UNIVERSITY OF CALIFORNIA, SAN DIEGO

Experimental studies on remanence acquisition processes and regional geomagnetic field variability from archeointensity studies

A dissertation submitted in partial satisfaction of the
requirements for the degree
Doctor of Philosophy

in

Earth Sciences

by

Ritayan Mitra

Committee in charge:

Professor Lisa Tauxe, Chair
Professor Catherine Constable
Professor Jeff Gee
Professor Tom Levy
Professor Hubert Staudigel

2012

Copyright
Ritayan Mitra, 2012
All rights reserved.

The dissertation of Ritayan Mitra is approved, and it is acceptable in quality and form for publication on microfilm and electronically:

_____

_____

_____

_____

_____

Chair

University of California, San Diego

2012

DEDICATION

To the one who kept me calm
The couple who brought me here
And to the curious explorers, many
Who made me who I am

EPIGRAPH

"What do we mean by 'understanding something'? We can imagine that this complicated array of moving things which constitutes 'the world' is something like a great chess game being played by the gods, and we are observers of the game. We do not know what the rules of the game are: all we are allowed to do is to watch the playing. Of course, if we watch long enough we may eventually catch on to a few of the rules. The rules of the game are what we mean by fundamental physics. Even if we knew every rule, however, we might not be able to understand why a particular move is made in the game, merely because it is too complicated." —*Richard Feynman*

TABLE OF CONTENTS

Signature Page iii

Dedication iv

Epigraph v

Table of Contents vi

List of Figures viii

List of Tables x

Acknowledgements xi

Vita and Publications xiii

Abstract of the Dissertation xiv

Chapter 1 Introduction 1
1.1 Remanence acquisition processes in paleomagnetic studies 1
1.2 Nature of the geomagnetic field 5

Chapter 2 Full vector model for magnetization in sediments 9
2.1 Introduction 10
2.2 Methods 12
2.3 Model 16
2.3.1 Floc Building 19
2.3.2 Floc Partitioning 21
2.3.3 Floc Rotation 23
2.4 Results 25
2.5 Discussion 27
2.6 Conclusions 36

Chapter 3 Detecting uniaxial single domain grains with a modified IRM technique 42
3.1 Introduction 43
3.2 Theory 47
3.2.1 Energy Calculations 47
3.2.2 Numerical Simulation 50
3.3 Experimental Evidence 54
3.4 Nature of anisotropy energy in MORB samples 57
3.5 Conclusions 62

Chapter 4 Two thousand years of archeointensity from West Africa . . . 67
4.1 Introduction . . . 68
4.2 Archeological Background . . . 71
4.2.1 The Middle Senegal Valley samples . . . 72
4.2.2 The Middle Niger Valley samples . . . 73
4.2.3 Chronology and Nomenclature . . . 77
4.3 Experimental Procedure . . . 78
4.3.1 Paleointensity Experiments . . . 78
4.3.2 Anisotropy . . . 82
4.3.3 Cooling-rate . . . 85
4.3.4 Rock Magnetism . . . 88
4.4 Discussion . . . 91
4.5 Conclusion . . . 99
4.6 Supplementary Material . . . 100

Chapter 5 Archeointensity in India: New constraints for the Iron Age . . 119
5.1 Introduction . . . 119
5.2 Archeology . . . 122
5.3 Rock Magnetic Experiments . . . 122
5.4 Archeointensity Experiments and Results . . . 123
5.5 Discussion . . . 124
5.6 Conclusion . . . 127

LIST OF FIGURES

Figure 1.1: Detrital remanent magnetization 3
Figure 1.2: Nature of the geomagnetic field 6

Figure 2.1: Normalized intensities in vertical fields 14
Figure 2.2: Experimental Data 15
Figure 2.3: Cartoon of model 18
Figure 2.4: 2-D cross-sections of flocs 19
Figure 2.5: Coordinate system for the model 24
Figure 2.6: Model results 26
Figure 2.7: Floc partitioning 28
Figure 2.8: Simultaneous variation of floc size and field intensity 31
Figure 2.9: RPI from site 983 and 984 33
Figure 2.10: Regimes of DRM acquisition 34

Figure 3.1: Energy density diargrams 48
Figure 3.2: Moment densities in response to fields 51
Figure 3.3: DIRM acquisition curves 52
Figure 3.4: Factors influencing IRAT 54
Figure 3.5: Hysteresis behavior 55
Figure 3.6: FORC distributions 56
Figure 3.7: DIRM in natural samples 57
Figure 3.8: IRAT of PH93-1 specimens 59
Figure 3.9: Ratio of IRM to NRM 60
Figure 3.10: M_{rs}/M_s vs IRAT of PH93-1 61

Figure 4.1: Global paleointensity data coverage and site locations 70
Figure 4.2: Excavation in progress 72
Figure 4.3: IZZI selection criteria 79
Figure 4.4: IZZI experimental results 81
Figure 4.5: Anisotropy correction 84
Figure 4.6: Cooling rate correction 87
Figure 4.7: Rock magnetic properties 90
Figure 4.8: Paleointensities from Africa 92
Figure 4.9: Paleointensities from Senegal and Mali 94
Figure 4.10: Latitudinal gradient in VADMs 96
Figure 4.11: Stratigraphy of Cubalel 101
Figure 4.12: Calibrated radiocarbon dates from Cubalel 102
Figure 4.13: Stratigraphy of Walalde 103
Figure 4.14: Calibrated radiocarbon dates from Walalde 104
Figure 4.15: Stratigraphy of Jenné-Jeno and Hambarketolo 105
Figure 4.16: Calibrated radiocarbon dates from Jenné-Jeno and Hambarketolo 106

Figure 5.1: Average VADMs from Europe and South East Asia 121
Figure 5.2: Rock Magnetism 123
Figure 5.3: IZZI experimental results 125
Figure 5.4: Paleointensities from India 127

LIST OF TABLES

Table 4.1: List of archeological sites 75
Table 4.2: List of samples and specimens 76
Table 4.3: Paleointensity parameters of selected specimens 107

Table 5.1: Archeointensity results from Varanasi, India 129

ACKNOWLEDGEMENTS

I am grateful to my doctoral committee without whose active guidance this dissertation would not have been possible. The chair of my committee, Lisa Tauxe, has been an advisor who has supported me in every way an advisor possibly can. She has listened to my bizarre plans, helped me come up with interesting questions to solve and has also taken an interest in helping me answer those questions to the satisfaction of journal reviewers. Words cannot express my deep sense of gratitude towards her. Jeff Gee, who is a coauthor of one publication, has been instrumental in the rest as well. His high standards were offered in a way that not only motivated me but also helped me immensely through every step of the scientific enquiry process. He also taught me how to spell 'remanence'. Cathy Constable helped me look at scientific questions from unique perspectives and I can definitely say that my interactions with her have been the most productive per unit time. Hubert Staudigel has been a strong sounding board and even though my plans changed mid-way, he remained his same gracious self throughout. Tom Levy has also been very kind and supportive and made important suggestions in one of the chapters.

During my stay at SIO I have met a lot of people and some have lingered on in my memory and I am sure they will for a long time to come. Roi Granot, Marcel Croon, Leah Ziegler, Elisenda Costa i Gisbert, Geoff Cromwell, Jesse Vavrek, Anita Di Chiara, Ron Shaar, Saiko Sugisaki and Shuhui Cai are some of the names, in the order they integrated with my life, that need to be mentioned. Their good advice, great insight (especially Roi and Ron) or just simple banter over coffee or beer have molded this dissertation in subtle ways.

This dissertation would not have been successful without the awesome folks at the graduate office and I would like to mention Laura Schaefer, Josh Reeves, Becky Burrola, Cerise Maue, Jan Hess, Gilbert Bretado and Monica Bailey. I am sure their involvement has helped me save unquantifiable hours of running around.

And, finally, I must mention the names of the few people who have seen me a little longer, chose to stick with me through a little more and willingly endured me, let's just say, in a more holistic way. Thanks Atreyee for all the support and

encouragement. Goutam, a dear friend, is sorely missed - he would have been very happy today. Back home, my sister Nandini Ghosh, an educator herself, has played a silent role in bringing this dissertation to fruition. Also, my Parents, really dealt with this 'doctoral epoch' much better than I thought they would - probably because they know me better than many, so Ma-Baba, thanks again for that.

Chapter 2, in full, is a reprint of the material as it appears in Mitra, R. and Tauxe, L. (2009), Full vector model for magnetization in sediments, Earth and Planetary Science Letters. The dissertation author was the primary investigator and author of this paper.

Chapter 3, in full, is a reprint as it appears in Mitra, R., Tauxe., L. and Gee, J. (2011), Detecting uniaxial single domain grains with a modified IRM technique, Geophysical Journal International. The dissertation author was the primary investigator and author of this paper.

Chapter 4, in full, has been submitted to Earth and Planetary Science Letters as: Mitra, R., Tauxe., L. and McIntosh, S.K., Two thousands years of archeointensity from West Africa. The dissertation author was the primary investigator and author of this paper.

VITA

2002	B.Sc. in Geology, Presidency College, Calcutta, India
2002-2004	M.Sc. in Earth Sciences, Indian Institute of Technology, Kharagpur, India
2006-2012	Ph.D. in Earth Sciences, Scripps Institution of Oceanography, University of California, San Diego

PUBLICATIONS

Mitra, R., Tauxe,L., 2009. Full vector model for magnetization in sediments. Earth. Planet. Sci. Lett., 286, 535-545, doi: 10.1016/j.epsl.2009.07.019

Mitra, R., Tauxe, L., Gee, J.S., 2011. Detecting uniaxial single domain grains with a modified IRM technique. Geophys. J. Int., 187,1250-1258, doi:10.1111/j.1365-246X.2011.05224.x

Mitra, R., Tauxe, L., McIntosh, S., Two thousand years of archeointensity from West Africa (submitted).

Mitra, R., Tauxe, L., Gee, J.S., Reply to comment on "Detecting uniaxial single domain grains with a modified IRM technique." (submitted).

ABSTRACT OF THE DISSERTATION

Experimental studies on remanence acquisition processes and regional geomagnetic field variability from archeointensity studies

by

Ritayan Mitra

Doctor of Philosophy in Earth Sciences

University of California, San Diego, 2012

Professor Lisa Tauxe, Chair

The dissertation comprises two separate topics. Chapters 2 and 3 are experimental studies on remanence acquisition processes. Chapters 4 and 5 investigate the geomagnetic field variability in Africa and India between 1000 BCE and 1000 CE.

Chapter 2 is a study in which the role of flocculation in sedimentary magnetization is analyzed with the help of laboratory redeposition experiments and a simple numerical model. At small floc sizes DRM acquisition is likely to be non-linear but it may record the directions with higher fidelity. In environments having bigger flocs the sediments are likely to record either intensities or directions with high fidelity, but not both. Also flocculation may inhibit a large frac-

tion of magnetic grains from contributing to the net remanence and this might have consequences for intensity normalization in sediments. Chapter 3 presents a fresh perspective on the long standing debate of the nature of magnetocrystalline anisotropy in Mid-Ocean Ridge Basalts (MORBs). A new parameter, IRAT, defined as the ratio of the isothermal remanences in antiparallel directions is used to differentiate between uniaxial single domain grains (IRAT $\sim$1) and multiaxial single domain grains (IRAT$<$1). The theoretical predictions were first validated with standard samples and then multiple MORB samples were analyzed. The observed IRAT ratios indicate a dominant non-uniaxial anisotropy in the MORBs. Chapters 4 and 5 are archeointensity studies from two data poor regions of the world viz., Africa and India. With stringent data selection criteria and well established archeological constraints these datasets provide important constraints on the field intensity from 1000 BCE to 1000 CE in Africa and 500 BCE to 1000 CE in India. The African dataset has a higher age resolution than the Indian dataset. The African dataset matches well with the global CALS3k.4 model and shows significant non-axial-dipolar contribution in the region. The Indian dataset is not of a similar resolution but shows that the field might have dropped by as much as 40% in the first half of the first century BCE and remained low during the first century CE.

Chapter 1

Introduction

1.1 Remanence acquisition processes in paleomagnetic studies

Paleomagnetism is the study of the remanent magnetization in sediments, rocks and other geological and archeological archives like pottery, slag, speleothems, etc. It attempts to understand the different processes through which the geomagnetic signal gets recorded at the time of formation of these ancient archives. As the nature of the archive changes, so does the way it records the geomagnetic signals and the magnetization recorded in such archives is called the natural remanent magnetization. In laboratories we have several ways of magnetizing a sample which often help us in understanding the underlying mineralogy. These often do not have an analogue in nature and are grouped under artificial remanences.

Among the natural remanences, thermoremanent magnetization (TRM) or the magnetization acquired by an archive when cooling from very high temperatures, is the best understood. Its foundation was laid out by the Nobel Prize winning work of Néel (1949). When a molten material like lava cools from a very high temperature then the thermal energy of the system is very high and the statistical orientation of the ferromagnetic grains is random. Below the Curie temperature the grains start to track the external field. As the temperature decreases and falls below the blocking temperature of the ferromagnetic minerals, the thermal energy

becomes less compared to the magnetic anisotropy energy of the system and the magnetization is locked in. A useful concept in understanding ferromagnetism is the relaxation time of the assemblage (τ), which is the time constant for the decay of the locked-in magnetization of the assemblage. It is given by

$$\tau = \frac{1}{C} e^{\frac{Kv}{kT}} \tag{1.1}$$

where C is a constant frequency factor, K is the dominant anisotropy, v is the grain volume, k is the Boltzmann constant and T is the temperature of the system. Therefore, the relaxation time is critically dependent on the size of grains, the temperature of the system and the kind of anisotropy present in the grains. As the temperature of a system increases the probability of a grain acquiring enough thermal energy to overcome the anisotropy energy increases and eventually at a high enough temperature the system unblocks or loses its remanent magnetization.

A very different process of locking-in the geomagnetic field is observed in detrital remanent magnetization (DRM). This is the remanence acquisition process in sediments and unlike TRM the theoretical foundation of DRM is not as well worked out. The detrital grains which already have a NRM align themselves with the ambient magnetic field as they settle in a fluid column. The degree of alignment is a function of the net magnetic field and when locked in can provide an estimate of the paleofield in which the sediments accumulated. A related process called the pDRM involves the post-depositional realignment of the detrital grains in the pore fluids of the unconsolidated sediments. Although it is largely agreed that the sediments acquire their magnetization as they settle through the water column and subsequent post-depositional processes play a role, their relative contribution or even the complete set of variables that affect these processes are poorly understood. For example, the role of flocculation, or loose aggregation of clay platelets into micron-sized porous bodies, has recently come to light (Fig. 1.1).

It has been shown that flocculation can explain the low remanence observed in sediments ($\sim$1% of saturation) and both theoretical and experimental work have shown that it can be one of the important variables affecting the DRM process

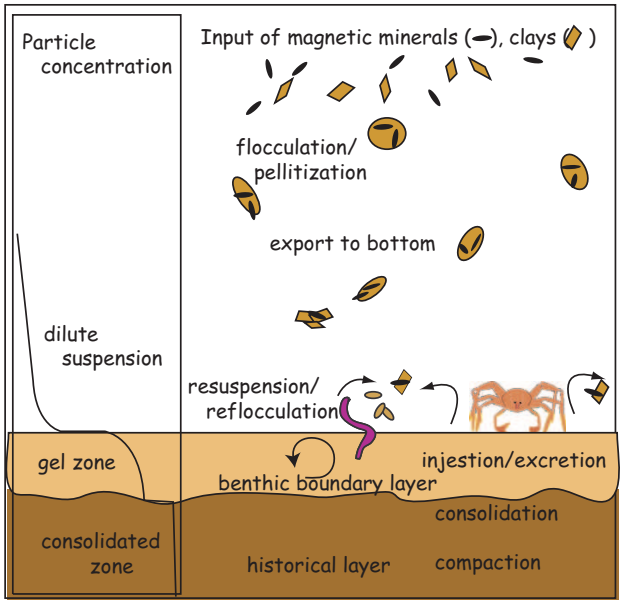


Figure 1.1: Schematic drawing showing the bottom water environment of a flocculating system. Tiny magnetic particles (black ellipse) attach themselves to platy clay minerals (brown rhomb) and pellets (brown ellipse) to settle together as a floc. A significant amount of re-suspension and re-flocculation occur near the boundary. Bioturbation also plays an important role in such systems. The concentration of the water changes with depth and at the interface there exists a gel-zone where the concentration of flocs is very high and they become largely immobile. Dewatering of this layer leads to further consolidation of the sediment (from Tauxe and Yamazaki, 2007).

(Scherbakov and Scherbakova, 1983; van Vreumingen, 1993b,a; Tauxe et al., 2006).

Other types of remanences observed in nature are viscous remanent magnetization (VRM) and chemical remanent magnetization (CRM). VRM involves gradual magnetization in the presence of weak magnetic fields. Natural VRM is considered as a secondary magnetization of a rock long after formation and therefore is treated as noise. Paleomagnetic techniques take care to remove this overprint to isolate the original remanence, also known as the characteristic remanent magnetization (ChRM). When a rock acquires a magnetization from growth of secondary magnetic minerals long after the formation of the rocks it is said to acquire a CRM. The red beds of China where pigmentary hematite imparts the red color is a good example. When rocks alter they may form new magnetic minerals which can also impart such a magnetization. The theoretical foundation of CRM

is not well worked out and is usually very difficult to interpret.

With the discovery of new archives that record ancient magnetization it is expected that more remanent acquisition processes will come to light in the future. Also, some archives may acquire their remanent magnetization from a combination of two different processes. Magnetization of speleothems is one such process where both DRM and CRM are supposed to play a role (Lascu and Feinberg, 2011).

Artificial remanent magnetization acquisition processes are usually of immense use in the laboratory for rock magnetic measurements. Isothermal remanent magnetization (IRM) is one such process in which the remanent magnetization results from the short term exposure to a very high magnetic fields, usually of the order of milliteslas and higher. In the laboratory a strong electromagnet is used to impart such a field. Similar to hysteresis processes the magnetization is entirely dependent on the coercivity of the ferromagnetic grains. All grain moments that have coercivities less than the applied field flip towards the field direction. In nature this kind of magnetization is possible when a lightning strikes a rock body. Anhysteretic remanent magnetization is the magnetization from a small DC field in the presence of an AF field. While the AF field serves to entrain similar coercivity fractions along opposite directions, the small DC bias field entrains moments along the field direction, thereby giving rise to a net moment along the direction of the bias field.

In this dissertation I have looked at two different remanence acquisition processes. Chapter 2 is a study of the role of flocculation in DRM. Previous workers have pointed out that flocculation of sediments could be an important control on the sedimentary magnetization process (Scherbakov and Scherbakova, 1983; van Vreumingen, 1993b,a). Tauxe et al. (2006) were the first to build numerical models to quantitatively explain the observed experimental results. They did not model the full vector but restricted their scope to intensities only. In this chapter I outline a new set of redeposition experiments and develop a numerical model to explain the full vector obtained from the experiments. Experimental details, model assumptions and implications are discussed in this chapter.

Chapter 3 is a study of magnetic anisotropy and how it influences the results

of a bidirectional stepwise IRM acquisition experiment. I develop a new experimental protocol to detect uniaxial anisotropy in single domain grains and apply this technique to Mid-Ocean Ridge Basalts (MORBs) to show that the dominant anisotropy in them is unlikely to be uniaxial.

1.2 Nature of the geomagnetic field

The dipolar nature of the Earth's internal magnetic field is well-known. According to this model the magnetic field of the Earth can be approximated to that of a huge bar magnet with the magnetic field lines pointing to the geographic North (Fig. 1.2a). Although this is a good approximation, especially when the field is averaged over thousands of years, the geomagnetic field is not a perfect dipole. This is to be expected because the magnetic field lines are a result of complex magnetohydrodynamical churnings of the dominantly iron-nickel fluid outer core and are not expected to show a perfectly symmetrical pattern. Thermal and topological imbalances across the core-mantle boundary, the presence of the solid inner core and the rotation of the earth all contribute to make the field lines more convoluted than what is required for a simple axial dipolar structure (Fig. 1.2b).

The key to understand the complexity of the geomagnetic field is surface field measurements from different locations spread around the globe. This kind of spatially distributed data collected over time is crucial to build complicated time-varying geomagnetic field models (Bloxham and Jackson, 1992; Jackson et al., 2000; Korte and Constable, 2011). Systematic field measurements are available for a relatively restricted period of the past 200 yrs. Historical measurements from the log books of the ancient mariners push back the available data till the sixteenth century. As time dependent variations of the internal geomagnetic field (secular variation) have longer time-scales we need to look at paleomagnetic archives for the necessary data.

The different kind of archives and the types of remanences they carry were discussed in the previous section. The most widely used paleomagnetic archives are sediments and volcanic rocks. While volcanic rocks can be used to determine the

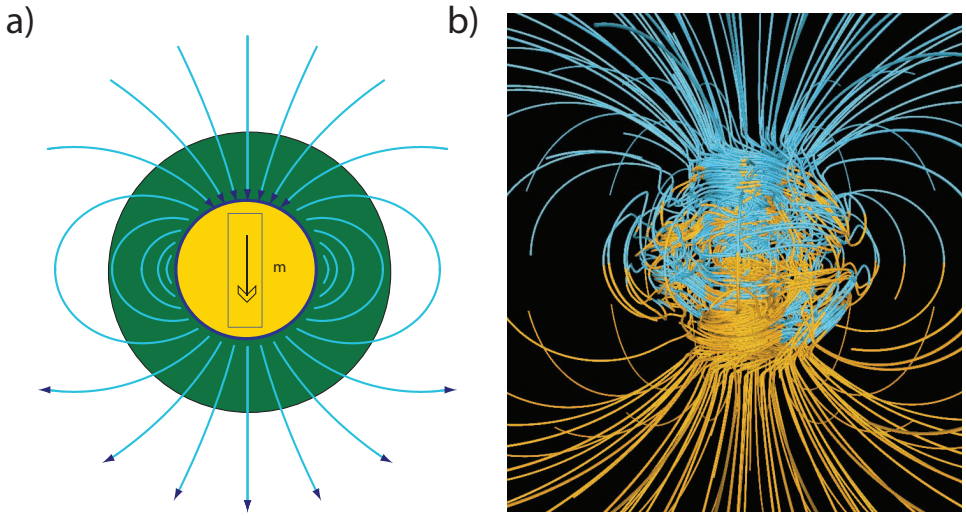


Figure 1.2: a) Geomagnetic field lines for an axial dipole approximation of the Earth's magnetic field (from Tauxe, 2010). b) Magnetic field lines according to the Glatzmaier-Roberts geodynamo model (from Glatzmaier and Roberts, 1996). Magnetic field lines are blue where the field is directed inward and yellow where directed outward.

full magnetic vector, sediments can only yield the field direction, not the intensity. But sediments provide a more continuous record than the volcanic rocks because of the relatively uninterrupted nature of the archive. Another archive which is especially useful during the Anthropocene (past $\sim$ 8 Ka) is that of archeological artifacts from past civilizations. Archeological artifacts like pottery, bricks and furnace clays acquire their magnetization in a manner analogous to that of volcanic rocks. The moments of the ferromagnetic minerals in the artifacts orient with the magnetic field and below a certain temperature remain in energetic equilibrium for a long time (Myr). Therefore, any archeological artifact which has been made at a high temperature has the potential to record the paleofield. These have become increasingly important to reconstruct the global geomagnetic field over the last few millennia because of the sparse distribution of dated lava flows and the abundance of ancient civilizations during this time.

To understand the global structure and evolution of the geomagnetic field homogenous distribution of data across both time and space is ideal. Unfortunately this is not true at present with most of the data coming from Europe and

neighboring countries in Asia. In this section of my thesis, I look at two such data deprived regions of the world. In chapter 4 I use archeological artifacts from West Africa to reconstruct the field intensity from 1000 BCE to 1000 CE. More specifically, in this chapter I provide the first paleointensity estimates from regions below 20°N in Africa. The experiments, results and implications of the study are discussed in this chapter. Chapter 5 is similar in its organization to chapter 4. Here I look at some Iron Age potsherds from North India. Pre-existing data from the sub-continent come from relatively old publications which used antiquated experimental techniques. This dataset is the only one from this region that conforms to stringent requirements of advanced paleointensity experiments. Results and implications of the study are discussed in this chapter.

Bibliography

J. Bloxham and A. Jackson. Time-dependent mapping of the magnetic-field at the core-mantle boundary. *J. Geophys. Res.*, 97(B13):19537–19563, 1992.

G.A. Glatzmaier and P.H. Roberts. An anelastic evolutionary geodynamo simulation driven by compositional and thermal convection. *Physica D: Nonlinear Phenomena*, 97(1-3):81 – 94, 1996.

A. Jackson, A. R. T. Jonkers, and M. R. Walker. Four centuries of geomagnetic secular variation from historical records. *Philos. Trans. R. Soc. A*, 358(1768): 957–990, 2000.

M. Korte and C. Constable. Improving geomagnetic field reconstructions for 0-3 ka. *Phys. Earth Planet. Inter.*, 188(3-4):247–259, 2011.

I. Lascu and J. M. Feinberg. Speleothem magnetism. *Quat. Sci. Rev.*, 30(23-24): 3306–3320, 2011.

L Néel. Théorie du trainage magnétique des ferromagnétiques en grains fins avec application aux terres cuites. *Anns. Géophys.*, 5:99–136, 1949.

V Scherbakov and V. Scherbakova. On the theory of depositional remanent magnetization in sedimentary rocks. *Geophysical Survey*, 5:369–380, 1983.

L. Tauxe. *Essentials of Paleomagnetism*. University of California Press, Berkeley, 2010.

L. Tauxe, J. L. Steindorf, and A. Harris. Depositional remanent magnetization: Toward an improved theoretical and experimental foundation. *Earth Planet. Sci. Lett.*, 244(3-4):515–529, 2006.

L. Tauxe and T. Yamazaki. Paleointensities. In G. Schubert, editor, *Geomagnetism*, volume 5 of *Treatise on Geophysics*, pages 509–564. Oxford: Elsevier Ltd., 2007.

M. J. van Vreumingen. The influence of salinity and flocculation upon the acquisition of remanent magnetization in some artificial sediments. *Geophys. J. Int.*, 114(3):607–614, 1993a.

M. J. van Vreumingen. The magnetization intensity of some artificial suspensions while flocculating in a magnetic field. *Geophys. J. Int.*, 114(3):601–606, 1993b.

Chapter 2

Full vector model for magnetization in sediments

Sediments provide a continuous record of past geomagnetic field variations. Although it is theoretically possible to get both the direction and intensity of the geomagnetic field from sediment records, the mechanism is not fully understood. Previous workers have postulated that flocculation plays an important role in detrital remanent magnetism (DRM). Flocs are porous, loose and highly fragile aggregates of microscopic clay particles and their behavior in a viscous medium is likely to be different than single particles of magnetic minerals. In order to understand the role of flocculation in sediment magnetization, we carried out a set of redeposition experiments at different field intensities and a quasi-constant field inclination of 45°. We present here a simple numerical model of flocculation, incorporating both magnetic and hydrodynamic torques to explain the experimental data. At small floc sizes DRM acquisition is likely to be non-linear in field strengths comparable to the Earth's, but the sediments may be able to record the directions accurately. With increasing floc sizes sediments may retain a record of the intensity that is linearly related to the applied field or a direction parallel to the applied field, but are unlikely to do both at the same time. Also, the majority

of the magnetic particles in the sediments may not be contributing significantly towards the net DRM and any bulk normalizing parameter may be unsuitable if the depositional environment has changed over the depositional period.

2.1 Introduction

Although it is generally accepted that sediments record past variations of the geomagnetic field, there is still no consensus on how sediments get magnetized. The theory of depositional remanent magnetism (DRM) was initially laid out by Nagata in which individual magnetic grains align themselves with the magnetic field while settling in a viscous medium at low Reynolds number Nagata (1961). According to this model, assuming reasonable terrestrial field intensities and magnetic moment of the settling particles, the time for the population of magnetic particles to become substantially aligned with the field is of the order of a few milliseconds. This is true irrespective of field and mineralogy, so, sediments should show saturation remanance. Yet nearly all laboratory redeposition experiments, dating from the first by Johnson et al. (1948), exhibit a strong field dependence of DRM which is nearly linear in fields like the Earth's.

Another aspect of DRM relevant to magnetic recording of the Earth's field is the observation that the remanent inclinations are often anomalously shallow compared to the applied magnetic field. This too has been observed in laboratory redeposition experiments. The first explanation for this inclination "error" was by King (1955). He proposed that magnetic grains could be divided into two populations; one which were plate-like and presumably would settle with their magnetic moments aligned in the horizontal plane and the other, which were spherical, would align perfectly with the field. The contributions of these two types of grains would give rise to a net shallowing of the inclinations. An alternative explanation was offered by Griffiths et al. (1960), who argued that having two distinct population of grain shapes was unlikely. They proposed instead a model whereby each

individual spherical grain would settle to the bottom where it would encounter a micro-landscape of crests and troughs owing to surface unevenness. If the particles rolled from an aligned position by a random angle there could be a net shallowing of the inclination. A third explanation involving sedimentary compaction was first proposed by Blow and Hamilton (1978) who found a dependence of inclination shallowing with reducing porosity. This model was further extended by Anson and Kodama (1987) who called upon a mechanical model in which the individual magnetic particles, attached to plate-like clay particles, rotate during compaction causing a net shallowing. Arason and Levi (1990) devised a suite of compaction induced inclination shallowing models in which they considered discrete rotation of individual grains in either a rigid or soft matrix and also rotation of magnetic grains attached to clay flakes.

Scherbakov and Scherbakova (1983) first recognized the importance of flocculation in DRM. They pointed out that microscopic clay and sub-micron sized magnetite particles acquire surface charges which make them stick together. In this view, magnetic grains settle embedded in loosely aggregated porous bodies of clay. The lower net moment of the flocs would explain the field dependence of DRM. The role of flocculation was further investigated by van Vreumingen (van Vreumingen, 1993a,b). With the help of an array of experiments he explored the role of sediment concentration, type, magnetic mineral concentration on DRM intensity and inclination. He demonstrated a dependence of intensity and inclination shallowing on increasing salinity (which controls the degree of flocculation). At very low salinities, there was only a moderate inclination error. The inclination error increased with increasing salinities. However, intriguingly, at higher salinities, the inclination error began to decline while the intensities remained low. Although the experiments were insightful a number of interpretations were ambiguous. The author was unable to explain the rise of inclination shallowing with a drop in intensity at moderate salinities stating that the phenomenon was "incompletely understood". More importantly, although the author suggested flocculation to be

the driver behind the observed variations in intensity and inclination, a coherent model was not suggested. One of the current authors developed a numerical model for the effect of flocculation on remanent intensities at a range of different field intensities and came to the conclusion that below a critical diameter magnetization in sediments is likely to be non-linear (Tauxe et al., 2006).

So far DRM models incorporating flocculating particles have not been able to quantitatively address both intensity and inclination variation with changing floc size. In this paper we present a series of redeposition experiments with different floc size distributions and field intensities. We confirm the experimental results of van Vreumingen that inclination shallowing can be partly depositional and can vary with the degree of flocculation. We extend the numerical modeling approach of Tauxe et al. (2006) to include processes (viz, hydrodynamic torques) which could give rise to the observed inclination shallowing. Further, with the model we aim to explain some of the ambiguities of earlier studies and make broad predictions about the suitability of depositional environments for paleomagnetic studies. To avoid confusion further on we define DRM strictly as the remanence acquired during the settling of sediments and is not to be confused with post-depositional remanent magnetism (pDRM) which we conceive as the remanence the sediment acquires after it has completely settled, in the presence of an external field due to rotation of individual magnetic particles.

2.2 Methods

We followed the recipe of van Vreumingen (1993a) for creating a synthetic mixture of sediment: we combined kaolinite and illite in the ratio of 2:1. Partially oxidized magnetite powder (W4000; 0.08 percent by weight) with an average diameter of 50 nm was added to the mixture. The mixture was crushed thoroughly in a rock crusher to ensure homogenization and thorough dispersal of the maghemite particles. A total of 12 samples of 0.9 gm of the mixture were given a saturation

isothermal remanance (sIRM) in a 700 mT impulse field. Uniformity of the sIRM values (11.85 $\pm$1.5 μAm^2) ensured between sample homogeneity. The samples were mixed with 300 ml of water and 4 ml of 0.1 M sodium pyrophospate was added to the mixtures to ensure a de-flocculated initial state. Van Vreumingen varied salinity to create a range of floc sizes. In our experiment, sodium chloride was added to the sediment slurries to obtain a range of salinities from 0 to 20 ppt in the 12 tubes. Before each settling experiment, the sediment slurries were shaken vigorously for 10 minutes.

Three pilot studies were done with all 12 tubes in vertical fields of 10, 30 and 60 μT. The tubes were placed in a solenoid generating a uniform field. The settling experiments were carried out inside a 1 m diameter μ-metal sheath to cancel external fields. After letting the slurry settle for two weeks, the tubes were carefully taken out and inserted into a CTF three axes cryogenic magnetometer housed in the magnetically shielded room at Scripps Institution of Oceanography in order to measure their remanence .

Fig. 2.1 shows the sIRM normalized remanent intensities for the twelve tubes after settling in three different fields. The intensity variations replicate those obtained by van Vreumingen (van Vreumingen, 1993b) in that there is an initial rise in DRM intensity with increasing salinity followed by a pronounced drop in intensity for salinities in excess of about 2 ppt. Van Vreumingen argued that isolated magnetic particles would tend to clump together suppressing the net magnetization. Increasing salinity of the solution resulted in increased tendency to flocculate which prevented the magnetic grains from clumping together. He explained the initial rise in DRM intensity with salinity as a result of the magnetic grains becoming increasingly attached to clays, instead of to each other, which would increase the net magnetization. In our experiments, however, we found that the tubes with salinities between 0 and 2.5 ppt were not fully settled and remained cloudy even after two weeks. Hence it is also possible that the rise in intensity was the result of inaccurate normalization. Because of the ambiguity in interpretation,

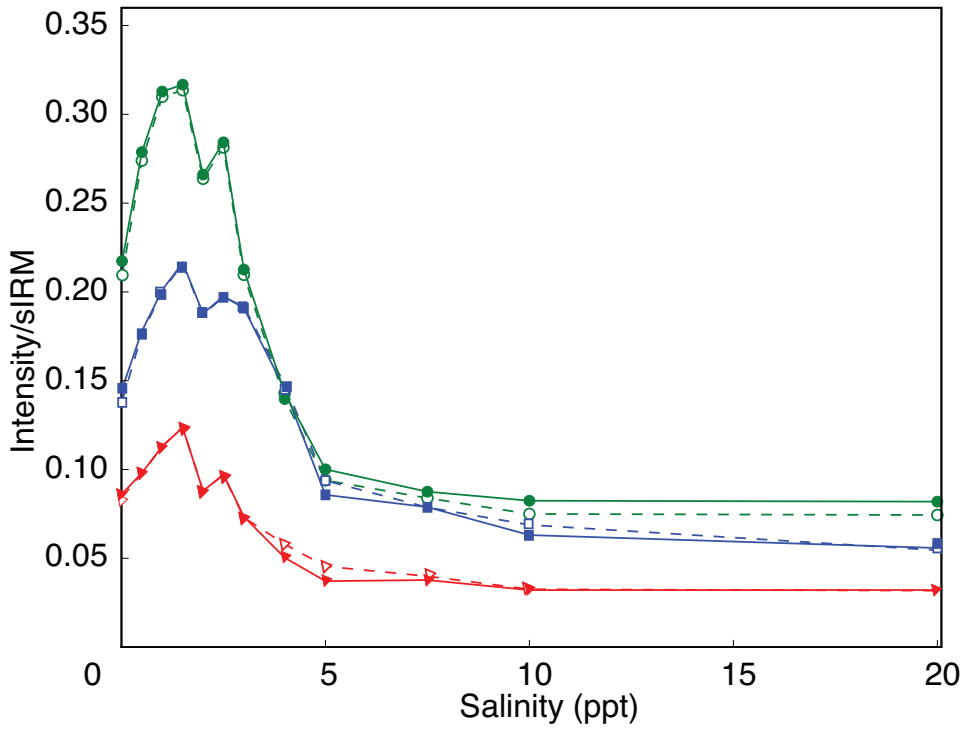


Figure 2.1: Normalized intensities from twelve tubes in vertical fields of 10 μT (red triangles), 30 μT (blue squares), 60 μT (green circles). Open symbols are the remanences measured after reversing the field direction for 12 hrs.

we use results from only fully settled tubes (salinity of 2.5 ppt or more).

To assess the role of post-depositional rotation of magnetic grains (pDRM), we reversed the vertical field direction and measured the intensity after 12 hrs. Comparison of the results (dashed and solid lines in Fig. 2.1) shows that pDRM was negligible in these experiments.

Our next experiment consisted of placing six tubes with salinities ranging from 3 ppt to 20 ppt in a two axis Helmholtz coil placed within a μ-metal sheath. Care was taken to ensure minimum field variations across the tubes. To further offset the effect of field variations, the tubes' positions with respect to the center of the Helmholtz coil was changed between experiments. Experiments were conducted in three fields (28.21 $\mu T\pm$ 0.21 inclined at 47.22°$\pm$ 0.68, 44.10 $\mu T\pm$0.25 inclined at 46.41°$\pm$1.31 and 57.55 $\mu T\pm$0.37 inclined at 44.58°$\pm$1.42).

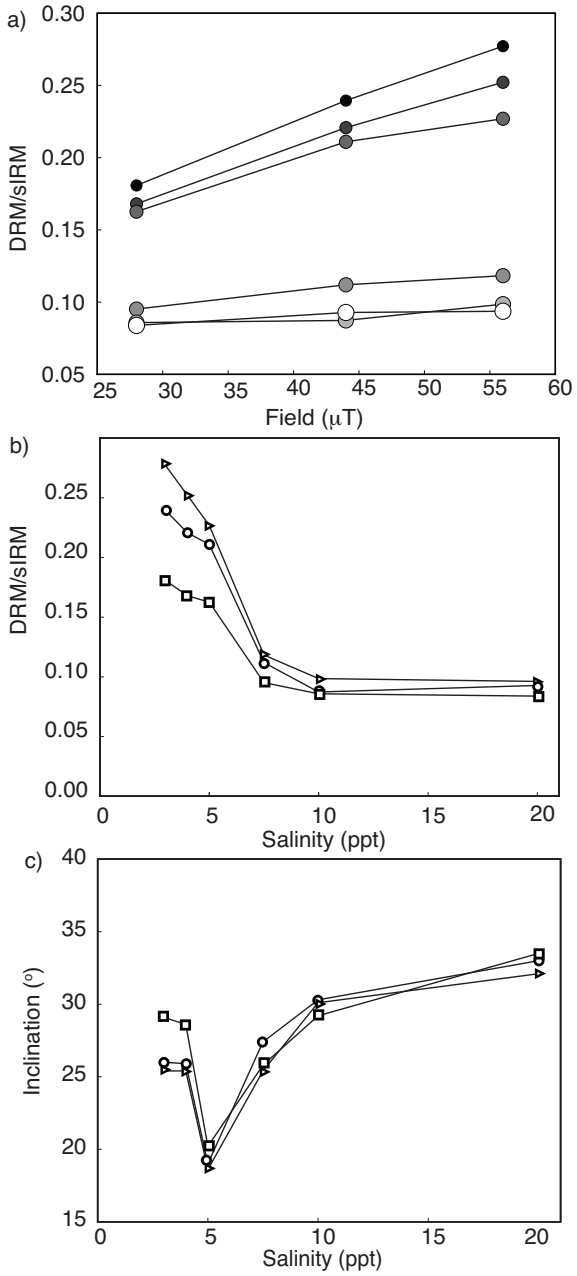


Figure 2.2: Experimental data. a) Normalized intensity as a function of the applied field. Smaller, darker circles indicate lower salinities. b) Normalized intensities as a function of salinity. Squares, circles and triangles indicate field strengths of 28.21 μT, 44.10 μT and 57.55 μT. c) Corresponding inclinations as a function of salinity.

Low salinity tubes (marked with smaller, darker circles) exhibit a non-linear field dependence while high salinity tubes are more linear (Fig. 2.2a). Increas-

ing salt content help in flocculation and the remanent intensities drop markedly (Fig. 2.2b). The inclinations show a concomittant drop (increasing inclination error) and subsequently bounce back at higher salinities (Fig. 2.2c).

The experimental data echo those from a single field intensity experiment observed in van Vreumingen (1993a). We have used a clay composition and salinity range very similar to his experiments and observe a similar drop of intensity in the 4-6 ppt range. This is particularly important because our experimental setup differs substantially from his. We have used 50 cm long settling tubes while his experiments were conducted in 2cm plastic cubes. Therefore, the observations of intensity and inclination dependence on salinity are independent of exact experimental setup.

We performed the settling experiments in three field strengths; our results suggest a possible (weak) field dependence of inclination shallowing (inclinations are slightly shallower at higher field strengths). However, this apparent field dependence of inclination shallowing could possibly be ascribed to the fact that the experiments were conducted at slightly different inclinations, with the stronger field strengths having slightly steeper field inclinations. We also note that DRM declinations tracked the field accurately, in keeping with earlier studies. In the following section we formulate a physical model to explain the key observations.

2.3 Model

Flocculated particles are hydrodynamically different from isolated particles. They are porous, loose and highly fragile. Instead of being perfectly spherical as has been hypothesized in models exploring flocculation as an explicit control on DRM (Katari and Bloxham, 2001; Tauxe et al., 2006), they tend to have highly irregular shapes. Studies of rigid ellipsoidal particles have shown that they exhibit complex motion while settling in the fluid column (Belmonte et al., 1998; Field et al., 1997). Although flocs are rigid ellipsoidal particles it is useful to attempt to

model their settling behavior as stemming from slight departures from sphericity. Heslop (2007) attempted such a study and showed that with increasing floc sizes the hydrodynamic torque would increase at a much higher rate than the magnetic torque and for a prolate ellipsoid with a particular aspect ratio there is a critical size beyond which flocs would tend to be dominated by hydrodynamic torques. A different approach was taken by Jezek and Gilder (2006). They considered remanence acquisition of ellipsoidal magnetic particles in a gently creeping viscous flow, conditions which are likely to be found in continental margins and slopes. While the two studies are complimentary to each other, Heslop (2007) showed that even in quiescent and non-sloping conditions like open ocean or lake interiors, the role of hydrodynamic torques could be quite significant.

The proposed model incorporates Heslop's findings into the flocculation model of Tauxe et al. (2006). It is conceptually similar to the model proposed by King (1955) to explain inclination shallowing but differs substantially in the processes involved. Instead of assuming two distinct magnetic grain shape populations, our model separates a continuous distribution of floc sizes into two behavioral groups: one small enough to be responsive to *only* magnetic torques and the other big enough to be governed *chiefly* by hydrodynamic torques. The smaller flocs in the distribution (population M, hereafter as M) would be dominated by magnetic torques. Their net magnetic moment would be quasi-parallel with the applied field. Larger flocs (population H, hereafter as H) would be more influenced by hydrodynamic torques. Flocs in H first attain hydrodynamic stability and subsequently align with the magnetic field trying to maintain its hydrodynamically stable situation. Therefore, the net declination of H would track the field azimuth, but the net inclination would be near zero. The resultant of moments from M and H could give rise to the observed DRM (Fig. 2.3). The reader is cautioned that in reality a floc is not expected to show a rotation scheme as envisaged in the model. Instead it is expected to follow a complicated trajectory under the simultaneous influence of magnetic and hydrodynamic torques. But if we consider a large ensemble of

flocs then such an approach would give us an 'average' value by ironing out the inconsistencies.

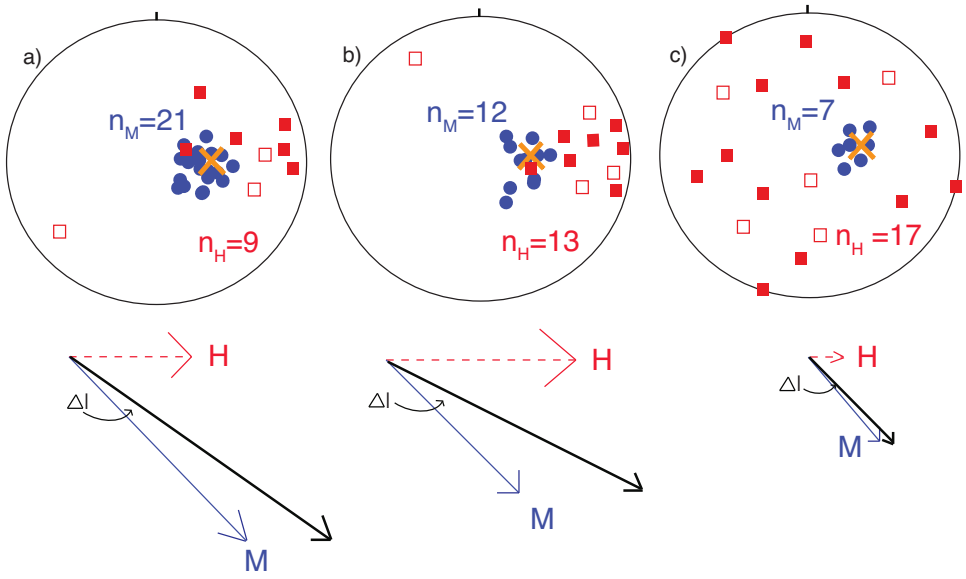


Figure 2.3: Schematic of equal area projections of individual floc moments showing the intensity and inclination dependence with increasing floc size. Blue circles represent M and red squares represent H. Solid and open squares represent moment directions in the lower and upper hemispheres respectively (see text). Orange cross is the field direction. Arrows show the contributions from M (blue solid arrow) and H (red dotted arrow) and the resultant (thick black arrow). a) Tubes with low salinity have small floc sizes and majority of the flocs (blue circles) are dominated by magnetic torques. Very few flocs are dominated by hydrodynamic torques (squares). The horizontal component is thus small, giving a low inclination shallowing (ΔI). b) With increasing floc sizes more flocs are influenced by hydrodynamic torques resulting in a higher net horizontal component. This increases ΔI. c) The floc sizes have become so large that most of the flocs are influenced by hydrodynamic torques and they cannot orient themselves as efficiently (as in b) with the field any more. This causes a very small net horizontal moment in the field direction and thus producing only a slight inclination shallowing. The net moment continues to decrease throughout (from a to c) because of less efficient alignment by increasingly bigger flocs.

Assuming a distribution of floc sizes, at low salinities (Fig. 2.3a), the fraction of flocs in the M population is greater than that in the H population because low salinity inhibits flocculation thus keeping the floc sizes small. Most of the flocs align with the field and this results in high DRM intensities and limited inclination

shallowing. With increasing salinity (Fig. 2.3b) the average floc size increases and the contribution of population H becomes significant, resulting in a net shallowing of the inclination and a reduction in the net moment. With further increase in salinity, net contribution of population H is strongly reduced (Fig. 2.3c); their moments are essentially randomly oriented, unable to align with the field at all. The randomization of H results in both a decrease in inclination shallowing and a reduction in strength of the net moment.

Our conceptual model involves three basic steps; building flocs, partitioning flocs into M and H, and finally rotating the flocs in response to the magnetic field. The key to a realistic yet simple numerical model involving such complex processes involves trade-offs in all the three steps. In the following sections we discuss the key assumptions and methods involved in each.

2.3.1 Floc Building

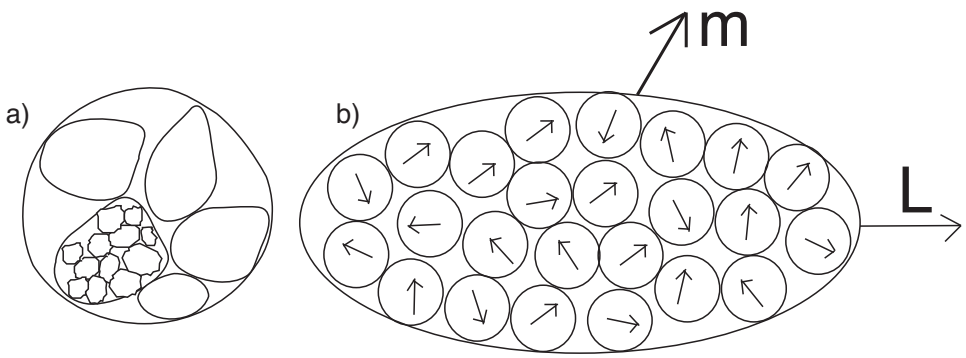


Figure 2.4: 2-D cross-sections of flocs. a) Hierarchical structure of flocs as envisaged by Krone (1986). Three levels of organization are shown. b) Flocs as envisaged in the current model. Small red arrows show the individual moment directions of the maghemite grains embedded in 1 μm clay balls. Thick arrow shows the net moment (m) of the floc. Long thin arrow is the long axis (L) of the ellipsoidal flocs.

Particulate clusters of clay sediments have a tendency to aggregate in a hierarchical fashion. Krone (1986) was the first to suggest a fractal nature of the

flocs (Fig. 2.4a). Clay flocs also tend to have a very open ended structure with high water content. Processes giving rise to fractal floc shapes can be broadly categorized into Diffusion Limited Aggregation (DLA) and Cluster-Cluster Aggregation(CCA). In the former, individual particles execute Brownian motion to collide and stick on to one another. The latter adds one more step of complexity by assuming collisions of clusters instead of single particles. The basic building blocks of any DRM model involving flocculation are the flocs and past workers have approached this problem in a number of ways. The first numerical model dealing with flocculation was by Katari and Bloxham (2001). To build flocs they assumed a single magnetite particle within a larger spherical mass of clay. Tauxe et al. (2006) developed this model by building flocs with micron sized "micro-flocs" each of which had a magnetite embedded in it. Tauxe's model was closer to Krone's original thesis of hierarchical nature of flocs without explicit declaration of the processes leading up to such a structure. Shcherbakov and Sycheva (2008) designed very realistic floc structures by explicitly using the CCA and the DLA models of flocculation. Although realistic, such flocs are difficult to incorporate within the framework of a DRM model because of the lack of studies of their hydrodynamic behavior. Keeping the foregoing in mind, the flocs in our models have been built as in Fig. 2.4b. Length of the long axis of each floc was drawn out of a lognormal distribution. The long axes of the ellipsoidal flocs were uniformly distributed over $\theta = [-\pi/2, \pi/2]$. It was assumed that the flocs were prolate spheroids with an axial ratio (p=b/a) of 0.5. We further assume that the larger ellipsoidal floc is made up of many small spherical micron sized clay flocs each of which has a magnetic particle embedded in it. To calculate the number of such microflocs necessary to form the bigger flocs we assumed a packing density of 0.64, in keeping with random close spaced packing of spheres (Scott and Kilgour, 1969). A final consideration was given to keeping the total mass of magnetic minerals constant in all the simulations. In contrast, Tauxe et al. (2006) kept the number of flocs constant implying an ever increasing magnetic mineral population with increasing

mean size of the distribution. This is physically unreasonable. Therefore in our model we have conserved total number of magnetic grains rather than the total number of flocs for each simulation. This translates to having fewer flocs with magnetic grains embedded in them as the mean size of the distribution increases. Given the high clay to maghemite ratio in the experiments we find this assumption to be a better approximation of the experimental conditions. Furthermore, we constrained the maximum number of maghemite grains available to build a floc to 500. Otherwise for distributions with sufficiently large means all the maghemite grains would be used up in building the first few flocs which can be argued to be unnatural. Raising the maximum limit would require more flocs to generate stable results without changing the model results. To calculate the net moment of each floc we use the expression by Rayleigh (1919) which gives the probability density function, F, of obtaining a resultant magnitude of R, from the summation of N randomly oriented vectors distributed uniformly in space.

$$f(R) \approx \frac{3\sqrt{6}R^2}{\sqrt{\pi}N^{\frac{3}{2}}} e^{\frac{-3R^2}{2N}} \tag{2.1}$$

The net moment directions of individual flocs were assumed to be oriented at a random angle with the floc's long axis (Fig. 2.4b).

2.3.2 Floc Partitioning

The current model aims at understanding the average behavior of an ensemble of flocs. It does not take into account the actual trajectory a floc would take when acted upon by hydrodynamic and magnetic forces. This requires a partitioning of the entire population of flocs into M and H, which are dominated by either magnetic or hydrodynamic torques. To this end we first consider the hydrodynamic torque (τ^H) on a rigid, ellipsoidal particle (the flocs), with a as the principle axis and $b = c$ as the semi-minor axes, in a stationary Newtonian fluid

at low Reynolds number. An approximate value for this is given by the following expressions (Kuusela, 2005; Heslop, 2007):

$$\tau^H \approx \frac{16a^4\rho_l^2(V_t)^3G}{\eta} sin2\theta[cos2\theta\left\{\left(\frac{cos\theta}{X^A}\right)^2-\left(\frac{sin\theta}{Y^A}\right)^2\right\} - \frac{cos4\theta}{2X^AY^A}]\sqrt{\frac{sin^2\theta}{(Y^A)^2}+\frac{cos^2\theta}{(X^A)^2}}, \quad (2.2)$$

where

$$X^A = \frac{8}{3}e^3\{-2e+(1+e^2)L\}^{-1},$$

and

$$X^B = \frac{16}{3}e^3\{2e+(3e^2-1)L\}^{-1},$$

are the resistance functions of a prolate ellipsoid with

$$L = ln\frac{1+e}{1-e},$$

where,

$$e = \sqrt{1-\left(\frac{b}{a}\right)^2},$$

and ρ_l, η, V_t are the density, viscosity of water and the terminal velocity of a sphere with radius b. G is the geometric factor of Galdi and Vaidya (2001) and for p=0.5, G = -0.96. θ is the angle the long axis of the floc makes with the vertical. The floc is stable (i.e, $\tau^H = 0$) when $\theta = \pi/2$. Eqn.2 is for prolate ellipsoids only. Although a similar expression exists for oblate ellipsoids no expression for the geometric factor, G is available.

The magnetic torque (τ^M) is given by:

$$\tau^M = \mathbf{m} \times \mathbf{B}, \tag{2.3}$$

where **m** and **B** are the net magnetic moment and magnetic field vectors respectively.

The flocs are separated into M and H depending on the magnitude of the torques τ^H and τ^M at a random point during their settling. A valid point to consider would be whether the torques should be calculated for a random instance of the flocs or to compare the maximum of the two torques. Since we are looking at the ensemble behavior and not the precise trajectories of individual flocs we believe that either assumption is equally plausible for the purpose.

2.3.3 Floc Rotation

If $|\tau^H|$ is less than $|\tau^M|$ then the magnetic torque dominates the floc's rotation and it changes its orientation along path a (Fig. 2.5). If $|\tau^H|$ is greater than $|\tau^M|$ then the floc is assumed to be in H and rotates from L_1 to L_2,to bring itself to the most stable orientation of $\theta = \pi/2$. The moment direction changes from M_1 to M_2 (path b_1). The floc undergoes a further rotation due to the magnetic torque acting on it while maintaining its hydrodynamically stable position at $\theta = \pi/2$ (path b_2).

In order to ascertain the role of magnetic field on the flocs we start from the classic equation proposed by Nagata (1961):

$$I\frac{d^2\alpha}{dt^2} = -\lambda\frac{d\alpha}{dt} - mBsin\alpha \tag{2.4}$$

where λ is the viscosity coefficient of water and I is the moment of inertia and α is the angle between the moment and the field directions. For non-spherical particles Equation 2.4 becomes

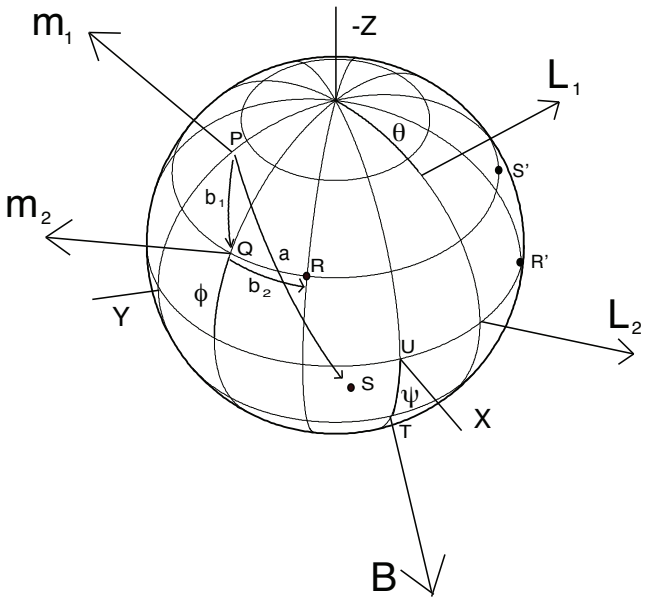


Figure 2.5: Coordinate system for the model. L_1 and $\mathbf{m_1}$ are the initial long axis and moment directions. L_1 makes $\theta = 90°$ with Z axis. B is the field direction. Flocs dominated by hydrodynamic torques rotate from P towards T in a stepwise fashion. L_1 goes to L_2 and in response $\mathbf{m_1}$ goes to $\mathbf{m_2}$ (path b_1). $\mathbf{m_2}$ goes to R and in response L_2 goes to R' (path b_2). Flocs dominated by magnetic torques take the shortest path towards B (a); $\mathbf{m_1}$ goes to S and in response L_1 goes to S'.

$$I\frac{d^2\alpha}{dt^2} = -F_p\lambda\frac{d\alpha}{dt} - mBsin\alpha, \tag{2.5}$$

where F_p is the Perrin friction factor (Perrin, 1934). For prolate ellipsoidal particles (with an axial ratio of 0.5) we have used an average value of 1.2.

Neglecting the inertial term and assuming Gibb's empirical relation between floc size and settling velocity Gibbs (1985) we have $v = 1.1r^{0.78}$

Equation 2.4 can be solved as in Katari and Bloxham (2001);

$$\tan\frac{\alpha}{2} = \tan\frac{\alpha_0}{2}\exp\left(\frac{-mBl}{8.8F_p\pi\eta r^{3.78}}\right) \tag{2.6}$$

where l is the length of the tube through which the flocs settle, r is the equivalent radius of the flocs, α_0 and α are the initial and the final angle between the moment and the field directions.

For particles in population H, constrained to lie in the horizontal plane for greater hydrodynamic stability, we have:

$$\tan\frac{\alpha}{2} = \tan\frac{\alpha_0}{2}\exp\left(\frac{-mB\cos(\phi)\cos(\psi)l}{8.8F_p\pi\eta r^{3.78}}\right) \tag{2.7}$$

where I is the field inclination. α_0 and α are the initial and the final angle between the horizontal components of the moment and the field directions. ϕ is the inclination of the floc moment after b_1 and ψ is the field inclination. The $\cos(\phi)$ and $\cos(\psi)$ terms are necessary because in this case we are considering rotation with the flocs long axis constrained to lie in the horizontal plane(Fig. 2.5). For a more detailed exposition of the governing equations the reader is directed to Tauxe et al. (2006)

2.4 Results

Our model replicates the primary characteristics of the data (Fig. 2.6). Smaller floc sizes show an increasingly non-linear rise of DRM intensity with field (compare Fig. 2.2a with Fig. 2.6a). Moreover, the distinct drop in intensity was accompanied by an increase in the degree of inclination shallowing (Fig. 2.6b). The declinations tracked the field azimuth in the experiments as well as the model.

In the model the floc size distribution plays an important role. In model instances with low mean floc sizes and low standard deviations we expect to see the majority of flocs to be dominated by magnetic torques. Also these flocs being small will be very efficiently oriented by the field. The few flocs that are dominated by hydrodynamic toques would show clustering towards the field azimuth because they are still small in size. The moments of these would form a cone around the field azimuth but their total number is not high enough to cause substantial shallowing in inclination (Fig. 2.7a). With increasing flocculation the mean floc size increases and a greater number of flocs are dominated by hydrodynamic torques.

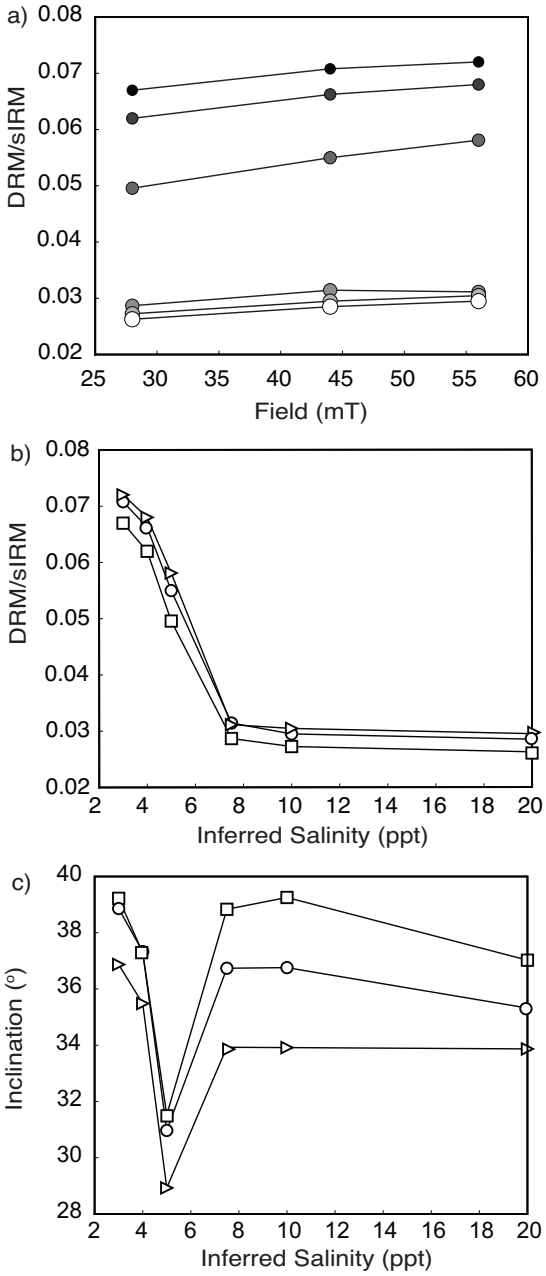


Figure 2.6: Modeled results with symbols having the same meaning as in Fig. 2.2. a) Normalized intensity as a function of applied field. b) Normalized intensity as a function of inferred salinity. c) Inclinations as a function of inferred salinity. For each salinity a lognormal distribution of floc size was assumed. In order of increasing salinities they were (μ,σ) 2.4 μm, 0.6; 2.5 μm, 0.6; 2.8 μm, 0.5; 3.5 μm, 2.0; 3.6 μm, 2.0; 3.7 μm, 2.0.

The number of flocs forming the cone increases and that causes the inclination shallowing (Fig. 2.7b). With very large floc sizes most of the flocs are dominated by hydrodynamic torques but because of extremely large sizes there is very little alignment thereby reducing the inclination shallowing (Fig. 2.7c).

We note that although the model replicates the broad character of the intensity variations it is on an average between 2-3 times less efficient than the observed data. The reason for such high DRM intensities in the experiments is not understood fully but we propose that this might be because of the way flocs are actually built. In the model we have assumed that maghemite particles are completely randomly oriented within the flocs. This might not be true and the maghemite particles could show some kind of alignment while being incorporated within the flocs. For example, if more than one maghemite particle attaches to a single clay particle, these would be randomly oriented in a plane and not on a sphere as envisaged in the model. Furthermore the clay particles to which the maghemite particles get attached would definitely show some alignment because of their plate-like structures. Modeled inclinations show the same trends as the data although they seem to underestimate the shallowing ($\sim 10^{\circ}$). The uniformly greater experimental inclination shallowing can be attributed to a flattening of the clay flakes upon deposition. In passing we note that any higher accuracy from a DRM model involving assumptions as made herein although possible is not desirable given the inherent deficiencies in the assumptions (e.g., flocs are not rigid ellipsoids as assumed here). Instead the model results should suffice to understand the relative importance of the processes involved in DRM acquisition and a starting point for more comprehensive models.

2.5 Discussion

An important question to ask is: "What is the likelihood of flocculation affecting the paleomagnetic record?" Clay particles in water have surface charges

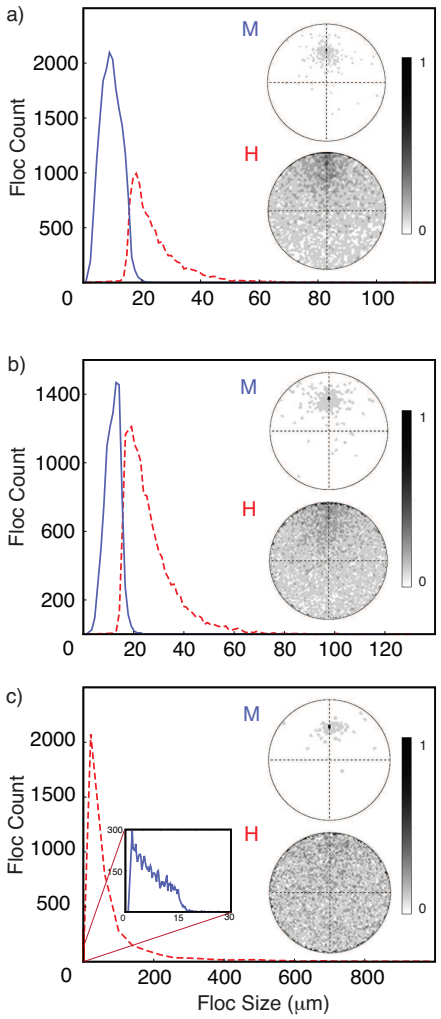


Figure 2.7: Partitioning of flocs into M (blue solid line) and H(red dotted line) with a field of 45 μT at 45° towards north for three different floc size distributions; a) $\mu = 2.4$ μm, σ =0.6, b) $\mu = 2.8$ μm, σ =0.5, c) $\mu = 3.5$ μm, σ =2.0. Semi-major axis of the floc is plotted on the abscissa. Insets show the corresponding equal area projections of floc moments for M (top) and H(bottom). No distinction is made between hemispheres and the plots are normalized by the maximum concentration. High (low) concentration is indicated by darker (lighter) colors and homogeneity (or lack of alignment) of moment direction is indicated by mid tones over the entire projection (as in c). Projections of M show small dark areas indicating that majority of moments are well aligned with the field direction.

on them which attract ions in solution. These build up a mixed double layer of cations-anions with their ratio changing away from the particle surface. Zeta-

potential is the electric potential in the double layer and is proportional to the width of the double layer or equivalently of the surface charge on the clay particles. With addition of more salt there is an abundance of ions and the surface charge gets neutralized over a shorter distance which lowers the double-layer width and the absolute value of the zeta potential (Winterwerp and Kesteren, 2004).

By measuring the zeta potential we can estimate the repulsive power of clay layers. As the zeta potential approaches zero, the van der Waals attractive forces become dominant and clay particles will tend to flocculate. The lowering of the zeta potential can be brought about by addition of an electrolyte or by changing the pH of the solution. It has been observed experimentally that zeta potential in kaolinite varies from -20 mV to -12 mV when the salt concentration varies from 10^{-4} M to 0.1 M salt concentration at constant pH (Vane and Zang, 1997). The dependence of zeta potential on pH is even stronger than on salinity and a charge reversal is observed at pH=2 for kaolinite. Bentonite on the other hand shows much less variability with both salinity and pH.

The dependence of zeta potential with salinity and pH has important consequences for the structure of clay flocs. When charges on the negative clay surfaces are not fully neutralized but are weak enough to let an adjacent oppositely charged clay particle come close enough so that van der Waals forces become dominant, clays usually form porous house-of-cards type structures. In such a structure positive edges attach themselves to negative faces. With further lowering of the zeta potential towards zero, the surface charge becomes so low that even similarly charged faces can come in close contact and form dense aggregates of clay flocs (e.g., (Olphen, 1977)). Environments having a high salinity gradient (viz., estuaries) have shown an increase in floc sizes with salinity (Allersma, 1980; van Leussen, 1999).

While sticking of particles due to reduction of surface potential is a likely mechanism for clay flocculation, binding of inorganic clays with adsorbed organic polymers (like polysaccharides) are equally important in nature. Polysaccharides

are non-ionic and are ubiquitous in the marine environment as they are produced by organisms like bacteria, algae, filter feeders, etc. They adsorb onto clay particles by strong bipolar forces which are much stronger than van der Waals forces. A long polymer string can attach itself to clay flakes at multiple locations and act as a bridge between such particles (Winterwerp and Kesteren, 2004; Hunter, 2001). Such union of inorganic and organic content of the sediment load gives rise to flocs which can be 10 to 100 times as strong as flocs made of purely inorganic material (Gregory, 1985). Therefore in the open ocean where salinity ranges are small, floc aggregation is likely to be a function of such particulate organic matter. Additionally, changes in sediment concentration and turbulence in the water column affect flocculation. Sediment concentration affects flocculation unidirectionally by promoting greater aggregation because of higher chance of mutual collisions (Dyer, 1989). Turbulence, on the other hand, affects flocculation in a contradictory manner. While turbulent motion promotes aggregation due to increased number of collisions, turbulent shear breaks down larger flocs into their constituent particles (van Leussen, 1997).

Therefore we can see that a number of mutually independent factors contribute to the distribution of floc sizes observed in nature and it is likely that these factors change considerably across the spectrum of fluvial environments (from glaciomarine lakes to open oceans) and geological time scales to give rise to considerably different floc size distributions. This in turn would play a role in the paleomagnetic recording process (Lu et al., 1990; Katari and Tauxe, 2000; Tauxe et al., 2006).

In order to assess the role of floc size variation on magnetic recording in sediments, we use our model to explore hypothetical scenarios. We simulated two regions each experiencing the same magnetic field variations. The two regions had different mean floc radii, one small (from 2.0 μm to 2.1 μm and σ =0.3) and one large (from 3.0 μm to 3.1μm and σ =1.3). Within each region we ran three simulations of magnetic recording by drawing populations of flocs whose mean floc

sizes were varied slightly and randomly through time (see mean floc size strips in Figs. 2.8a and b respectively).

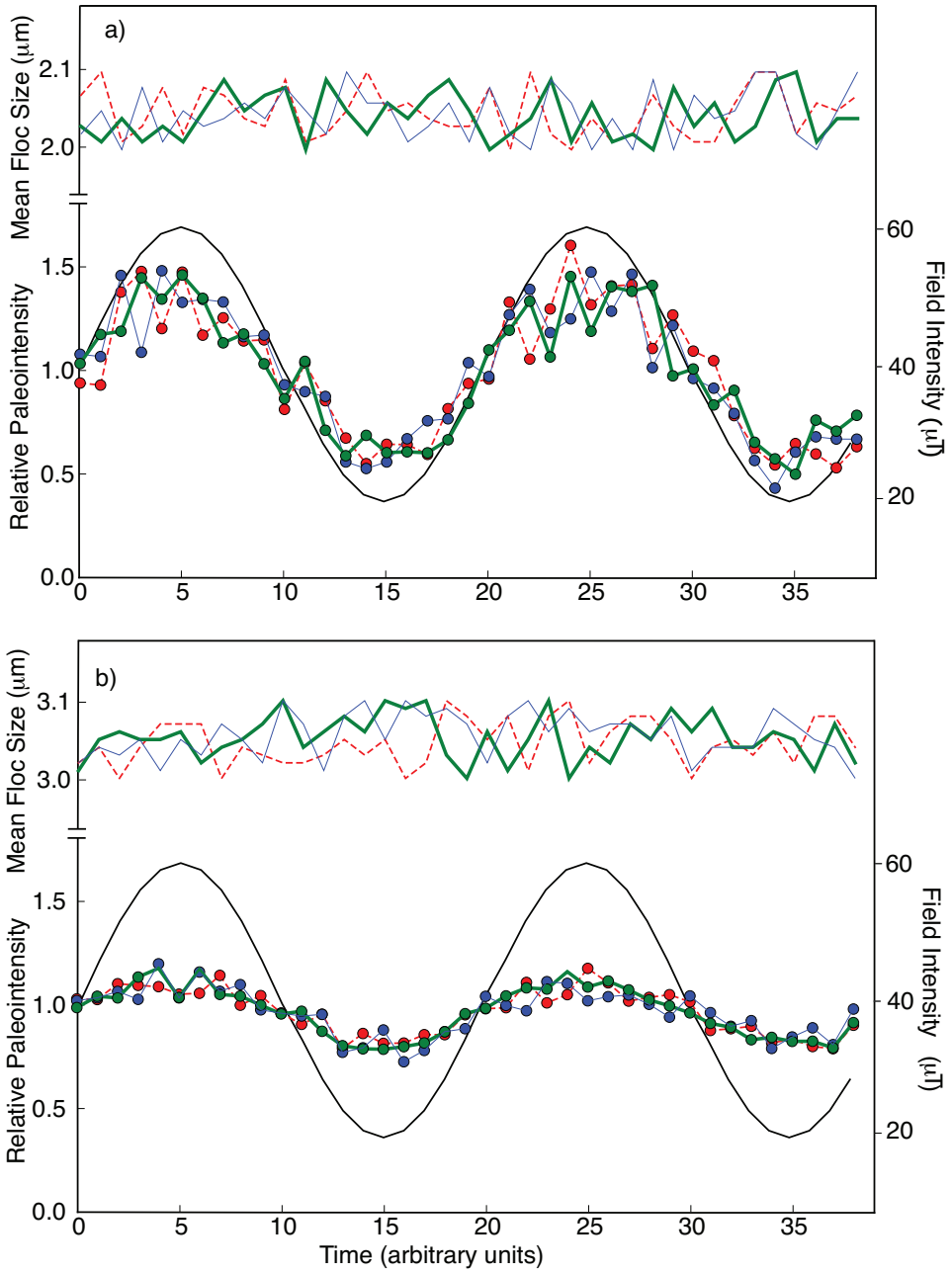


Figure 2.8: Effect of floc size variation and sinusoidal field intensity fluctuations on sediments. The field intensity (black) was varied between 20 μT and 60 μT. Relative paleointensities, normalized by mean values are shown in dotted red, thin blue and thick green lines for the corresponding floc sizes (length of long axis) at the top.

We imposed an input magnetic field which varied sinusoidally between 20 μT and 60 μT to simulate geomagnetic field variation (see smooth black line in Figs. 2.8a and b corresponding to "Field Intensity" on right of plots). The inclination was kept constant at 45°. All six records "observed" the same magnetic field, but because of slight differences in floc size distribution, the remanent vectors generated by the model were somewhat different.

The relative paleointensity (shown with circles and lines in Figs. 2.8a,b) generally followed the input field variation but was also sensitive to floc size variation. In both scenarios we found that the floc size distribution introduced substantial fluctuations in the relative paleointensity records. The first order amplitude of the record became attenuated with increasing floc size (compare Fig. 2.8a with Fig.. 2.8b) because larger flocs orient less efficiently with the field. The second order amplitude variations (the minor "wiggles") decrease substantially because with increasing standard deviation the distribution becomes more positively skewed. The positively skewed distribution makes the proportion of M/H less variable with increasing mean floc size.

The appearance of minor "wiggles" due to variation of floc sizes has a direct consequence for natural systems. Relative paleointensities from globally distributed sites have been successfully used to build a global stack which is thought to represent the geomagnetic field variation (e.g., (Guyodo and Valet, 1996, 1999)). But neighboring cores, which should have similar variations in the geomagnetic field have been shown to differ significantly (see Fig. 2.9). The simulations show that tiny fluctuations in floc size could be the source of such a discrepancy although the magnitude of this fluctuation would depend on actual floc size distribution. Furthermore, small floc size systems would be prone to greater fluctuations with changing floc size. This might also explain the large scatter associated with paleointensity records from freshwater lakes because they are expected to have smaller mean floc sizes (Constable, 1985).

An important aspect of sedimentary paleointensity studies is the assump-

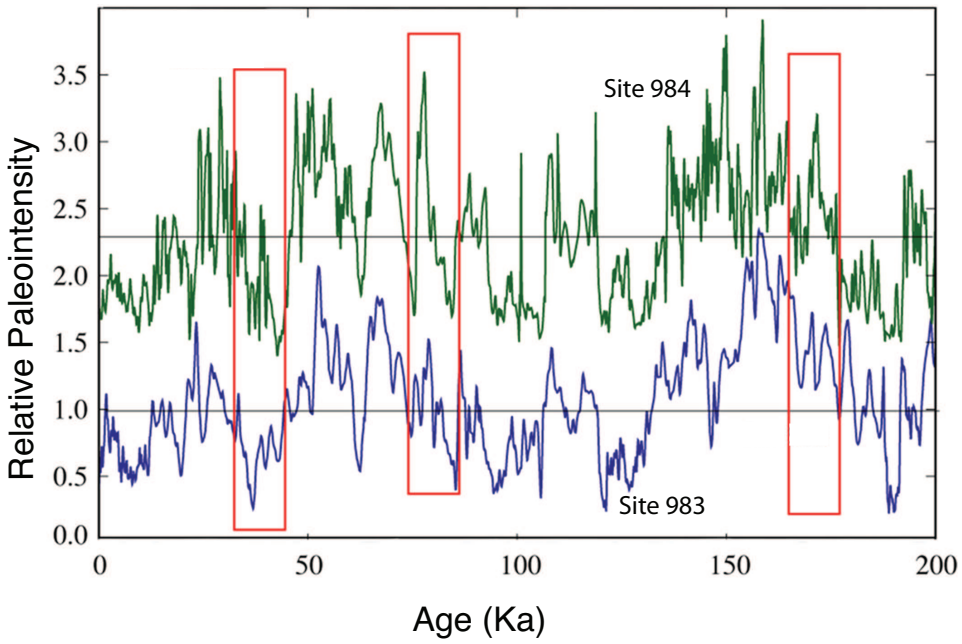


Figure 2.9: Relative paleointensity (ARM normalized) record from Site 983 and the adjacent Site 984. Red boxes highlight areas showing subtle difference in amplitude and trend of the normalized paleointensity. Data from Channell et al. (1997, 1998, 2004). Figure modified after Tauxe and Yamazaki (2007).

tion of linearity of the remanence with respect to the applied field (Kent, 1973). It is evident from the experiments as well as from the model that this cannot be true for all floc sizes. Tauxe et al. (2006) predicted a narrow range of floc sizes where the DRM response to the field behaves linearly. With our model we can explore the problem further by incorporating the possibility of inclination error into the model: "Are there distinct regimes where the field is linear?" " Are there regimes where we expect a low inclination error?"

In order to "map out" the floc distributions whose DRM acquisition was essentially linear with applied field versus those that behaved with a significantly non-linear response, we use the extra sum-of-squares F test with a critical ratio of 1 and a p value of 0.05. In our simulation, we draw lognormal populations of varying floc size and standard deviations. For each population we calculated the normalized field intensities at fields ranging from 0 to 100 μT at steps of 10 μT and

a constant inclination of 45°. The inclinations were calculated for a representative field of 40 μT.

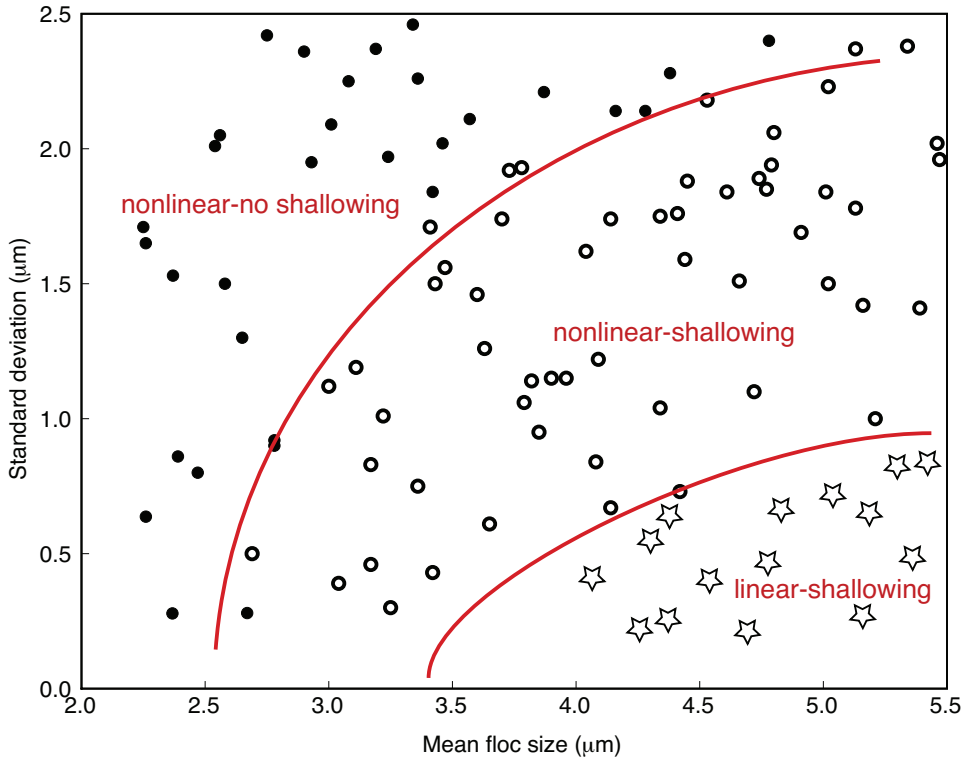


Figure 2.10: Regimes showing linear/non-linear behavior of DRM intensity acquisition and inclination shallowing. Each point represents a simulation with the given mean size and standard deviation. For each point the simulation was run in fields ranging from 0 to 100 μT at steps of 10 μT at 45° to decide whether DRM acquisition is increasing linearly with the applied field. Corresponding inclination shallowing at field strength of 40 μT was also calculated. Filled circles: non-linear DRM acquisition with $< 5°$ inclination shallowing; Open circles: non-linear DRM acquisition with $> 5°$ shallowing. Stars: Linear DRM acquisition with $> 5°$.

In general agreement with Tauxe et al. (2006), increasing mean floc sizes makes the DRM response more linear. At low mean floc sizes the flocs tend to have low inclination shallowing and DRM response is largely nonlinear (filled circles). With increasing floc sizes the inclination shallowing increases (open circles). A perfectly linear DRM acquisition with field is possible but with a high degree of inclination shallowing (stars). Increasing standard deviation pushes the linear regimes to larger mean floc sizes. At very large standard deviation the DRM

response remains largely non-linear Fig. 2.10.

At very low salinities we expect to have smaller flocs. Freshwater lakes have salinities typically less than 5 ppt and can be expected to form small flocs. For such flocs the DRM acquisition curve is likely to be non-linear for a large range of standard deviation. It is thus unlikely that lake sediments would give a consistent record of past field variations. Flocculation processes in the oceans are more dominated by the organic content which is capable of producing very large flocs. Depending on the nature of the floc size distribution the sediments might record either no inclination shallowing or linear DRM acquisition Fig. 2.10. However, it is unlikely that sediments would be able to capture true field intensities and directions simultaneously.

Both in the experiments and the model, DRM efficiency decreases dramatically as the salinity increases (Figs. 2.2b and 2.6b). This is similar to what we observe in natural sediments and is a direct consequence of flocculation; with higher salinities the flocs grow bigger and a higher fraction is dominated by hydrodynamic torques which do not align with the field direction, hence contribute little towards the net DRM. Even the fraction which is dominated by magnetic torques do not orient very well with the field direction. The resultant field intensity is thus very low. Based on a similar reasoning, we predict that sIRM normalized paleointensity records from lakes should have a higher average efficiency than those from proximal marine records because sIRM overcompensates for the bulk amount of magnetic material present for larger mean floc sizes. This would provide an independent test for the model.

We come now to another important consideration – the choice of an appropriate normalizer (see, e.g., (Tauxe, 1993)). An ideal normalizer should account for the total volume of magnetic minerals contributing to the remanence and its efficiency. From our model we see that the total volume of magnetic particles reflected in bulk magnetic parameters like sIRM is but part of the answer. The distribution of floc sizes controls efficiency and is equally or perhaps even more

important than bulk content of magnetic particles. For instance, if flocculation partitions higher concentrations of magnetite particles into bigger flocs then the horizontal component is likely to increase, giving rise to greater inclination shallowing. The contribution towards the net magnetization is much less because of their inability to fully align with the field. So, if mean floc sizes were to increase over geological time scales in a particular sedimentary basin, the normalized remanence might decrease in spite of no change in the field intensity or the magnetic content of the sediments.

2.6 Conclusions

A basic premise of our experimental setup was to control flocculation by varying salinity. Salinity variations are most likely to be important in freshwater lakes where a minor change in salinity could affect flocculation dynamics. Seawater salinity is largely constant (35 ppt) and salt concentration is unlikely to play a dominant role in the flocculation processes. More important processes which could affect flocculation in the open ocean include microbial glue coating inorganic particles, clay/carbonate ratio and bottom water turbulence. The conclusions of this study however, are independent of how flocculation takes place. Irrespective of how the flocs form, this study shows that the absolute size distribution of the flocs play an important role in DRM acquisition.

Our simple numerical model serves to capture the major trends in the experimental data but is not meant to be a comprehensive and/or predictive model for DRM acquisition. Instead, this model should be used as a starting point for more complicated models involving precise trajectories of flocs and more realistic redeposition experiment using natural sediments. In spite of the obvious disadvantages in constructing a realistic DRM model the current study shows that hydrodynamic torques could be an important factor in DRM acquisition and outlines the following caveats:

1. Flocculation can explain the full DRM vector obtained from laboratory redeposition experiments.

2. Minute variations in flocculation dynamics may explain the differences observed in paleointensity records from nearby cores.

3. Paleointensity estimates from some glacial or freshwater lakes which show very little flocculation can be difficult because the smaller mean floc sizes could lead to non-linear acquisition of remanence. On the brighter side, these sediments can be ideal recorders for paleosecular variation studies.

4. Marine sediments having large mean floc sizes and standard deviations; these could be suitable for paleointensity or paleosecular variation studies, but a particular region may not be suitable for both. If proper techniques for estimating past floc size distributions become available in the future we might be able to predict the suitability of sediment cores for a particular study.

5. Irrespective of how the magnetic fraction partitions with increasing floc sizes it is important to recognize that not all magnetic grains contribute equally to the remanence. Magnetic grains in large flocs are practically neutral to the ambient field. Therefore any bulk parameter aimed at normalizing the data is susceptible to error. Depending on the variability of the initial depositional environment this could pose a challenge for interpretation of relative paleointensity records.

2.7 Acknowledgement

We are grateful to ACS Petroleum Research Fund for supporting the research. We would like to thank Brooks Ellwood for facilitating replacement of the SQUID electronics package for our vertical access magnetometer, without which this project could not have been completed. We would also like to thank David

Heslop, Gustaf Arrhenius, Jason Steindorf and Roi Granot who helped in various stages of the project.

Chapter 2, in full, is a reprint of the material as it appears in Mitra, R. and Tauxe, L. (2009), Full vector model for magnetization in sediments, Earth and Planetary Science Letters. The dissertation author was the primary investigator and author of this paper.

Bibliography

E Allersma. Mud in estuaries and along coasts. In *International Symposium of River Sedimentation*, pages 663–685 and 1285–1289, Beijing, 1980.

G. L. Anson and K. P. Kodama. Compaction-induced inclination shallowing of the post-depositional remanent magnetization in a synthetic sediment. *Geophs. J. Roy. Astron. Soc.*, 88(3):673–692, 1987.

P. Arason and S. Levi. Models of inclination shallowing during sediment compaction. *J. Geophys. Res.*, 95(B4):4481–4499, 1990.

A. Belmonte, H. Eisenberg, and E. Moses. From flutter to tumble: Inertial drag and froude similarity in falling paper. *Phys. Rev. Lett.*, 81(2):345–348, 1998.

R. A. Blow and N. Hamilton. Effect of compaction on acquisition of a detrital remanent magnetization in fine-grained sediments. *Geophs. J. Roy. Astron. Soc.*, 52(1):13–23, 1978.

J. E. T. Channell, J. H. Curtis, and B. P. Flower. The Matuyama-Brunhes boundary interval (500-900 ka) in North Atlantic drift sediments. *Geophys. J. Int.*, 158(2):489–505, 2004.

J. E. T. Channell, D. A. Hodell, and B. Lehman. Relative geomagnetic paleointensity and $\delta^{18}O$ at ODP site 983 (Gardar Drift, North Atlantic) since 350 ka. *Earth Planet. Sci. Lett.*, 153(1-2):103–118, 1997.

J. E. T. Channell, D. A. Hodell, J. McManus, and B. Lehman. Orbital modulation of the Earth's magnetic field intensity. *Nature*, 394(6692):464–468, 1998.

C. G. Constable. Eastern Australian geomagnetic-field intensity over the past 14000 yr. *Geophs. J. Roy. Astron. Soc.*, 81(1):121–130, 1985.

K. R. Dyer. Sediment Processes in Estuaries - Future-Research Requirements. *J. Geophys. Res.*, 94(C10):14327–14339, 1989.

S. B. Field, M. Klaus, M. G. Moore, and F. Nori. Chaotic dynamics of falling disks. *Nature*, 388(6639):252–254, 1997.

G. P. Galdi and A. Vaidya. Translational steady fall of symmetric bodies in a Navier-Stokes liquid, with application to particle sedimentation. *J. Math. Fluid Mech.*, 3:183–211, 2001.

R. J. Gibbs. Estuarine Flocs - Their Size, Settling Velocity and Density. *J. Geophys. Res.*, 90(Nc2):3249–3251, 1985.

J. Gregory. Flocculation, Sedimentation and Consolidation. Engineering Publication Services, University of Florida, 1985.

D. H. Griffiths, R. F. King, A. I. Rees, and A. E. Wright. The remanent magnetism of some recent varved sediments. *Proc. R. Soc. Lond., A Math. Phys. Sci.*, 256 (1286):359–383, 1960.

Y. Guyodo and J. P. Valet. Relative variations in geomagnetic intensity from sedimentary records: The past 200,000 years. *Earth Planet. Sci. Lett.*, 143(1-4): 23–36, 1996.

Y. Guyodo and J. P. Valet. Global changes in intensity of the Earth's magnetic field during the past 800 kyr. *Nature*, 399(6733):249–252, 1999.

D. Heslop. Are hydrodynamic shape effects important when modelling the formation of depositional remanent magnetization ? *Geophys. J. Int.*, 171(3): 1029–1035, 2007.

R.J. Hunter. *Foundation of Colloid Science*. Oxford University Press, 2nd edition, 2001. p. 806.

J. Jezek and S. A. Gilder. Competition of magnetic and hydrodynamic forces on ellipsoidal particles under shear: Influence of the Earth's magnetic field on particle alignment in viscous media. *J. Geophys. Res.*, 111(B12), 2006.

E.A. Johnson, T. Murphy, and O.W. Torreson. Pre-history of the Earth's magnetic field. *Terr. Magn. Atmos. Electr.*, 53:349–372, 1948.

K. Katari and J. Bloxham. Effects of sediment aggregate size on DRM intensity: a new theory. *Earth Planet. Sci. Lett.*, 186(1):113–122, 2001.

K. Katari and L. Tauxe. Effects of pH and salinity on the intensity of magnetization in redeposited sediments. *Earth Planet. Sci. Lett.*, 181(4):489–496, 2000.

D. V. Kent. Paleomagnetism of some Neogene sedimentary-rocks on Oga-Peninsula, Japan. *J. Geomagn. Geoelectr.*, 25(1):87–103, 1973.

R.F. King. The remanent magnetism of artificially deposited sediments. *Mon. Not. R. Astr. Soc. Geophys.*, Supp. 7(115), 1955.

R.B. Krone. The significance of aggregate properties to transport processes: Proceedings of a Workshop on Cohesive Sediment Dynamics with Special Reference to Physical Processes in Estuaries, Tampa, Florida. Technical report, 1986.

E. Kuusela. *Steady-state sedimentation of non-brownian particles with finite Reynolds numbers*. PhD thesis, Helsinki University of Technology, 2005.

R. Lu, S. K. Banerjee, and J. Marvin. Effects of clay mineralogy and the electrical-conductivity of water on the acquisition of depositional remanent magnetization in sediments. *J. Geophys. Res.*, 95(B4):4531–4538, 1990.

T. Nagata. *Rock Magnetism*. Mazuren Co, Tokyo, 1961.

Hendrick van Olphen. *An introduction to clay colloid chemistry for clay technologists, geologists, and soil scientists*. Interscience Publishers, New York, 1977.

F. Perrin. The brownien movement of an ellipsoide. - the dielectric dispersion of ellipsoidal molecules. *J. Phys. Radium*, 5:497–511, 1934.

Lord Rayleigh. On the problem of random vibrations, and of random flights in one, two, or three dimensions. *Phil. Mag.*, 37(220):321–347, 1919.

V Scherbakov and V. Scherbakova. On the theory of depositional remanent magnetization in sedimentary rocks. *Geophys. Surv.*, 5:369–380, 1983.

G. D. Scott and D. M. Kilgour. Density of random close packing of spheres. *J. Phys. D Appl. Phys.*, 2(6):863–867, 1969.

V. P. Shcherbakov and N. K. Sycheva. Flocculation mechanism of the acquisition of remanent magnetization by sedimentary rocks. *Izv. Phys. Solid Earth*, 44(10): 804–815, 2008.

L. Tauxe. Sedimentary records of relative paleointensity of the geomagnetic-field - theory and practice. *Rev. Geophys*, 31(3):319–354, 1993.

L. Tauxe, J. L. Steindorf, and A. Harris. Depositional remanent magnetization: Toward an improved theoretical and experimental foundation. *Earth Planet. Sci. Lett.*, 244(3-4):515–529, 2006.

L. Tauxe and T. Yamazaki. Paleointensities. In G. Schubert, editor, *Geomagnetism*, volume 5 of *Treatise on Geophysics*, pages 509–564. Oxford: Elsevier Ltd., 2007.

W. van Leussen. *The Kolmogorov microscale as a limiting value for the floc sizes of suspended fine-grained sediments in estuaries*. Cohesive Sediments. Wiley, Chichester, 1997.

W. van Leussen. The variability of settling velocities of suspended fine-grained sediment in the Ems estuary. *J. Sea Res.*, 41(1-2):109–118, 1999.

M. J. van Vreumingen. The influence of salinity and flocculation upon the acquisition of remanent magnetization in some artificial sediments. *Geophys. J. Int.*, 114(3):607–614, 1993a.

M. J. van Vreumingen. The magnetization intensity of some artificial suspensions while flocculating in a magnetic-field. *Geophys. J. Int.*, 114(3):601–606, 1993b.

L. M. Vane and G. M. Zang. Effect of aqueous phase properties on clay particle zeta potential and electro-osmotic permeability: Implications for electro-kinetic soil remediation processes. *J. Hazard. Mater.*, 55(1-3):1–22, 1997.

J. C. Winterwerp and W.G. M. v. Kesteren. volume 56 of *Developments in Sedimentology*. Elsevier, Amsterdam ; Boston, 2004.

Chapter 3

Detecting uniaxial single domain grains with a modified IRM technique

Mid-ocean ridge basalt (MORB) specimens have often been found to have high ratios of saturation remanence to saturation magnetization (M_{rs}/M_s). This has been attributed to either dominant cubic anisotropy (Gee and Kent, 1995) or to insufficient saturating field leading to overestimation of M_{rs}/M_s of a dominantly uniaxial single domain (USD) assemblage (Fabian, 2006). To resolve this debate, we develop an independent technique to detect USD assemblages. The experimental protocol involves subjecting the specimen to bidirectional impulse fields at each step. The experiment is similar to the conventional IRM acquisition experiment but the field is applied twice, in antiparallel directions. We define a new parameter, IRAT, as the ratio of the remanences at each field step and show it to have characteristic behavior for the two assemblages; IRAT ~ 1 at all field steps for USD and < 1 with a strong field dependence for multi-axial single domain (MSD) grains. We verified the theoretical predictions experimentally with representative USD and MSD specimens. Experiments with MORBs gave low IRATs

for specimens having high M_{rs}/M_s. This is consistent with the hypothesis of Gee and Kent (1995). While undersaturation of the specimens as proposed by Fabian (2006) could indeed be a contributing factor for the high M_{rs}/M_s ratios, this study shows that the nature of anisotropy in those specimens cannot be USD.

3.1 Introduction

The ratio of saturation remanence to saturation magnetization (M_{rs}/M_s) is commonly used to identify uniaxial single domain (USD) particles although the interpretation is not always straightforward. For example, the M_{rs}/M_s for randomly distributed USD grains has a theoretical upper limit of 0.5 (Stoner and Wohlfarth, 1948), but mixing of USD grains with finer superparamagnetic (SP) or coarser multidomain (MD) grains inevitably reduces this ratio (Day et al., 1977). Day et al. (1978) and more recently Gee and Kent (1995), noted exceptionally high M_{rs}/M_s ratios (> 0.5 and as high as 0.67) in some mid-ocean ridge basalts (MORBs). Gee and Kent (1995) attributed this to the dominance of grains with cubic anisotropy (as opposed to uniaxial anisotropy) because the theoretical limit for SD grains with cubic anisotropy is 0.83 ($K_1 > 0$) or 0.87 ($K_1 < 0$), where K_1 is the magnetocrystalline anisotropy (Joffe and Heuberger, 1974). Fabian (2006) offered an alternative explanation, arguing that the samples were essentially uniaxial but not saturated leading to an underestimation of M_s, making the M_{rs}/M_s ratio greater than 0.5. Using a saturating field as high as 7 T, he showed for a single specimen that M_{rs}/M_s could be brought down from 0.5 (measured at 1 T) to 0.39, thereby obviating the need for cubic anisotropy. While lowering of M_{rs}/M_s with increasing field would be an indication of sample undersaturation, the evidence it presents for uniaxial anisotropy is inconclusive. Gee and Kent (1995) measured hysteresis parameters of one specimen at a 5T field. The resulting M_{rs}/M_s ratio dropped from 0.63 (measured at 1T) to 0.49. However, the presence of abundant observable multidomain (MD) grains in this specimen suggests that a ratio of 0.49

is the result of mixing of a population with ratios much higher than 0.5 (hence not USD) with grains having much lower ratios (the MD grains).

The assumption of uniaxial anisotropy of titanomagnetites in MORBs stems from the low K_1 compared to magnetoelastic anisotropy (K_λ). In titanomagnetites with moderate to high Ti content, equant grains lacking significant shape anisotropy have been shown to be dominated by stress anisotropy which is assumed to be uniaxial (Appel and Soffel, 1984; Appel, 1987). Sahu and Moskowitz (1995) showed that $K_\lambda > K_1$ for most temperatures in TM60, a titanomagnetite with 60% mole fraction of ulvöspinel, an important constituent of MORBs. Although stress control of the dominant anisotropy is largely agreed upon, the assumption of its uniaxial nature is more of a mathematical simplification than an empirical observation (Dunlop and Özdemir (1997), p44). In light of such findings, an independent test for detecting USD grains could prove to be useful. In this paper we propose such a test.

The magnetization acquired by a specimen at room temperature through the application of an impulse field is known as isothermal remanent magnetization (IRM). In SD grains, there are a finite number of directions in which the magnetic moment tends to reside in the absence of an external field. Because moments in these directions have the minimum magnetic energy, they are known as 'easy directions'. With the application of a sufficient field, the moment can attain enough energy to cross the energy barrier between adjacent easy directions. In such a situation the moment jumps, suddenly and irreversibly, from one easy direction to another, closer to the direction of the field. In SD grains, the field strength required to flip the moments is a function of the angular relation between the field and the moment. Therefore the bulk coercivity of an assemblage could change depending on the angular relationship between the field, the available easy directions and the distribution of magnetic moments.

An IRM aquisition experiment generally involves subjecting a specimen to a stepwise increasing field. Here we explore a double IRM experiment (DIRM) in

which each field step comprises applying the same field strength twice, but, in anti-parallel directions. The remanence is measured after *each* field application. We define the IRM ratio (IRAT) as the ratio of the absolute remanences, second over the first, at every step. IRAT has distinctive signatures for USD grains as opposed to SD grains showing multiaxial anisotropy (MSD) and is useful in addressing the controversy regarding the cubic anisotropy (a form of MSD) of some MORBs as proposed by Gee and Kent (1995) and disputed by Fabian (2006).

USD grains have by definition two easy directions in which the moment has minimum energy in the absence of an applied field. The first application of an instantaneous field in a dominantly USD assemblage will flip moments in some grains towards the easy direction closer to the field. When the field is applied in the reverse direction the angular relationships between the field and the moments remain unchanged because the inherent uniaxial symmetry of the grains is symmetric with respect to a bidirectional field. For example, if a grain moment makes an angle of 120° with the field and the field is sufficient to overcome the energy barrier, the moment will flip to the only other easy direction, at an angle of 60° with the field. Now when the field direction is reversed the moment again makes an angle of 120° with the field, hence a second field of the same magnitude is sufficient to flip the moment back. This ensures that the bulk coercivity does not change in USD grains under a bidirectional application of a field and consequently IRAT remains very close to one.

In the case of a dominantly MSD assemblage, the first application of the field would flip moments in some grains into easy directions closer to the field. But in this case, when the field is reversed, the coercivity changes because the easy directions do not necessarily maintain the same symmetry with the field. For example, let us consider a grain of hematite showing six fold anisotropy in the basal plane. There are six easy directions, each 60° apart. The first application of a sufficiently high field acting in the basal plane of a grain would cause a moment at an angle of 90° with the field to overcome the necessary energy barrier and flip

to an easy direction closer to the field. This direction would be at an angle of 30° with the field. Now when the field direction is reversed, the new angle between the field and the moment would be 150° and the field strength could be inadequate to flip back the moment.

In essence, any departure from uniaxial symmetry is likely to show a change in coercivity with changing field directions. In fact it will be shown in the following sections that this anisotropy is enough to exhibit substantially *higher* coercivities during the second application of the field. As a result IRAT will be always less than one in MSD grains for fields less than saturation.

Wohlfarth (1958) was the first to derive a simple relationship between the forward and backward remanences and suggested that the lack of reciprocity of the two could be due to non-uniaxial anisotropy, particle interaction or domain state. He did not comment on the exact mechanism of how these apparently dissimilar properties would affect the result or the nature of their influence. Although non-uniaxiality of anisotropy had been cited as one of the reasons for the observed phenomenon, the other reasons seem to have been invoked more often to explain similar phenomenon. Tauxe et al. (1990) in an experiment similar to DIRM, observed a 'sawtooth' in a sample containing specular hematite and ascribed that to relict MD signature in SD grains. A similar propensity is sometimes observed in the interpretation of Henkel plots, where IRM acquisition and DC demagnetization are plotted against each other (Henkel, 1964). Instead of alternating the field direction at each step as in the DIRM experiment, this entails exposure of the sample to succesively higher fields in one direction and subsequent demagnetization by applying increasingly negative fields in the opposite. This type of plot has long been used to analyze the strength of particle interaction. Much like an Arai plot for a paleointensity experiment, where sagging of the curve is often ascribed to MD grains, non-linearity in the Henkel plots are often used as an indicator of interacting SD grains. More recently though, attention has been drawn to the fact that multiaxial anisotropy can also cause Henkel plots to be curved, with

the remanence during the IRM acquisition leg being greater than during the DC demagnetization leg; a result in keeping with our tenet (Geshev and Mikhov, 1992; Garcia-Otero et al., 2000). Garcia-Otero et al. (2000) further showed that this curvature would be in a direction opposite to that observed due to particle interaction and warned that the combined effect of the two could yield a straight line in a Henkel plot leading to erroneous interpretation.

In this paper we will use numerical models and experimental evidence to demonstrate the difference in response of USD and MSD grains to DIRM acqusition. We will be using USD magnetite and MSD hematite to be representative of the two categories. We will then use DIRM acquisition curves to address the issue of the dominant anisotropy in MORBs. We will provide strong evidence for the presence of multiaxial anisotropy in the high M_{rs}/M_s MORB samples.

3.2 Theory

3.2.1 Energy Calculations

The total energy of an SD grain, assuming only coherent rotations of moments, is the sum of the anisotropy energy (E_{anis}) and the magnetostatic energy (E_{ms}) due to the external field. An SD grain showing n-fold anisotropy has n easy directions where the total free energy density E_{tot} (energy per unit volume) is minimum. E_{tot} is given by the sum of the anisotropy energy, E_{anis} and the magnetostatic energy, E_{ms};

$$E_{tot} = E_{anis} + E_{ms} = K \sin^2(\frac{n}{2}\theta) - M_s B_{eff} \cos(\theta - \phi), \tag{3.1}$$

where K is the anisotropy constant (e.g., K_1, K_u or K_λ), M_s is the saturation magnetization, B_{eff} is the effective field, θ the angle between the moment and the easy direction and ϕ is the angle between the easy direction and B (Dunlop, 1971).

For any grain in the absence of a field the total energy per unit volume is

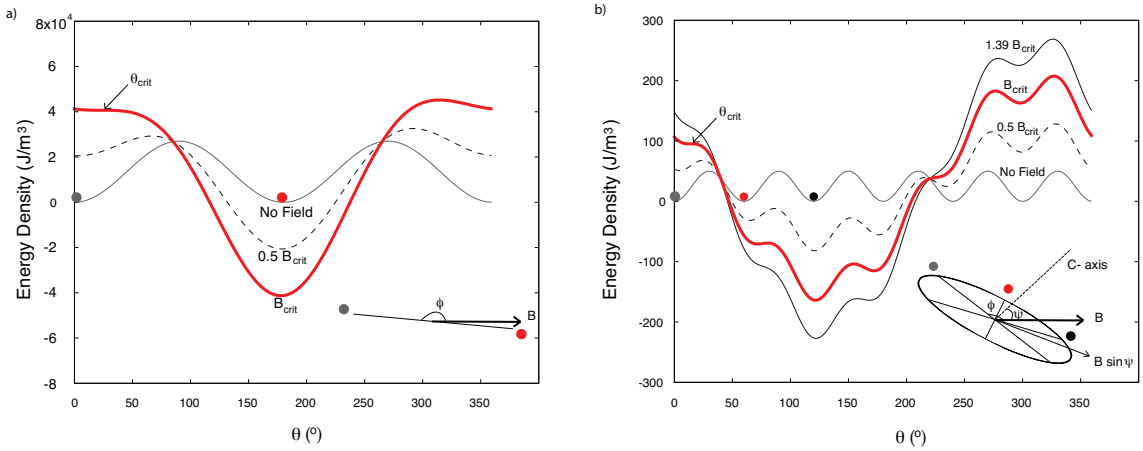


Figure 3.1: Energy density for $\theta = [0, 360]$ in a) magnetite grains with $\phi = 175°$ and b) hematite grains with $\phi = 130°$. Insets show the corresponding grains with easy directions (thin line) and field direction (thick). In b) the C-axis is orthogonal to the plane containing easy directions. a) In absence of a field the energy profile (grey) shows two energy minima (easy directions). For a field $0.5B_{crit}$ the profile changes (dashed line) but the moment (grey dot) cannot flip to the other easy direction. Only when $B_{eff} \geq B_{crit}$ can the moment overcome the energy barrier and flip to a position 180° apart (red dot). b) Without any field, the energy profile (grey) shows six energy minima (easy directions). As in the USD case, at any field less than B_{crit} the energy profile changes but the moment (grey dot) cannot overcome the energy barrier. At B_{crit} the moment flips instantaneously to an adjacent easy axis 60° apart (red dot). If the field was even higher ($1.39B_{crit}$ for this particular grain) then the moment would have had its least energy configuration at an easy axis 120° (black dot) apart. Calculations are based on values used in text. See Fig. 2 in Dunlop (1971) for additional graphs showing dependence of B_{crit} with ϕ for the two cases.

equal to the anisotropy energy. With the application of an external field the contribution of the magnetostatic energy rises. Using Eqn. 3.1 we can plot the energy profiles of a single grain of magnetite, having $n = 2$ easy directions (uniaxial), and a hematite grain, having $n = 6$ easy directions in the basal plane (multiaxial) (Figs. 3.1a and b respectively). It is to be noted that hematite shows a dominant six-fold basal plane anisotropy only between the Morin transition ($\sim$ -10°C) and the Néel temperature ($\sim$ 675 °C) (Besser et al., 1967). Below the Morin transition the moments are not constrained to lie in the basal plane, showing a pronounced uniaxiality along the c-axis instead.

In Fig. 3.1 the energy minima in the solid grey curves (no field) represent the easy directions. As we apply a field, the energy density curves change. A small applied field moves the curves to the dashed lines but it is not large enough to remove barriers entirely from between the easy directions and the moment may stay trapped in the local energy minimum (grey dot). At a critical field value, B_{crit}, however, the curve changes to the heavy (red) line and the energy barrier is removed; the moment is able to flip to the adjacent energy minimum and remains there when the field is switched off (red dot on grey lines). The value of θ at B_{crit} is the critical angle, θ_{crit}. It is worth mentioning at this stage that the moment flips instantaneously from one direction to the other, hence θ_{crit} is more of a mathematical construct than a physical quantity . Also it is noteworthy that B_{eff} is the effective field. So for uniaxial magnetite, when the moment is free to rotate in any direction under the influence of the field, B_{eff} equals the applied field (B). But for a grain where the moments are constrained to lie in a particular plane, as in hematite, only the basal plane component i.e., $B\sin\psi$ makes up B_{eff} (Fig. 3.1 insets).

The condition for flipping is to remove the energy barrier (e.g., the humps between the grey and red dots in Fig. 3.1). This can be mathematically expressed in terms of the derivatives of the energy density curves when the first and second derivatives are both zero, i.e., $dE/d\theta = d^2E/d\theta^2 = 0$. Solving for θ and B_{crit}, we get:

$$\tan(n\theta_{crit}) = n\tan(\theta_{crit} - \phi), \tag{3.2}$$

and

$$B_{crit} = -\frac{nK}{2M}\frac{\sin(n\theta_{crit})}{\sin(\theta_{crit} - \phi)}. \tag{3.3}$$

The flipping condition is met when $B_{eff} \geq B_{crit}$.

3.2.2 Numerical Simulation

To simulate DIRM as a function of applied field, we start with an assemblage of magnetic grains with randomly oriented moment directions along randomly oriented easy axes. A large number of grains in the simulation ensures a low initial remanence reflecting a completely demagnetized state. We used 20,000 grains for our simulations which gave an initial remanence of $\sim 1\%$ of saturation remanence. Increasing the number of grains gives even lower initial remanence but also increases the total runtime without significantly affecting the result. This is also more representative of our experimental conditions where we use the natural remanence (NRM) as the initial state. This is a fair approximation as long as the NRM is significantly lower than the IRM. We will discuss this in greater detail in Section 4.

We assumed shape dominated uniaxial anisotropy in magnetite and used $M_s = 480$ KAm^{-1} for simulating a USD assemblage (Tauxe (2010), p68). A uniform prolate grain shape with axial ratio, $c/a = 1.9$ translates to a uniaxial anisotropy constant K_u of 27 KJm^{-3}. For simulating MSD grains we used hematite which has a six fold basal plane anisotropy. A range from 10-100 Jm^{-3} is suggested for magnetocrystalline anisotropy in hematite (Dunlop and Özdemir, 1997). For the purpose of this simulation we chose a value of 50 Jm^{-3}, noting that the results do not depend critically on the precise value. We used $M_s = 2.1$ KAm^{-1} for hematite (Tauxe, 2010). An iterative routine of increasing field steps, with each field step comprising a $+B$ and $-B$ simulated DIRM acquisition. For each grain, the critical field, B_{crit}, for the moment to jump to the adjacent easy direction closer to the applied field B was calculated using Eqns. 3.2 and 3.3. For those grains in which B_{crit} was found to be less than B_{eff} the moments were transferred to the easy directions closer to the field direction. For USD grains this is a single step process for each B because the moments can reside only in two directions. For MSD grains this can be a multi step process depending on the strength of the

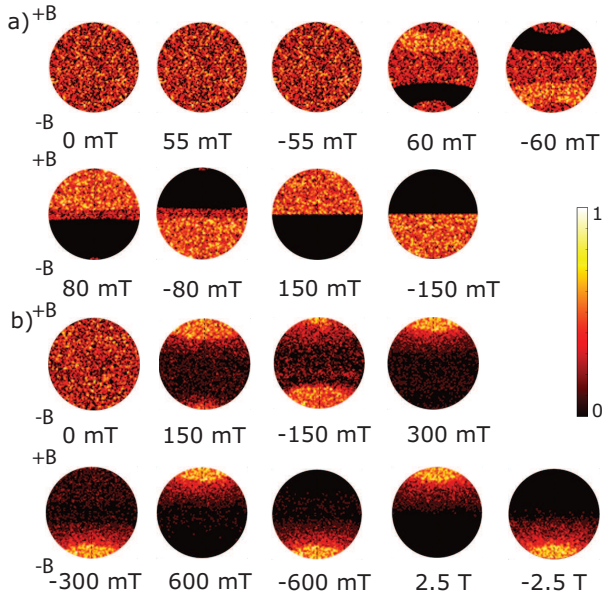


Figure 3.2: Kamb plots showing density of moments in response to different field steps for a) USD magnetite and b) MSD hematite. Only absolute value of inclinations were considered and the density was normalized by the maximum density of moments for that particular field step. Therefore similar colors from different plots do not signify similar density.

applied field (Fig. 3.1b). The simulations yielded Mrs/Ms values of 0.5 and 0.94 for the uniaxial and triaxial cases respectively. For the latter, the moment was constrained to lie in the basal plane.

In USD assemblages, reversing the field direction flips the moments from one direction to the opposite. As a result there is no difference in net magnetization of the bulk distribution of moments at any B or $-B$ (Fig. 3.2a). At $\pm$60 mT all moments having the lowest coercivity flip towards the field. Since we have assumed that all grains have the same size and shape, coercivity is strictly a function of ϕ. Hence, the moments which are flipped to the antipodal easy directions at any particular field all lie on a cone around the field direction. This is manifested in the form of small circles in Fig. 3.2. The number of such circles increases (note the expanding dark patch in Fig. 3.2a from 60 to 150 mT) with increasing field until saturation at which all the moments are confined to one hemisphere. At

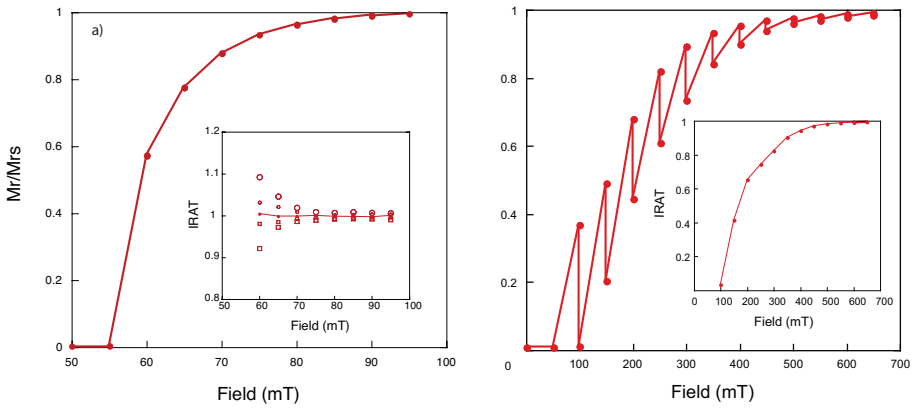


Figure 3.3: DIRM acquisition curves for a) USD magnetite. Inset shows IRAT for the corresponding field steps (solid line). Open circles/squares show IRAT for a 2%(small symbols), 5%(big symbols) NRM at 0°/180° to the initial field direction and b) MSD hematite. Inset shows IRAT for the corresponding field steps. Remanence (Mr) is normalized by saturation remanence (Mrs).

each field step the distribution of moments is symmetric with respect to the field direction (e.g., at 60 mT and -60 mT), thereby, giving the same net remanence. As a result, the remanence acquisition curve is smooth and IRAT is ~ 1 at all field steps (Fig. 3.3a). This is strictly true only for a completely demagnetized initial state (solid circles in inset to Fig. 3.3a). For a simulated sample with an initial remanence of $\sim 2\%$ of the saturation remanence (either parallel to or antiparallel to the first field direction), the ratio changes to a value more (small open circles in inset to Fig. 3.3a) or less than unity (small open squares in inset to Fig. 3.3a) approaching unity as the field increases from 60 mT to 100 mT. The ratio is more or less than unity when the natural remanence is parallel or antiparallel to the direction of the first applied field. If the NRM is $\sim 5\%$ of saturation remanence IRAT shows at most $\sim 10\%$ departure from unity (larger symbols in the inset to Fig. 3.3a). As NRM of natural samples is usually weak and is unlikely to be 5 % of saturation remanence, IRAT is expected to be within 10% of unity in natural USD assemblages.

In MSD assemblages, coercivity changes as a function of the history of fields applied. This effect is especially marked at low fields. Fig. 3.2b shows that

at 150 mT, the concentration of moments is near the field azimuth in the +B hemisphere (direction of the first field application and top of diagrams). When the field is reversed there are distinct concentrations in both the hemispheres. This is because at -150 mT, the field is not strong enough to sweep away the moments which are already at a high obtuse angle, ϕ, to the -150 mT field direction owing to prior application of the +150 mT field. Therefore a fraction of the moments from the 150 mT step do not flip and effectively cancel out the contribution from the concentration of moments in the -B hemisphere after the -150 mT step. This gives rise to a pronounced sawtooth pattern in the DIRM acquisition plot (Fig. 3.3b). IRAT increases from 0.06 at 100 mT to 0.99 at 600 mT(Fig. 3.3b inset). At higher fields the field strength compensates partially for this effect. Thus the moment distribution at $\pm$ 600 mT and higher fields are almost mirror images of each other while those at $\pm$150 mT are markedly different (Fig. 3.2b).

These results have a bearing on alternating-field (AF) demagnetization. In AF demagnetization a specimen is exposed to an alternating field which has a sinusoidal waveform. The field decreases linearly with time and traps comparable number of moments along opposite directions. This gives rise to a net zero moment. Although our experiment is very different from an AF demagnetization, both are affected by the coercivity spectrum in an analogous manner. The linearly reducing alternating field can trap disproportionately more moments along one direction giving rise to strong remanence. This could explain spurious ARMs sometimes observed in the laboratory even when no detectable field bias or bad waveform is present.

The sawtooth is more pronounced at low fields and is also sensitive to the spacing of the field steps (Fig. 3.4). For example, at 200 mT, IRAT varied between 0.56 to 0.81 depending on the choice of field steps, which in these experiments ranged between 20 and 100 mT. Increasing the number of field steps lowers the difference in coercivity of the successive field steps. The intermediary field steps help to 'soften' the coercivity by churning the moment directions multiple times.

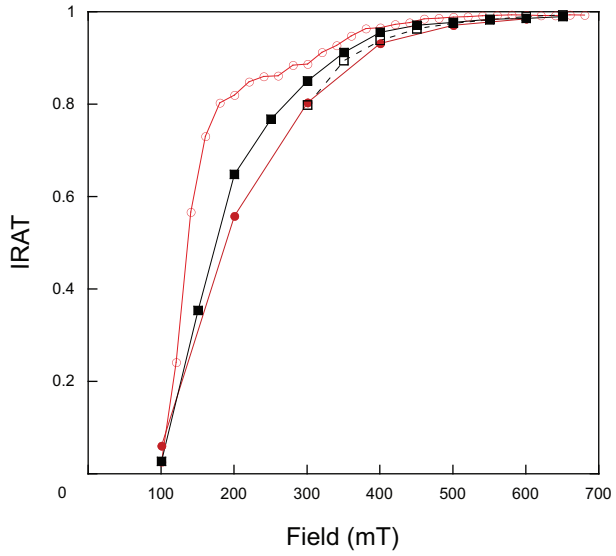


Figure 3.4: IRAT as a function of field spacing and initial field in MSD grains. Circles show IRAT for field spacing of 20 mT (open red) and 100 mT (closed red). Squares show IRAT for an initial field of 50 mT (closed black) and 300 mT (open black).

The choice of the initial field step has a similar, albeit less pronounced, effect on IRAT. For example, at 300 mT, IRAT varies from 0.79 to 0.85 for initial fields of 50 and 300 mT respectively, with the same field step spacing of 50 mT. These results together with the variability of grain size and coercivity of natural rocks suggest that the absolute IRM values from very different samples might not be comparable. Despite these caveats the property of IRAT being close to unity and showing little change with field step for USD grains can be used to distinguish between dominantly USD and dominantly MSD assemblages.

3.3 Experimental Evidence

The theory and modeling in the preceding sections predict that USD and MSD assemblages will behave differently in a DIRM acquisition experiment. In order to test this experimentally we investigate two sample types: the Tiva Canyon tuff and a specularite hematite sample from the Dhok Pathan formation in Pak-

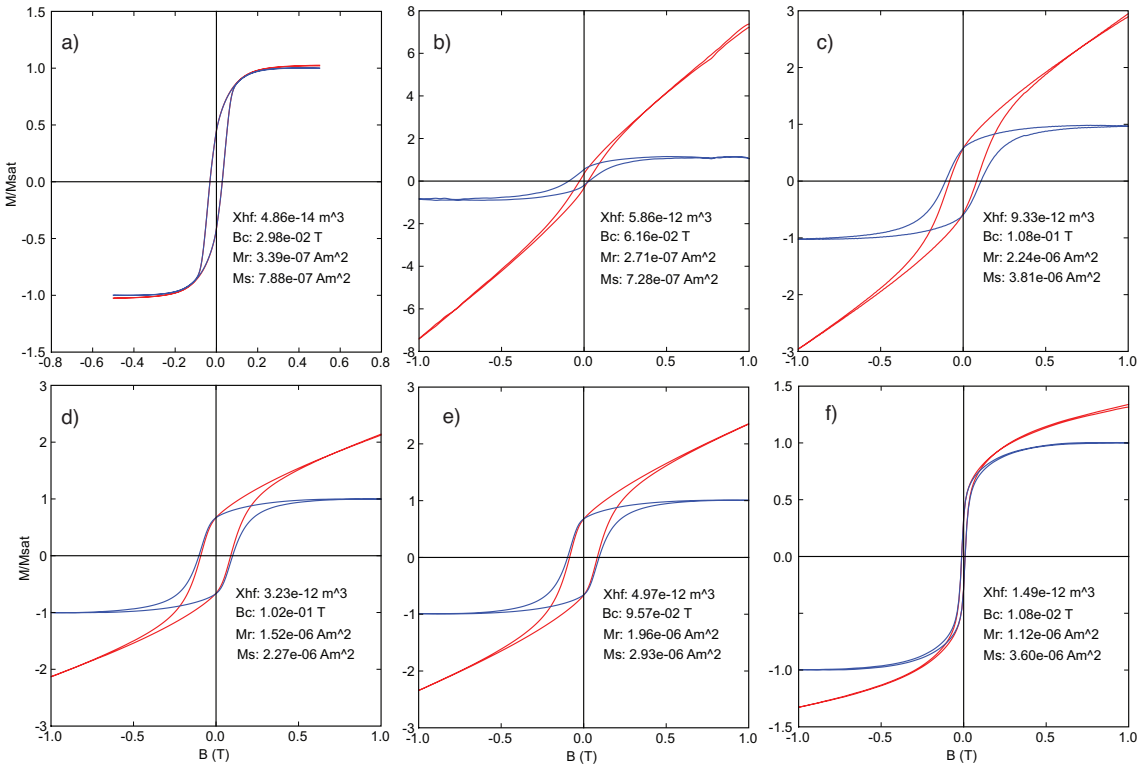


Figure 3.5: Representative hysteresis behavior for a) Tiva Canyon tuff b-f) Ph93-1 at 1, 3, 5, 7 and 30 mm from the glassy margin.

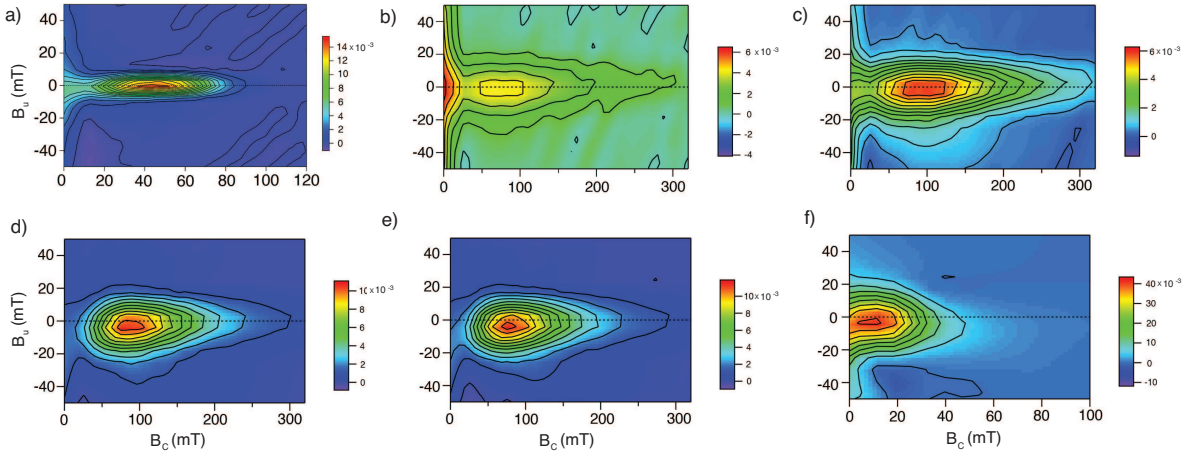


Figure 3.6: FORC distributions for a) Tiva Canyon tuff b-f) Ph93-1 at 1, 3, 5, 7 and 30 mm from the glassy margin. FORC distributions were prepared with the software described in Harrison et al. (2008).

istan. The Tiva Canyon tuff has been proposed as a standard USD material (Carter-Stiglitz et al., 2006). Hysteresis loops (Fig. 3.5a) look like classic SD loops predicted by Stoner and Wohlfarth (1948). FORC distributions (Pike et al., 1999; Roberts et al., 2000) show typical non-interacting SD behavior with closed contours parallel to the B_c axis, a density peak near 40 mT and a small spread along B_u (Fig. 3.6a).

Tauxe et al. (1990) characterized the hematite found in the Dhok Pathan formation of the Siwalik Group in Pakistan as either specular or pigmentary types. The sedimentary sequence comprising gray to red siltstones have varying proportions of these phases. In this study we chose one of the gray specimens which was reported to have primarily specular hematite with low coercivity.

The experimental protocol involved subjecting a specimen to an impulse DC field (B) in a pulse magnetizer and measuring the remanence. The specimen was then placed in the opposite direction in the pulse magnetizer and subjected to the same field (now, $-B$) and the remanence was remeasured. This was repeated at successively higher fields.

In a DIRM acquisition plot, no substantial sawtooth was observable in the

Tiva Canyon tuff and the lowest IRAT was as high as 0.94 at 30 mT (Fig. 3.7a). Specularite hematite on the other hand, showed a substantial sawtooth with IRAT increasing gradually from 0.57 at 50 mT to 0.97 at 600 mT (Fig. 3.7b). As predicted from theory: 1) the lowest IRAT was observed at the lowest field, 2) USD and MSD assemblages have distinct DIRM signatures, and 3) IRAT at the first field step shows the most difference for USD and MSD assemblages and can be used to effectively discriminate between the two. In the following section we will be using the first field IRAT to understand the dominant source of magnetic anisotropy enegy in the MORBs initially studied by Gee and Kent (1999).

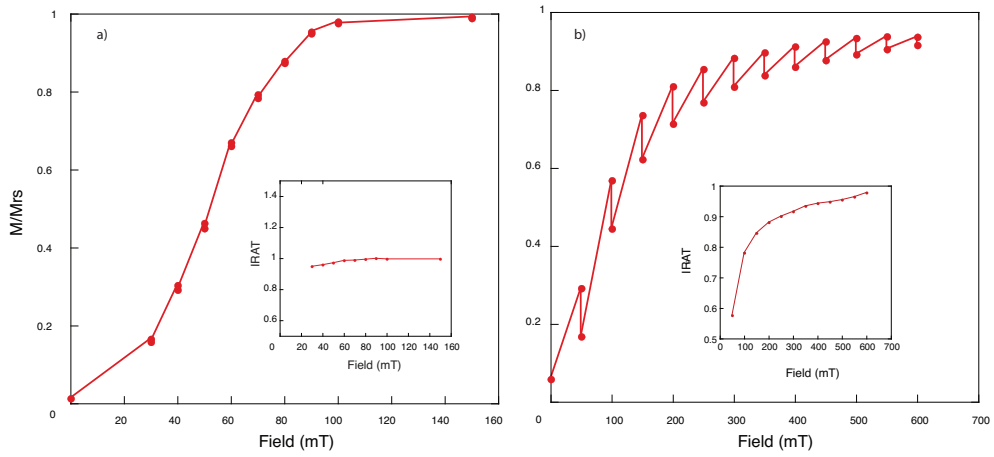


Figure 3.7: DIRM acquisition in natural samples. M_{rs} measured at 2.4 T. Inset shows corresponding IRATs. a) Tiva Canyon tuff. b) Dhok Pathan hematite.

3.4 Nature of anisotropy energy in MORB samples

To investigate the nature of anisotropy in MORBs, we started with a 0.18 Ma sample (PH93-1) from the Phoenix expedition near 10°N on the East Pacific Rise (Batiza et al., 1996). Gee and Kent (1999) used specimens from this sample

to show that magnetic granulometry varied as a function of the distance from the chilled margin. The M_{rs}/M_s ratios of some of the specimens were extremely high (> 0.5).

For the present study we cut four slices of PH93-1 at ∼1-2 mm resolution parallel to the chilled margin for the outermost 1 cm. Multiple specimens weighing between 20 and 100 mg were obtained by breaking apart each thin slice. The specimens were subjected to a complete DIRM acquisition experiment. Subsequently FORCs were determined for all specimens. The slices had distinct hysteresis behavior (Fig. 3.5b-e) and derived FORC distributions (Fig. 3.6b-e), consistent with the inferred increasing magnetic grain size away from the quenched margin. Peaks near $B_c = 0$ and FORC distribution contours parallel to B_u reflect a dominantly SP fraction (Fig. 3.6b). As we move away from the margin the coercivity peak moves towards higher B_c values, consistent with an increasing SD fraction (Fig. 3.6c). For specimens ∼0.5 - 0.8 cm away from the glassy margin the contours close and the spread along B_u reduces, suggesting a dominantly SD contribution (Fig. 3.6d,e). Further away, the contours open up again but with higher coercivity peak than in Fig. 3.6b, showing substantial MD contribution (Fig. 3.6f).

We subjected all specimens to the DIRM experiment (Fig. 3.8). DIRM acquisitions of the samples show IRAT increasing with field (Fig. 3.8). Specimens closest to the margin have the highest IRAT values (0.81 at 50 mT) and IRAT decreases with distance from the margin. At higher fields (200 mT) the difference in IRAT vanishes because the field strength overwhelms the difference in coercivity as the specimens approach saturation.

To further investigate the nature of the anisotropy energy we analyzed two more approximately zero age MORB samples; a pillow basalt (PH99-1) from 10°N on the East Pacific Rise (Batiza et al., 1996) and a 8 cm thick sheet flow (MW86-5) from the southern East Pacific Rise (Sinton et al., 1991). These were systematically sampled at $\sim 1 - 2$ mm resolution over the cm closest to the rim. Each horizon yielded 2-6 specimens measuring 20-100 mg. Three more specimens

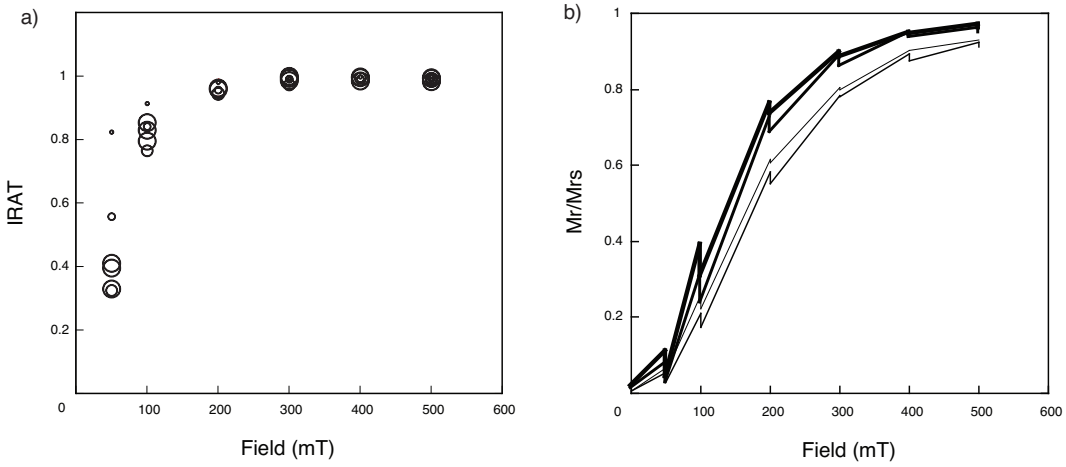


Figure 3.8: a)IRAT as a function of field for PH93-1 specimens. Circle size represents distance from the margin ie., 1(smallest circle), 3, 5 and 7 mm. b) Corresponding DIRM acquisition in representative specimens. Line thickness increases with distance from the margin. Only one specimen shown from each zone.

were sampled from the interior of the three basalts (> 3 cm). A curtailed double IRM protocol, involving just the initial step was carried out. The initial field was 50 mT for PH93-1 and 75 mT for the rest. Subsequently, hysteresis loops were determined and M_{rs}/M_s ratios were calculated using paramagnetic slope correction from 0.7 to 1 T.

To avoid high temperature alteration of the specimens we avoided thermal demagnetization. Instead, the NRM was used as the initial state. The potential bias introduced as a result should be negligible as long as the IRM after the first applied field is substantially higher than the NRM. This would show that the potential bias due to existing NRM is negligible. For our purposes we needed a selection criterion which would recognize specimens which were affected by the NRM bias. When IRM exceeded the NRM by a factor of six or more it was assumed that the bias due to such a low NRM was negligible. Ten of the 58 samples did not meet this criteria and were excluded from this discussion (Fig. 3.9). IRAT data

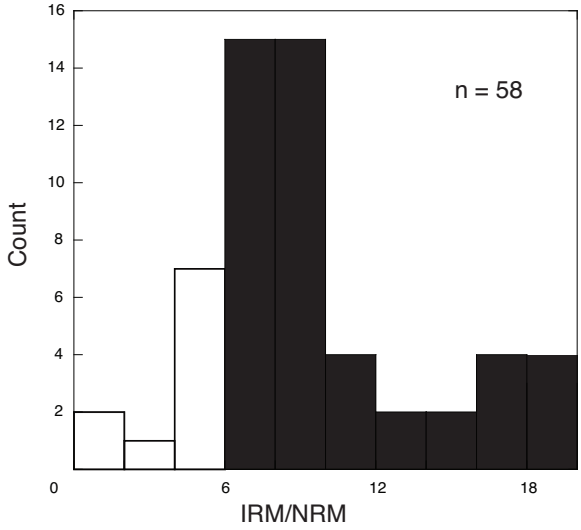


Figure 3.9: Histogram of the ratio of IRM at the first field step to NRM. Values 38.5 and 60 have been omitted from the figure. White bars denote samples which did not meet our selection criteria.

versus M_{rs}/M_s data for the remaining specimens are shown in Fig. 3.10. Three specimens had IRATs slightly above 1 and although this is arguably due to an initial NRM bias (as shown in Fig. 3.3a inset), the IRM was strong enough not to warrant an exclusion of these specimens.

We see a gradual transition from high M_{rs}/M_s, low IRAT specimens to low M_{rs}/M_s, high IRAT specimens. More importantly, specimens having M_{rs}/M_s above 0.5 all have IRAT values below 0.8 and sometimes as low as 0.3 (Fig. 3.10). Such low values of IRATs are consistent with our hypothesis of substantial MSD contribution in MORBs. The mostly glassy MW86-5 specimens all cluster in a low M_{rs}/M_s, high IRAT section of Fig. 3.10 (squares). On the other hand, pillow specimens, especially PH93-1(triangles), show a moderate dependence of IRAT with distance from the margin with higher IRAT in specimens closer to the margin. The high IRAT can be either due to a greater contribution of USD magnetite or

an effect of SP fraction as shown in Garcia-Otero et al. (2000). Specimens from the flow interiors have MD hysteresis behavior (Fig. 3.5f) and the derived FORC distributions have open contours and low coercivity (Fig. 3.6f) showing dominant MD contribution. These specimens typically have a high IRAT values. Although a theoretical treatment of IRAT in MD grains is beyond the scope of the current work it is postulated that the mobile walls of the MD grains, being less coercive than the anisotropy of SD grains, are easier to flip towards the field directions thereby contributing to substantially higher IRATs, even at low fields.

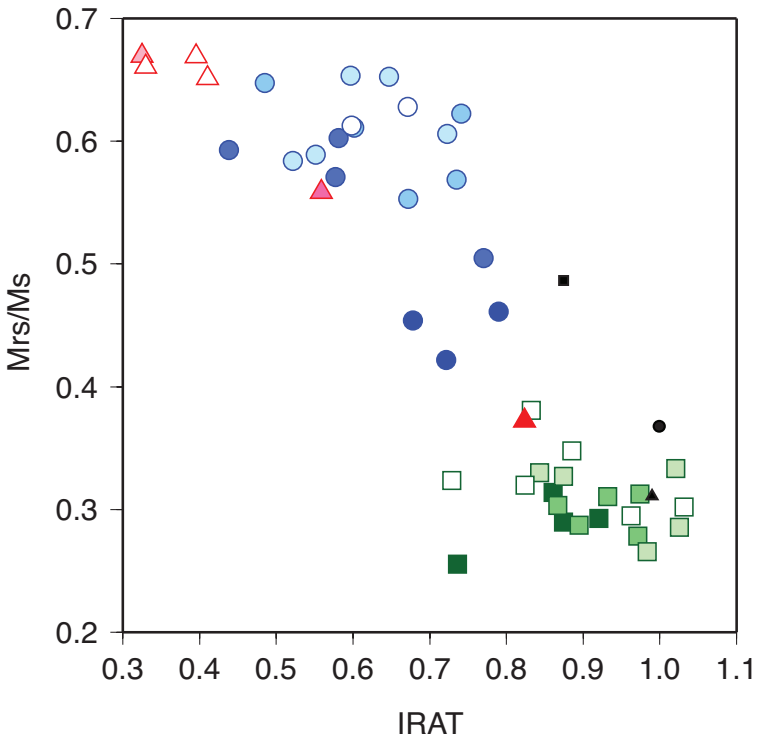


Figure 3.10: M_{rs}/M_s vs IRAT at the first field step for PH93-1 (red triangles, n=7), PH99-1 (blue circles, n=20) and MW86-5 (green squares, n=21). Color tones indicate distance from the chilled margin with deeper tones being closer to the margin and white symbols represent farthest (∼1 cm) from the margin. Specimens lying >3 cm from the margin are shown with smaller black symbols.

An independent case for the presence of multiaxial anisotropy in MORBs has been presented by Lanci (2010) in which he used anisotropy of susceptibility to establish the presence of dominant cubic anisotropy. Another proposed mech-

anism for high M_{rs}/M_s as well as the high coercivity as observed in these basalts was the 3-D cross structure of Tauxe et al. (2002). These cross structures are composed of three parallelepipeds intersecting in three mutually orthogonal directions. Although reversals in magnetization in such complicated shapes show flower and vortex states and is not possible to model sensu-stricto within the framework discussed in this paper, the presence of more than one easy direction would arguably lower the IRAT. Hence, while it is possible that the anisotropy is indeed cubic, this work does not rule out more complicated possibilities.

3.5 Conclusions

- We define a new parameter IRAT (the ratio of two opposing low field IRMs imparted in a double IRM acquisition experiment) for differentiating between USD and MSD grains. With numerical simulation and experimental data we show that IRAT is ~ 1 for USD grains for all fields. For MSD grains, IRAT approaches 1 from lower values with increasing field.

- We have shown that in a system with dominant multi-axial anisotropy coercivity varies with application of a field. At fields close to saturation both USD and MSD grains have IRAT values of ~ 1. This suggests that, for samples where MSD grains may be present, experiments like anisotropy of isothermal remanence should be conducted at fields close to saturation where the difference of remanences become negligible. Otherwise the experiments will always show a substantial anisotropy even when there is none. Presence of MSD grains can impart strong remanences during AF demagnetization and can be a source of spurious ARMs, sometimes observed in the laboratory. On the other hand, parameters such as HIRM and S-ratios, which are chiefly used as proxies for the relative amount of goethite/hematite as compared to softer minerals like magnetite/maghemite, are unlikely to be affected much

by this because of the large difference in coercivity between the two groups.

- All our hysteresis parameters have been measured at 1T maximum field. As noted earlier, Fabian showed that such a field might be underestimating the saturation magnetization which could potentially explain the high M_{rs}/M_s in some specimens. In spite of that, our work shows, the specimens cannot have a dominant USD fraction.

- If $K_\lambda > K_1$ for most MORBs then contrary to the popular assumption, stress anisotropy could be non-uniaxial.

3.6 Acknowledgement

We gratefully acknowledge useful discussions with Luca Lanci and David Dunlop. This work was supported in part by NSF grant EAR1013192 to Lisa Tauxe. Reviews by two anonymous editors helped to improve the manuscript.

Chapter 3, in full, is a reprint as it appears in Mitra, R., Tauxe., L. and Gee, J. (2011), Detecting uniaxial single domain grains with a modified IRM technique, Geophysical Journal International. The dissertation author was the primary investigator and author of this paper.

Bibliography

E. Appel. Stress anisotropy in Ti-rich titanomagnetites. *Phys. Earth Planet. Int.*, 46(1-3):233–240, 1987.

E. Appel and H. C. Soffel. Model for the domain state of Ti-rich titanomagnetites. *Geophys. Res. Lett.*, 11(3):189–192, 1984.

R. Batiza, Y. L. Niu, J. L. Karsten, W. Boger, E. Potts, L. Norby, and R. Butler. Steady and non-steady state magma chambers below the East Pacific Rise. *Geophys. Res. Lett.*, 23(3):221–224, 1996.

P. J. Besser, A. H. Morrish, and C. W. Searle. Magnetocrystalline anisotropy of pure and doped hematite. *Phys. Rev.*, 153(2):632–642, 1967.

B. Carter-Stiglitz, P. Solheid, R. Egli, and A. Chen. Tiva Canyon Tuff (II): Near single domain standard reference material available. *The IRM Quarterly*, 16(1), 2006.

R. Day, M. Fuller, and V. A. Schmidt. Hysteresis properties of titanomagnetites - grain-size and compositional dependence. *Phys. Earth Planet. Int.*, 13(4):260–267, 1977.

R. Day, S. Halgedahl, M. Steiner, K. Kobayashi, T. Furuta, T. Ishii, and A. Faller. Magnetic properties of basalts from DSDP Leg 49. *Init. Rep. DSDP*, 49:781–791, 1978.

D. J. Dunlop. Magnetic properties of fine-particle hematite. *Ann. de Geophys.*, 27 (3):269–283, 1971.

D. J. Dunlop and Ö. Özdemir. *Rock Magnetism:Fundamentals and Frontiers*. Cambridge University Press, Cambridge ; New York, 1997.

K. Fabian. Approach to saturation analysis of hysteresis measurements in rock magnetism and evidence for stress dominated magnetic anisotropy in young mid-ocean ridge basalt. *Phys. Earth Planet. Int.*, 154(3-4):299–307, 2006. doi:10.1016/j.pepi.2005.06.016.

J. Garcia-Otero, M. Porto, and J. Rivas. Henkel plots of single-domain ferromagnetic particles. *J. of App. Phys.*, 87(10):7376–7381, 2000.

J. Gee and D. V. Kent. Magnetic hysteresis in young mid-ocean ridge basalts - Dominant cubic anisotropy? *Geophys. Res. Lett.*, 22(5):551–554, 1995.

J. Gee and D. V. Kent. Calibration of magnetic granulometric trends in oceanic basalts. *Earth Planet. Sci. Lett.*, 170(4):377–390, 1999.

J. Geshev and M. Mikhov. Remanence curves for a disordered system of 3-axial and 4-axial fine particles - Henkel-Type Plots. *J. of Magn. and Mag. Mat.*, 104: 1569–1570, 1992.

R. J. Harrison and J. M. Feinberg. FORCinel: An improved algorithm for calculating first-order reversal curve distributions using locally weighted regression smoothing. *Geochem. Geophys. Geosyst.*, 9(Q05016), 2008. doi:/2008GC001987.

O. Henkel. Remanenzverhalten und Wechselwirkungen in Hartmagnetischen Teilchenkollektiven. *Phys. Stat. Sol.*, 7(3):919–929, 1964.

I. Joffe and R. Heuberger. Hysteresis properties of distributions of cubic single-domain ferromagnetic particles. *Phil. Mag.*, 29(5):1051–1059, 1974.

L. Lanci. Detection of multi-axial magnetite by remanence effect on anisotropy of magnetic susceptibility. *Geophys. J. Int.*, 181(3):1362–1366, 2010. doi:10.1111/j.1365-246X.2010.04588.x.

C. R. Pike, A. P. Roberts, and K. L. Verosub. Characterizing interactions in fine magnetic particle systems using first order reversal curves. *J. Appl. Phys.*, 85 (9):6660–6667, 1999.

A. P. Roberts, C. R. Pike, and K. L. Verosub. First-order reversal curve diagrams: A new tool for characterizing the magnetic properties of natural samples. *J. Geophys. Res.*, 105(B12):28461–28475, 2000.

S. Sahu and B. M. Moskowitz. Thermal-dependence of magnetocrystalline anisotropy and magnetostriction constants of single-crystal $Fe_{2,4}Ti_{0.61}O_4$. *Geophys. Res. Lett.*, 22(4):449–452, 1995.

J.M. Sinton, S.M. Smaglik, J.J. Mahoney, and K.C. Macdonald. Magmatic processes at superfast spreading mid-ocean ridges: glass compositional variations along the East Pacific Rise ,13°-23° S. *J. Geophys. Res.*, 96:6133–6156, 1991.

E. C. Stoner and E. P. Wohlfarth. A mechanism of magnetic hysteresis in heterogeneous alloys. *Phil. Trans. R. Soc. Lond.*, 240(826):599–642, 1948.

L. Tauxe. *Essentials of Paleomagnetism*. University of California Press, Berkeley, 2010.

L. Tauxe, H. N. Bertram, and C. Seberino. Physical interpretation of hysteresis loops: Micromagnetic modeling of fine particle magnetite. *Geochem. Geophys. Geosyst.*, 3(10), 2002. doi:10.1029/2001GC000241.

L. Tauxe, C. Constable, L. Stokking, and C. Badgley. Use of anisotropy to determine the origin of characteristic remanence in the Siwalik red beds of northern Pakistan. *J. Geophys. Res.*, 95(B4):4391–4404, 1990.

E. P. Wohlfarth. Relations between different modes of acquisition of the remanent magnetization of ferromagnetic particles. *J. of App. Phys.*, 29(3):595–595, 1958.

Chapter 4

Two thousand years of archeointensity from West Africa

This study presents 17 archeointensity estimates from Senegal and Mali, two neighboring countries in West Africa, for the period 1000 BCE to 1000 CE. The archeological artifacts used in this study were collected during the course of two separate projects, together spanning 22 years and 8 separate excavations. A primary objective of this study was to acquire paleointensities with accurate dates, hence, only samples with independent age constraints from pottery style, detailed stratigraphy and ^{14}C dates were used. A total of 263 specimens from 63 samples were subjected to a double heating paleointensity experiment (IZZI method) from which 95 specimens were selected using a set of very strict selection criteria. Paleointensity results were corrected for differential cooling rate effects and remanence anisotropy. Additionally, we demonstrate the equivalence of using tensors derived from anhysteretic and thermal remanences for correcting remanent anisotropy of the specimens and use the former for the anisotropy correction. Our data show good agreement with the most recent paleosecular variation model but are lower than the pre-existing data, mostly from Egypt and Morocco. The presence of substantial non-axial-dipolar contributions in the region is evident when virtual

axial dipole moments (VADMs) from the published literature are calculated for 20° latitudinal bands and compared with ours - the average VADM show a distinct latitudinal gradient. A prominent feature of this dataset is an intensity high observed prior to 700 CE in both Senegal and Mali. Comparing this peak with existing records from regions further to the north suggests a small but significant temporal offset and is interpreted to be additional evidence for a geomagnetic field with a significant and rapidly changing non-axial-dipolar contribution.

4.1 Introduction

Archeomagnetism provides a unique window to the changes in the Earth's magnetic field over the last few millennia. Compared to lavas, archeological artifacts are numerous, especially, in more recent times. They can be used to construct regional reference curves, which can then, in principle, be used for dating of other archeological artifacts from the region. The magnetic elements obtained from these items are also inputs for global field models such as the CALSxK generation of models (Korte and Constable, 2003, 2005, 2011) which often form the basis for answering fundamental geodynamo questions (e.g., Amit et al., 2011).

In spite of its potential, obtaining the full vector information from an archeological, or for that matter any kind of sample, is not a trivial task. While obtaining the direction of the ancient field is relatively simple, intensity measurements are more complicated because of the sensitivity of the experimental protocol to mineralogical alterations and domain states of the remanence carrier. Furthermore, there is no consensus yet on the experimental protocol and data reduction criteria and workers often use very different methods (Biggin, 2010). These could add to the scatter observed in an already impoverished dataset. Experimental difficulties and lack of access to suitable materials makes the global coverage of data extremely heterogeneous, with respect to space as well as time.

In Fig. 4.1a we plot the absolute paleointensity estimates for the last 10

millennia from Genevey et al. (2008). In general, the distribution of data with time is skewed towards the last two millennia where more than 50% of data are concentrated. Moreover, the data are heavily biased to the northern hemisphere and even there, there is a high concentration of data from Europe.

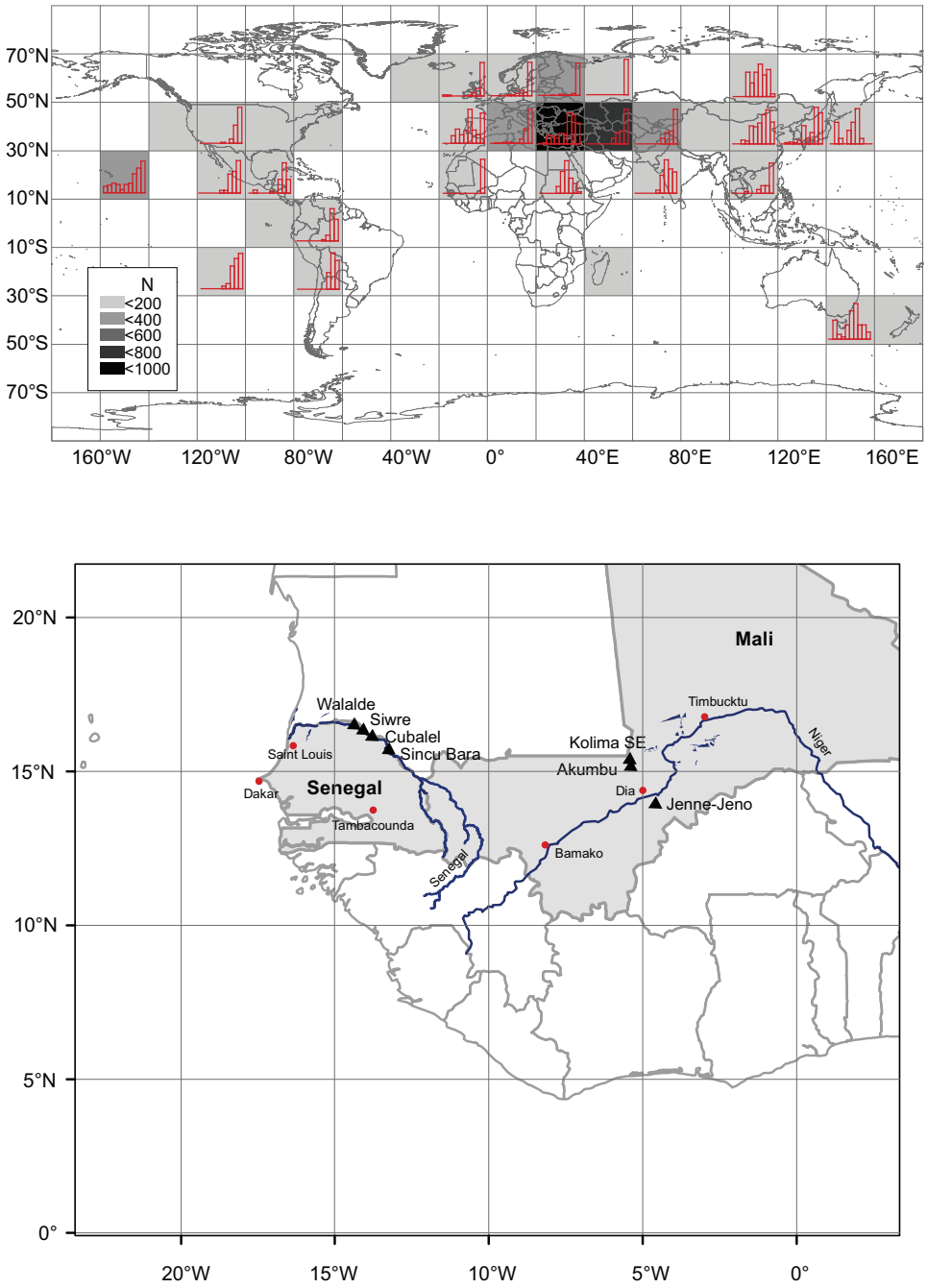


Figure 4.1: a) Spatial and temporal distribution of paleointensity data from the last 10 millennia as available in the Archeoint database (Genevey et al., 2008). Color-coded grid shows the absolute number of paleointensity estimates (N) available in each box and the histograms show its distribution with time. Each bin in the histogram represents 1000 years with left being older. Boxes having less than 20 paleointensity estimates have no histograms. b) Location of archeological sites in Senegal and Mali (triangles). Important cities and ports are shown with red dots.

In an effort to redress the paucity of high quality data from under-represented parts of the globe, we turn to the archeological findings from two areas of West Africa with rich iron age sites, the Middle Senegal Valley in Senegal and the Niger Valley in Mali (Fig. 4.1b). West Africa, a geographically extensive region, comparable in size with contiguous United States has sparse coverage in terms of archeomagnetic data (Kovacheva, 1984; Gomez-Paccard et al., 2012). The archeological samples in the present study come from two groups of sites separated by 1200 km. These archeological artifacts were collected during two multi-phase, decade-long archeological projects by one of the authors.

In this study, we reconstruct the evolution of the geomagnetic field intensity in the region, between 1000 BCE and 1000 CE. The location of the sites falls to the south of a pronounced geomagnetic flux patch over Europe during that time which may have influenced our sites (Korte and Constable, 2011). The passage of such a flux patch under a region would result in large swings in paleointensity which would be non-axial-dipolar in nature. Recently it has been proposed that the 'archeomagnetic jerks' of Gallet et al. (2003), or rapid changes in field strength coupled with long term directional changes in the field, are caused by the waxing and waning of geomagnetic flux patches in a region (Dumberry and Finlay, 2007; Amit et al., 2011). Here we find evidence for large non-axial-dipolar intensity swings which may or may not be associated with long term directional changes and are likely to be the outcome of rapid paleosecular variation (PSV) in a region influenced by geomagnetic flux patches.

4.2 Archeological Background

The potsherds used in this study were collected in the course of two separate multi-year projects designed to gain initial insights into the origin of complex iron-using societies along the Middle Niger Valley, Mali and the Middle Senegal Valley, Senegal (Fig. 4.1b and Fig. 4.2). In the rest of this section we discuss briefly the

archeological context of these two neighboring localities.



Figure 4.2: Excavation in progress at Cubalel mound C-3 in Senegal.

4.2.1 The Middle Senegal Valley samples

Between 1990 and 1999, five seasons of NSF-funded archaeological research were conducted at a variety of sites in the central region of the Senegal Valley, where the historical polities of Takrur and Sila – first mentioned in an eleventh century Arab chronicle – were thought to be located. The research aimed to investigate the origins and development of these early Sudanic polities. Prior archaeological work in the Senegal Valley was sparse and of variable quality, so chronology-building was a primary goal of the research. The numerous settlement mounds, up to six meters in height, along the river between Cubalel and Walaldé proved to be well-suited for this purpose, representing in each excavated instance between three to ten centuries of domestic deposits that accumulated between 2600-1000 BP(Deme and McIntosh, 2006; McIntosh et al., 2012). The pottery samples and radiocarbon dates used in this article come from five of these mounds, viz., Walaldé, Siwré, Cubalel C-1,C-3

and C-6, and one non-mound site, Sincu Bara, located 80 kilometers downriver (Table 1).

During excavation, individual deposition contexts were identified and excavated separately. This maximized the likelihood that cultural materials and charred organics recovered from each context were deposited contemporaneously. Within each excavation unit, stratigraphy is an important source of information on chronology, allowing reconstruction of the sequence of deposition for the different contexts. These events may range from very brief (such as the scatter of ashes from a small hearth) to lengthy (e.g., the slow decay and wall melt of an abandoned wattle-and-daub house). Detailed analysis of ceramics from all excavated contexts resulted in identification of characteristic changes in style that allowed the identification of time-successive pottery phases within the mound deposits. The most salient time-sensitive changes in pottery on which phase designations were based involve decorative techniques and vessel shape. Separate Phase sequences were defined for Walaldé (Deme and McIntosh, 2006), the Cubalel/Siwré site group (McIntosh, 2012) and Sincu Bara (McIntosh and Bocoum, 2000). Contemporaneity of ceramic phases present in the excavation units in different sites was verified by radiocarbon dating of charcoal samples from reliable (uncontaminated) contexts in all the units. Charcoal from hearths was abundant at these sites; only 1 of every 6 samples collected was submitted for radiocarbon analysis. This permitted great selectivity and let us focus on charcoal from the most secure contexts.

4.2.2 The Middle Niger Valley samples

Most of the Mali samples come from two adjacent settlement mounds, Jenné-Jeno and Hambarketolo, that were built up largely contemporaneously in the first and early second millennia CE. Together they cover an area of over 110 acres. The samples come from four units excavated in 1977 (M1, see McIntosh and McIntosh, 1980), 1981(LX-N, HAMB, see McIntosh, 1995) and 1997 (DT, unpub-

lished) (Table 1). While several other units have additionally been excavated at these mounds (see Supplemental Material), reinforcing the ceramic phase chronology and the radiocarbon dating of the deposits, Table 1 includes only the units from which pottery samples were analyzed for archeomagnetism. At their highest points, both mounds revealed from 4.5 - 5.5 meters of accumulated occupation deposits. The methodology employed for excavation and for the establishment of a ceramic phase chronology was identical to that described for the Senegal Valley sites. Detailed stratigraphy and chronological information for the sites discussed so far are available in the Supplemental Material.

The remaining Mali samples were recovered from excavations in 1999 at two occupation mound clusters ∼100 km north-north-west of Jenné-jeno in a now-desiccated alluvial region known as the Méma: Kolima SE and Akumbu. At the low mound of Kolima SE, two units, 1 and 3, were situated close together and yielded a similar pottery assemblage throughout the 1.5 meters of deposits. The material from both units can be considered as part of the same ceramic phase. This material has not yet been fully studied but the radiocarbon dates obtained in this study are in agreement with the stratigraphy.

Akumbu comprises several occupation mounds up to 4 m in height. In 2000, Unit 1 was excavated at one of these mounds to a depth of 1.5 m, when the excavation was ended before reaching sterile soil. The pottery assemblage in the upper levels 1-9 belongs to the Middle ceramic phase identified from prior excavations at another mound in the Akumbu cluster and radiocarbon dated between the sixth and fourteenth centuries CE (Togola, 2008). The pottery below level 9 is identical to the Early Phase ceramics identified by Togola, which date to the early first millennium CE. The sherd samples used in the analysis come from levels 6 and 13, separated by over 50 centimeters of deposits. The new radiocarbon dates obtained during the course of this study, 271±58 CE for Level 13 and 899±56 CE for Level 6 were found to be in excellent agreement with the previously established chronology of Togola (2008).

Table 4.1: List of archeological sites with dimensions of excavated units and pottery phases excavated at each unit. Site acronyms in brackets are the paleomagnetic sites corresponding to the archeological sites (see text).

Archeological Sites	**Excavation Units (size)**	**Depth**	**Phases**
Walalde (WA)	WAL 1 (4x3m)	4.5 m	WAL I, II
	WAL 2 (3x2m)	4.5 m	WAL I, II
Siwré (SW)	1S (4.3m)	5.5 m	CUB/S I
Cubalel (CB)			
C-1	C-1 (4x3m)	3.0 m	CUB/S II,III
C-3	C3-A (5x6m)	5.5 m	CUB/S I,II,III
	C3-B (5x6m)	5.5 m	CUB/S I,II,III
C-6	C-6 (4x3m)	3.8 m	CUB/S II,III,IV
Sincu Bara(SB)	SB1 (3x3m)	3.2 m	SB 1, II, III[1]
Jenné -jeno(JJ)	LXN (5x6m)	5.5 m	JJ I, II, III, IV
	DT (2x3m)	2.0 m	JJ I
	M1 (3x3m)	5.0 m	JJ I, II, III, IV
Hambarketolo (JJ)	HAMB (2x2m)	4.5 m	JJ II, III, IV
Kolima SE (KS)	UNIT 1 (2x3m)	1.5 m	NA
	UNIT 3 (2x3m)	1.5 m	NA
Akumbu (AK)	UNIT 1 (3x3m)	1.5 m	NA

[1] SB Phase III had pottery identical to CUB/S Phase III. SB Phases I and II were similar but not identical to CUB/S I and II, and contemporaneous with them, according to radiocarbon dates.

Table 4.2: Table showing list of samples and specimens. Sample (Specimen) column shows number of samples (specimens) selected/ number of samples(specimens) measured. Age calibrated according to OxCal program (Ramsey et al., 2010).

Sites	**Latitude**	**Longitude**	**Samples**	**Specimens**	**Claibrated Age**	**Intensity** (μT)	**VADM** (x10^{22}Am^2)
SB1	15.8°N	13.3°W	2/3	4/8	502±72	35.32±3.34	8.26±0.78
SB2	15.8°N	13.3°W	2/2	6/8	502-624	38.75±1.27	9.06±0.3
SB3	15.8°N	13.3°W	1/1	5/5	624±52	42.23±1.54	9.88±0.36
SB4	15.8°N	13.3°W	2/4	6/14	815±81	36.96±4.08	8.64±0.95
WA1	16.5°N	14.3°W	2/4	7/12	-628±92	40.66±2.04	9.43±0.47
CB1	16.0°N	13.6°W	2/2	5/6	124±73	38.89±3.08	9.07±0.72
CB2	16.0°N	13.6°W	2/4	4/7	221±70	36.17±1.61	8.43±0.37
CB5	16.0°N	13.6°W	1/3	4/8	485±75	36.40±2.70	8.49±0.57
CB6	16.0°N	13.6°W	1/2	4/8	221-410	34.93±1.23	8.15±2.86
JJ5	13.7°N	4.5°W	3/3	8/12	27±47	40.06±2.49	9.58±0.6
JJ6	13.7°N	4.5°W	1/2	3/8	125±48	41.88±0.38	10.0±0.09
JJ7	13.7°N	4.5°W	1/1	3/4	664±31	43.37±3.51	10.4±0.84
KS1	15.4°N	5.5°W	1/1	4/4	-662±72	40.82±1.11	9.59±0.26
KS2	15.4°N	5.5°W	1/1	4/4	-812±12	40.09±0.66	9.41±0.15
KS3	15.4°N	5.5°W	1/1	4/4	-865±25	42.71±2.25	10.03±0.53
AK1	15.3°N	5.5°W	1/2	4/8	899±56	39.62±1.01	9.32±0.24
AK2	15.3°N	5.5°W	1/2	4/8	271±58	35.87±1.45	8.44±0.34

4.2.3 Chronology and Nomenclature

As is evident from the foregoing discussion, the chronology of the excavated sites has been iteratively constrained by the archeologists with independent evidence from pottery style, stratigraphy and ^{14}C dating. Within a single unit, stratigraphy and pottery style served to corroborate the available ^{14}C dates. Often in archeological excavations, we have events such as pit digging or other disturbances that can complicate the stratigraphic interpretation. Therefore care was taken so that all the pottery and charcoal samples came only from the most unambiguous strata. Across units, pottery/occupation phase offered an independent check for the ^{14}C dates. Samples for which pottery style, stratigraphy and ^{14}C dating did not agree were deemed unfit for the study and were rejected (See Fig. 4.13 and 4.15 in Supplemental Material). Table 4.2 shows the list of all the successful sites. For two sites, viz., SB2 and CB6, the age was constrained using stratigraphic constraints and ^{14}C dates from adjoining strata.

The sense of the term paleomagnetic site as used in this study is different from its archeological equivalent, the archeological site. While an archeological site comprises a number of excavation units, a paleomagnetic site is defined as being made up of a number of samples from a particular horizon within a *single* excavation unit of an archeological site. For example, the paleomagnetic sites starting with CB (Table 4.2) each refer to a distinct layer in one of the Cubalel mound site excavation units (Table 4.3). Detailed stratigraphic and chronological contexts of the paleomagnetic sites and their respective archeological sites are presented in the Supplementary Material. Samples, as used in this study, refer to individual sherds (eg., cb07) while specimens refer to the multiple pieces, ranging between three to six, sub-sampled from the sherds (eg., cb07a. See Supplementary Material for the full list of specimens).

4.3 Experimental Procedure

4.3.1 Paleointensity Experiments

A total of 236 specimens from 63 samples were prepared for the archeointensity experiments. From each pottery sample, 3-6 specimens were chosen for the paleointensity experiments. Care was taken to sand off the slip (possibly a low temperature addition) that is a common feature in potteries. Thick edges and rims of potteries showing an even red coloration signify that high temperatures were reached and were therefore sampled wherever possible. All the specimens were wrapped in glass microfibre and completely immersed in potassium silicate, which dried over time.

Archeointensity experiments were carried out using the IZZI protocol of Tauxe and Staudigel (2004) in the magnetically shielded paleomagnetic laboratory of the Scripps Institution of Oceanography. Measurements were made on a horizontal 2G cryogenic magnetometer. Two water-cooled ovens were used for the experiments. The IZZI experiments consisted of double heating at each step from 100°C to 585°C (or 600°C in some). We used coarser steps of 100°C up to 200°C, 50°C steps up to 500°C and smaller steps for higher temperatures. After every zero field heating in the zero-field and in-field pair, an additional in-field step was inserted, heating to a temperature two steps lower than the current. This ensured that the specimen had not altered during the intervening steps and served as an alteration (pTRM) check.

Acceptable paleointensity estimates should have a linear Arai plot (Nagata et al., 1963) and a single NRM component decaying to the origin. Such behavior is expected for single domain grains that have been heated once to very high temperatures. Larger grain sizes, alteration during laboratory experiments, multiple heating of household potteries during their period of use and experimental errors invariably lead to significant departures from the aforementioned criteria. The acceptability limits for this departure are still a matter of discussion and are

critically dependent on the choice of a set of parameters that can quantitatively classify the quality of the data. As a result, selection of data remains subjective because of the wide array of parameters from which to choose (Tauxe, 2010) and also the broad range of acceptance thresholds for each of those parameters.

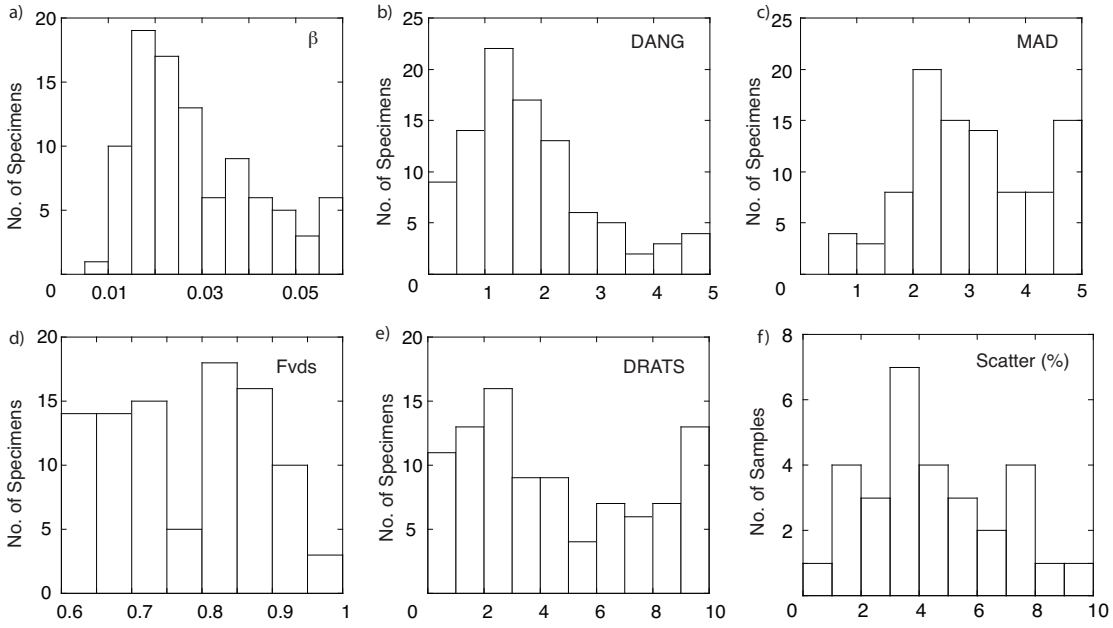


Figure 4.3: Selection criteria for the IZZI experiments. a-e) Histograms showing the distribution of the acceptance criteria for selected specimens (see text for description) f) Histogram showing sample level scatter as percent relative standard deviation.

In this study we have used a fairly strict set of criteria (Fig. 4.3). For a specimen to be selected, at least 60% of the remanence, as estimated by the f_{vds} (Tauxe and Staudigel, 2004), spanning at least 6 double heating steps were used to define the stable component. The parameter β is the error of the best fit slope in an Arai plot normalized to the slope (Coe et al., 1978) and we constrain it to be less than 0.06. Furthermore, DANG (Tauxe and Staudigel, 2004), the angular deviation of the best fit line from the line joining the center of mass to the origin in the Zijderveld plot, and MAD (Kirschvink, 1980), which is a measure of the scatter of the points about the best- fit line, were both restricted to a maximum value of 5°. Alteration, as measured by DRATS (Tauxe and Staudigel, 2004) was

kept below 10 for all selected specimens. A successful sample with a mean of μ had at least two successful specimens with a within-sample scatter, measured by the percent standard deviation ($100\sigma/\mu$), less than 10%. For a site level average to be included in the study it should have at least one sample and a minimum of three specimens. So, a site having only one successful sample with two successful specimen level estimates would be rejected but a site with two samples each having two specimen level estimates or a site with one sample and three specimen level estimates would be included in the study.

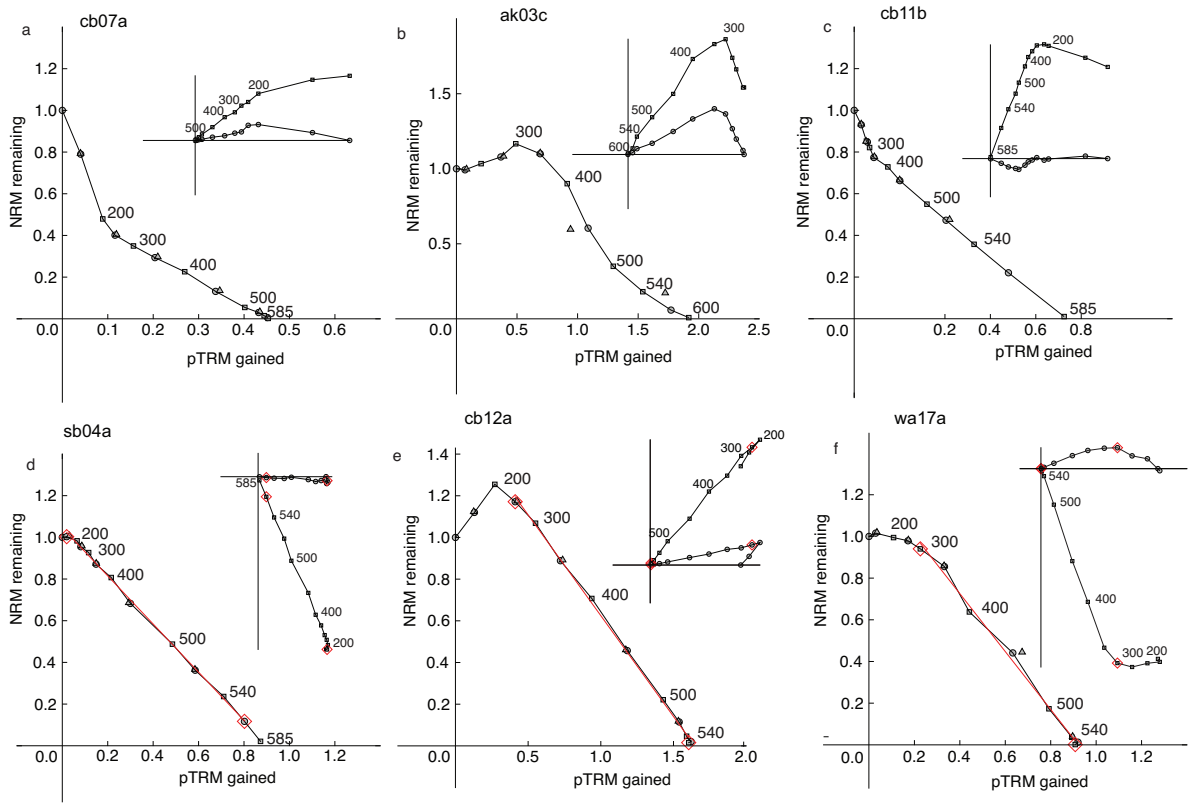


Figure 4.4: IZZI experiment results. a-c) Arai plots and Zijderveld diagrams of specimens which failed to pass the selection criteria. d-f) Representative plots for specimens which passed the selection criteria. The temperature interval used for isolating the characteristic remanence is marked with a red line and squares. The insets are the vector components of the zero field steps with x in the abscissa and y, z in the ordinate. The circles are (x, y) pairs and the squares (which have the temperature steps marked alongside) are (x, z) pairs. The directions are in the specimen coordinate system. The laboratory field was applied along the z-axis in the in-field steps.

Choosing the temperature limits for the paleointensity estimate includes some amount of discretion on the part of the worker but such strict criteria help to ensure unambiguous interpretations such as those shown in Fig. 4.4 a-c. For example, in cb07a, if temperature bounds between 200°C and 585°C were chosen, then the sample would be excluded on the basis of low f_{vds} while using bounds from 100-585°C would discard the specimen because of low β and high MAD. While keeping looser criteria, say $\beta \leq 0.1$ and, MAD ≤ 8 or $f_{vds} > 0.4$ would have lead to an acceptable intensity estimate with either selection criteria, the value would hardly be unambiguous. It would be 62.4 μT for the former and 49.2 μT for the latter. The low β used in the study made sure that Arai plots with pronounced concavity were rejected. Similarly specimens like cb11b were discarded because of high MAD and/or DANG.

The fairly strict criteria we have used for selecting specimens ensured that only the most robust estimates were retained. About half of all the selected specimens decayed straight to the origin with little to no viscous component (eg., Fig. 4.4d), while most of the rest ($\sim$ 40%) had a sharp low temperature secondary component which was removed by $\sim$ 200°C and the remanence decayed linearly to the origin thereafter (Fig. 4.4e). Only a few ($\sim$ 10%) had some curvature in the vector plots, but not significant enough to warrant exclusion (Fig. 4.4f). Of the 236 specimens 103 passed the selection criteria at the specimen level. Of these, specimens, 98 passed the sample level criteria and 95 passed the site level criteria (Table 4.2 and Table S1 in the Supplementary Material).

4.3.2 Anisotropy

TRM anisotropy in pottery is largely believed to be the result of alignment of the remanence carrying fraction during the creation of the pot when the minerals get aligned at a tangent to the surface of the pottery. Bricks, which do not undergo any flattening processes, are largely found to be isotropic lending credence to this

hypothesis. As a result of partial alignment of magnetic particles, the strength of the TRM depends on the direction of the applied field. One way to partially correct for this is to align the laboratory field along the NRM direction (e.g., Aitken et al., 1984). However, this is not foolproof because the NRM in an anisotropic material is unlikely to be exactly parallel to the ancient field. A better way is to find the anisotropy tensor of the specimen, which can then be used to correct the ancient field estimate obtained from a Thellier-type experiment. It is largely agreed that anisotropy of magnetic susceptibility (AMS) is carried by grains which are larger than the remanence carrier and hence should not be used to correct for the anisotropy (Selkin et al., 2000). Anisotropy of ARM (AARM) and TRM (ATRM) have long been known to have very similar properties in single domain magnetite and are carried by the same grain fraction (Levi and Banerjee, 1976). While some authors eschew using AARM because of the widely held belief that AARM tensors are different from the ATRM tensors (Chauvin et al., 2000), others (e.g., Selkin et al., 2000; Ben-Yosef et al., 2008) have continued using AARM because of the purported similarity in the grain sizes of the remanence carrying population and the lack of additional alteration while heating at high temperatures. In order to resolve which of the two is more suitable for our sample set we decided to correct the data with tensors obtained from both the methods. The specimens were given an ARM (180 mT alternating field; 0.05 mT bias field) along 9 directions. A zero-field demagnetization step was inserted between each position and was used for baseline subtraction. Subsequently we conducted partial TRM anisotropy experiments at 520°C in six positions with an initial zero step which acted as the baseline. An additional step in the end was used to detect alteration. It is worth noting that all the specimens had at least 60% of the remanence fraction removed by 520 °C.

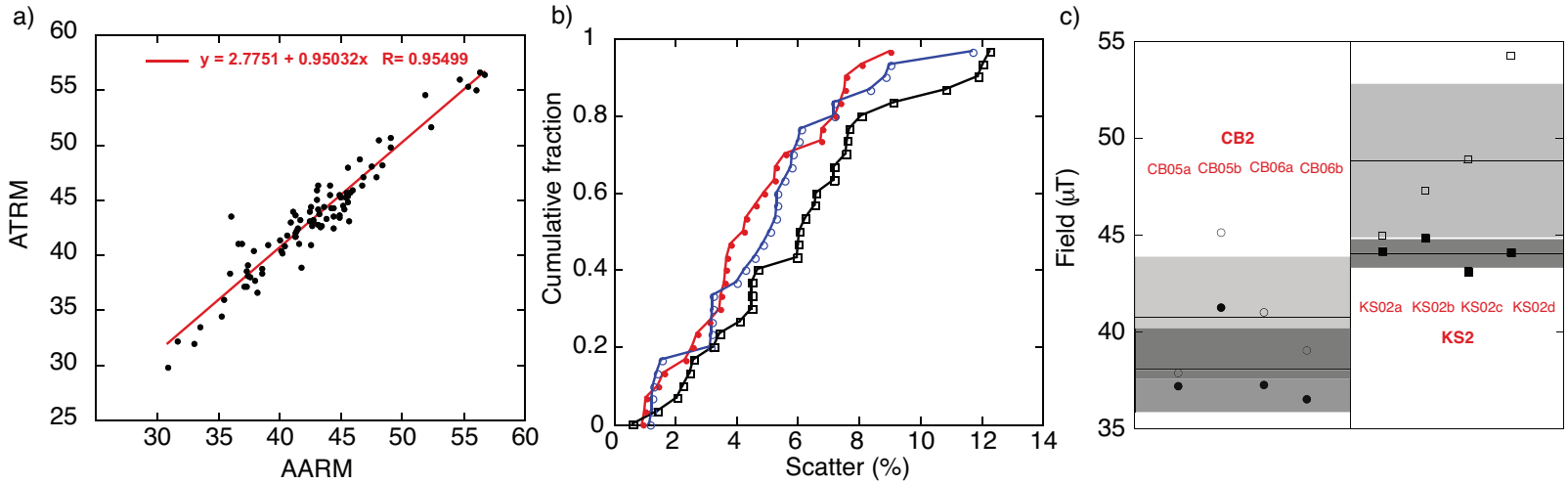


Figure 4.5: a) Correlation between ATRM and AARM corrected sample intensities. b) Cumulative distribution function of raw (black squares), ATRM corrected (blue open circles) and AARM corrected (red solid circles) intensities. Median values are 6.05, 4.98 and 4.03 respectively. Scatter is expressed as the percent relative standard deviation. c)Anisotropy correction using AARM tensors for two different sites. Open(solid) circles show uncorrected(corrected) specimen level intensity. Thin (thick) line and light (dark) grey area shows the site level mean and standard deviation of the uncorrected(corrected) specimens.

The specimen intensities corrected with the AARM and ATRM tensors showed a marked correlation (r=0.95) (Fig. 4.5a). Ideally, correction for anisotropy should be able to reduce the scatter at the sample level. Site level reduction in scatter should only be a natural consequence of this but is not inevitable because a single horizon may have potteries from considerably different periods of time. Therefore, in order to test which method is better, we plot the cumulative distribution of the sample level scatter (Fig. 4.5b). The within sample scatter in the raw data (black squares) improved with both the ARM tensors (red solid circles) and the TRM tensor (blue open circles) although the AARM has a lower median of 4.03% as opposed to 4.98% of the ATRM. The two were otherwise indistinguishable as revealed by a two sample Kolmogorov-Smirnov test with the test statistic, D=0.17, being less than the critical value of D, $D_{crit} = 0.35$, at 95% confidence level. We believe that the slightly (but insignificantly) higher scatter found in the ATRM corrected intensities could be a result of blocking temperature dependent anisotropy as was originally suggested by Aitken et al. (1981). If so, then if ATRM tensors are used to correct paleointensity, we recommend doing the experiments close to the maximum blocking temperature of the specimens.

For this study, we have shown the effectiveness of using either AARM or ATRM tensors for correcting anisotropy in specimens. Therefore, we report here specimen intensities that were corrected using the tensor obtained from AARM. The specimens in our study were found to be moderately anisotropic with ARM anisotropy degree (τ_1/τ_3) varying between 1.05 to 1.50 with 78% of the specimens yielding values less than 1.20. Correcting for anisotropy markedly reduced site level scatter in the data as specimens from different samples converged towards a mean value (examples shown in Fig. 4.5c).

4.3.3 Cooling-rate

Dodson and McClelland-Brown (1980) and Halgedahl et al. (1980) first

pointed out that if during cooling, an assemblage of single domain grains is allowed to equilibrate at a particular temperature for a longer period of time, it will acquire a higher magnetization. In other words, a magnetic assemblage in a slowly cooled system can maintain equilibrium with the field to a lower temperature before the magnetization gets blocked. In traditional paleointensity experiments the sample is cooled in the lab for typically less than an hour. Archeological artifacts could have taken anywhere from a few hours to a few days to cool. Because of the different cooling rates in the laboratory and the original environment, the same field could have induced a higher remanent magnetization when the artifact cooled in its ancient environment than when it cooled in the laboratory. Therefore, in a paleointensity experiment, where the laboratory field is multiplied by the ratio of ancient magnetization to laboratory magnetization to get an estimate of the ancient field, the ancient field strength would be overestimated.

Theoretical calculations have shown that for single domain magnetite, an order of magnitude of cooling rate difference gives rise to a 7% (Dodson and McClelland-Brown, 1980) to 10% (Halgedahl et al., 1980) overestimation. In other words, although for most ancient artifacts a cooling rate correction is mandatory, some uncertainty in the precise knowledge of ancient cooling time can be accommodated. This fact is especially useful because often the ancient cooling time depends on factors like the kind of oven (open hearth, pit etc.) and fuel (twigs, branches, leaves, coal etc.) and is often a matter of speculation. For example, in Fig. 4.6a, we see that even if an extreme misjudgment of cooling time was to occur and an ancient cooling time of two days was mistaken as six hours, the difference of overestimate is unlikely to be more than 5% for grains with low blocking temperatures. For grains with higher blocking temperatures this difference is expected to be even lower. This is also borne out by experimental studies where multiple cooling rates were used to account for the uncertainty of ancient cooling time (Hartmann et al., 2010).

In order to find the possible overestimates in our samples we have designed

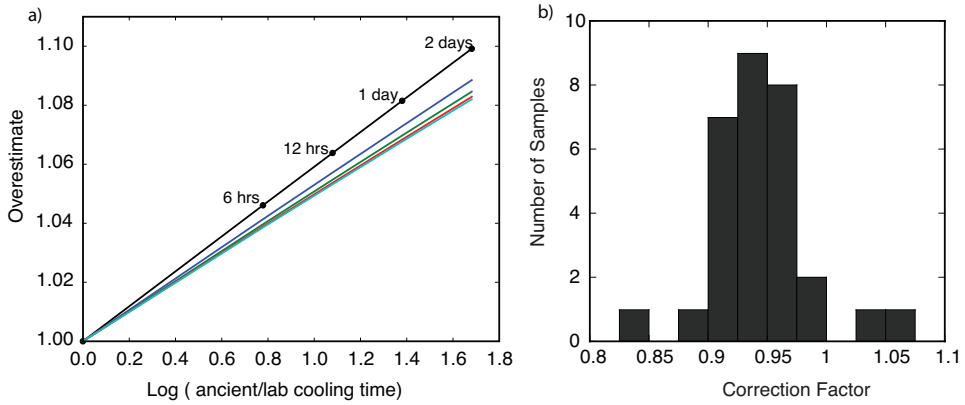


Figure 4.6: a) Predicted overestimates for SD magnetites having five grain sizes with axial ratio=1.6. Each line represents a single grain size with laboratory blocking temperatures of 308°C(black), 436°C(blue), 486°C(green), 512°C(red) and 528°C(cyan). Black dots show representative time intervals. E.g., a potsherd which was cooled in a furnace for 1 day is expected to overestimate the ancient field by 8% if it is found to unblock around 436°C in the lab. Calculations as in Halgedahl et al. [1980]. b) Histogram showing the correction factors for the specimens assuming a 10 hr cooling time.

a cooling rate experiment very similar to Chauvin et al. (2000) and Genevey and Gallet (2002). A sister sample was used from every potsherd. Three partial TRMs were measured from a high temperature. The temperature was high enough to cover the blocking temperatures of grains carrying at least 60 % of the remanence. In our experiments 525°C is an appropriate temperature for this purpose. The first experiment involved cooling for the normal laboratory time of 30 minutes (TRM_{fast1}). The second involved cooling at a slower rate. For this we turned off the cooling fan which gave us an exponential cooling from 520°C to 40°C in 10 hrs (TRM_{slow}). The third was exactly like the first (TRM_{fast2}) and the difference bewteen TRM_{fast1} and TRM_{fast2} was used to detect alteration. The correction factor is given by the ratio of the average of TRM_{fast1} and TRM_{fast2} to TRM_{slow}. The alteration cutoff was kept at 5%. The cooling rate correction of the samples varied between 0.85 to 1.05 with a median of 0.95 (Fig. 4.6b). A factor greater than unity could suggest the presence of interacting single domain or multi domain grains (McClelland-Brown, 1984).

4.3.4 Rock Magnetism

To identify the major magnetic mineral phases in the samples we carried out a three-axis IRM demagnetization experiment (Lowrie, 1990). Three DC pulse fields of 1.2 T, 0.4 T and 0.2 T were used. The samples were subsequently thermally demagnetized up to 600°C. Finally, hysteresis loops (peak field of 1T) were measured on these specimens. Together, these reveal varying contributions of different phases of magnetite and hematite.

The single most important remanence contributor in most of the samples had a low coercivity (<0.2 T) and distributed unblocking to maximum temperatures of 580°C were consistent with titanomagnetite as the remanence carrier (Fig. 4.7a). A typical hysteresis plot displays a narrow, saturated loop with hysteresis parameters ($0.5 > M_r/M_s > 0.05$ and $1.5 < H_{cr}/H_c < 5$ falling well within the PSD domain in Day plots (Day et al., 1977) (Fig. 4.7e).

In some samples, the presence of a harder component (>1.2T) with maximum unblocking above 600°C is indicative of somewhat higher contribution from hematite (Fig. 4.7b). The remanence contribution of this higher coercivity mineral in such samples is still secondary to the lower coercivity mineral. The hysteresis loop is constricted in the middle confirming the presence of two phases with different coercivities (Fig. 4.7f), presumably magnetite and hematite.

A totally different mineralogical makeup was evident in some samples (Fig. 4.7c,d,g,h). The goose-necked (sensu Tauxe et al., 1996) hysteresis loops showing non-saturation at 1 T with a heavily constricted middle indicate an equal or in some cases greater contribution of higher coercivity minerals (Fig. 4.7g,h). The IRM demagnetization experiments supported these observations (Fig. 4.7c,d). The medium and high field components showed a marked unblocking between 200 and 250°C. This component carried the bulk of the remanence in these specimens. Goethite which although has a very high coercivity of > 5T (Roberts et al., 1995) has a maximum unblocking temperature of 120°C (Strangway et al., 1968) and is

therefore not a suitable candidate. Even dehydration of goethite to form a more stable phase of hematite as suggested by Roberts et al. (1995) is unlikely because of the remarkable stability shown by specimens from the same samples in the paleointensity experiments. We therefore believe these minerals to be similar to those found by McIntosh et al. (2011, 2007) where they showed widespread occurrence of minerals with similar rock magnetic properties in archeological artifacts collected from 12 European countries. They called this mineral phase HCSLT, an acronym for High Coercivity, thermally Stable, Low unblocking Temperature phase. Ubiquitous in most archeological samples (Hartmann et al., 2010; McIntosh et al., 2011) these are yet to be identified unambiguously but possibilities such as hemoilmenite, ferri-cristobalite or a substituted hematite are currently being considered (McIntosh et al., 2011).

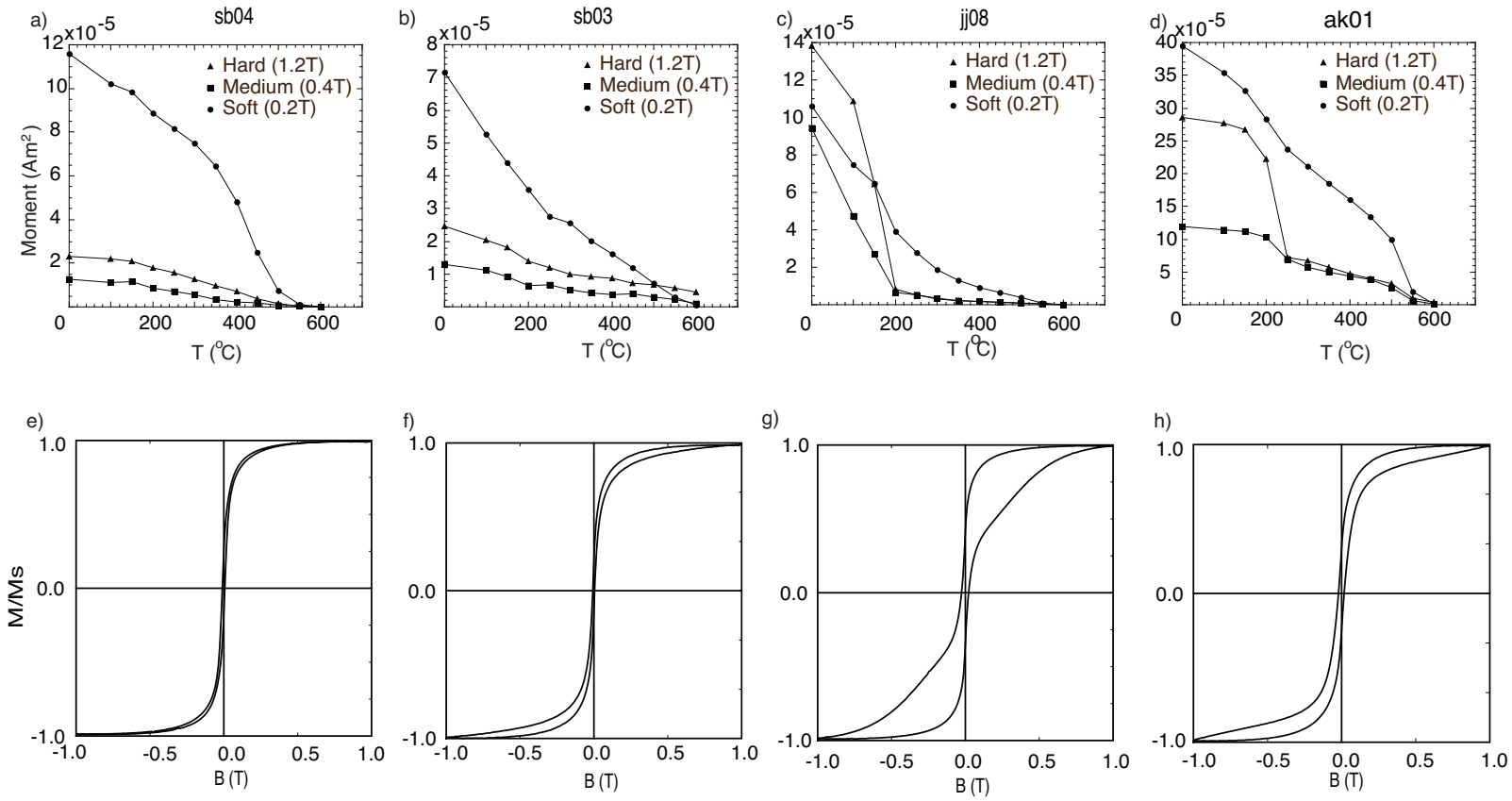


Figure 4.7: Rock magnetic measurements on sister specimens from samples which yielded successful paleointensities. a-d)Three component IRM demagnetization experiments. e-h) Hysteresis loops of the same specimens at 1T after heating.

4.4 Discussion

Africa is a large continent with limited archeointensity data. In the northern hemisphere it has a latitudinal extent of 37° from the equator and a longitudinal extent from 17°W to 51°E. In the last three millenia we have only 74 paleointensity estimates from the region (http://geomagia.ucsd.edu). Most of these come from Egypt and Morocco and all of these estimates are from latitudes greater than 25°N latitude. Our data from West Africa are the first to be reported from a lower latitude (∼15°N). Coupled with other studies from Africa, mostly from Egypt and few from Morocco, it helps us to reconstruct the geomagnetic field evolution in Africa between 1000 BCE to 1000 CE.

Data from Aitken et al. (1984) show that the field increased from present day values to 1.6 times that value during 1500 BCE to 1000 BCE (Fig. 4.8). Our data show that the field could have dropped after that, between 1000 BCE and 600 BCE. We had no successful samples between 500 to 0 BCE. Results from Hussain (1987) show that the field might have reached a value as high as twice that of the present day field near 500 BCE. The rapid decline of the field during the first half of the first millennium CE is quite evident in our results. An interesting feature of our data is the marked cusp observed around 300-500 CE when the field was as low as the present field. Leonhardt et al. (2010) also found a decisive low during this period from Egyptian ceramics. Walton (1984, 1990) and Walton and Balhatchet (1988) found similar low values from Greece. Western European data also suggest a low around 250 CE (Chauvin et al., 2000). Similar low values are also observed in the Levantine curve of Ben-Yosef et al. (2008). The broad picture arising out of these disparate datasets is that of a pronounced low over Europe and the northern part of continental Africa between 300 - 500 CE. In the global context we find no evidence for this (see Fig. 9 in Genevey et al., 2008) that suggests that the marked low around this period is likely to be a regional feature.

The high scatter observed in the Egyptian data (black symbols in Fig. 4.8)

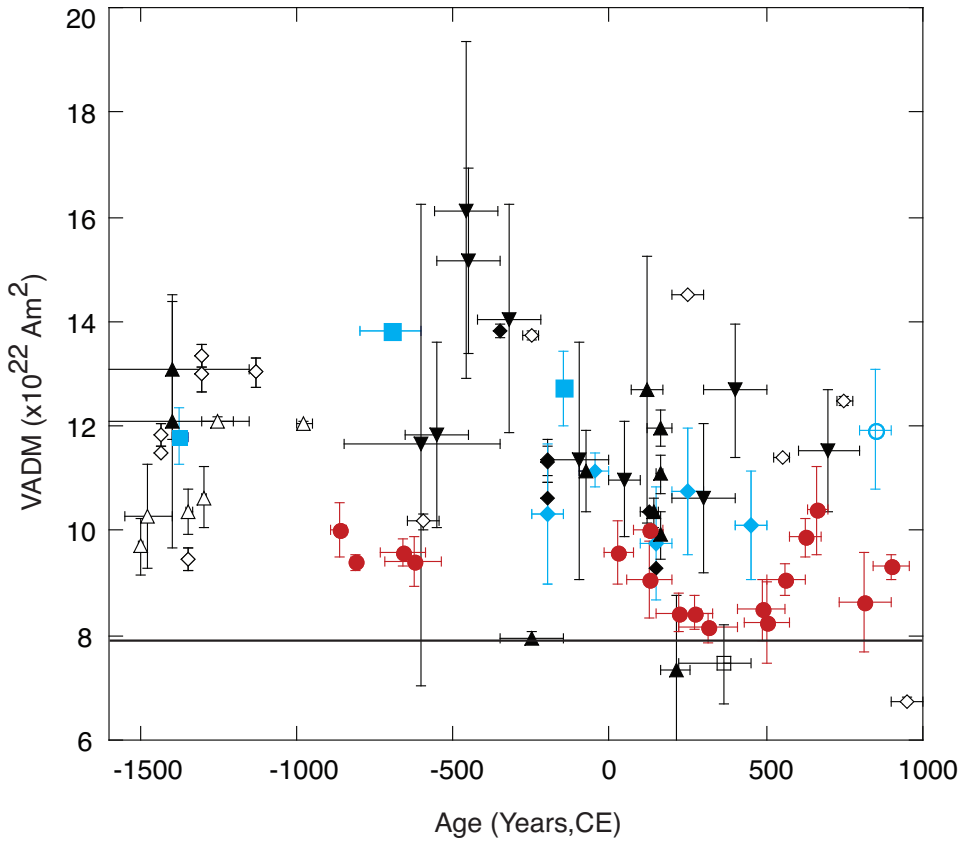


Figure 4.8: Collection of data from continental Africa for the period 1500 BCE to 1000 CE. The data are from Morocco (blue symbols) and Egypt (black symbols). Symbols are for different studies: Aitken et al. (1984)(open triangle), Odah (1999)(closed diamond), Thellier (1959)(blue solid square), Odah et al. (1995)(open diamond), Kovacheva (1984) (blue solid diamond), Hussain (1983)(up solid triangle) , Hussain (1987)(down solid triangle), Leonhardt et al. (2010)(open square), Gomez-Paccard et al. (2012)(blue open circle). Horizontal line shows present day IGRF field at Mali converted to VADM. Our data are shown as solid red circles. Geomagia database (Korhonen et al., 2008; Donadini et al., 2009) was queried and only experiments using a double-heating paleointensity technique were included. Aitken et al. (1989) show up in this search query but the sites are from an unspecified location near Iraq and was therefore excluded.

and the paucity of data from West Africa (blue symbols) make it difficult to draw strong conclusions. The scatter observed in the Egyptian data has been previously discussed in Leonhardt et al. (2010). They attributed this to experimental techniques in general which were ill equipped to detect errors arising from difference in cooling rates, anisotropy, multi-domain grains and undetected alteration of the samples. Data from Morocco provides an interesting perspective - they plot higher than our data for all contemporaneous periods. This is unlikely to be a result of systematic and undetected experimental error because three different studies with very different experimental controls (Thellier, 1959; Kovacheva, 1984; Gomez-Paccard et al., 2012) report similar results. Morocco is located 2000 km north of Mali and Senegal. Therefore it is possible that there is a significant latitudinal gradient in the field intensities which cannot be explained by an axial-dipole. This would also suggest that the very high values of Hussain (1987) could well be a true geomagnetic signal, because the sites were located east of Cairo (30°N, 31°E), at a latitude similar to the sites from Morocco. In spite of that, the scatter observed in the site estimates could indeed be as speculated in Leonhardt et al. (2010).

Our data generally agree well with the global CALS3K.4 model (Fig. 4.9) with a few exceptions (JJ6, SB3, and JJ7). The predicted range from 35 μT to 43 μT for the region is in close agreement with our data. It is important to note that although the sites from Mali and Senegal are separated by 1000 km, neither the CALS3K.4 predictions nor the data show significant differences in the two regions. The close agreement between the model and our data in general allows us to infer that during the period where we have no data viz., 500 BCE to 0 CE, the field likely increased but not to the extent observed in Hussain (1987). This suggests that the field could have been different in Northern Egypt during this time. To estimate the magnitude of the difference in intensity of the field which cannot be explained by an axial dipole we make use of VADM predictions from the CALS3K.4 model (Fig. 4.10a). Model results for four different locations separated

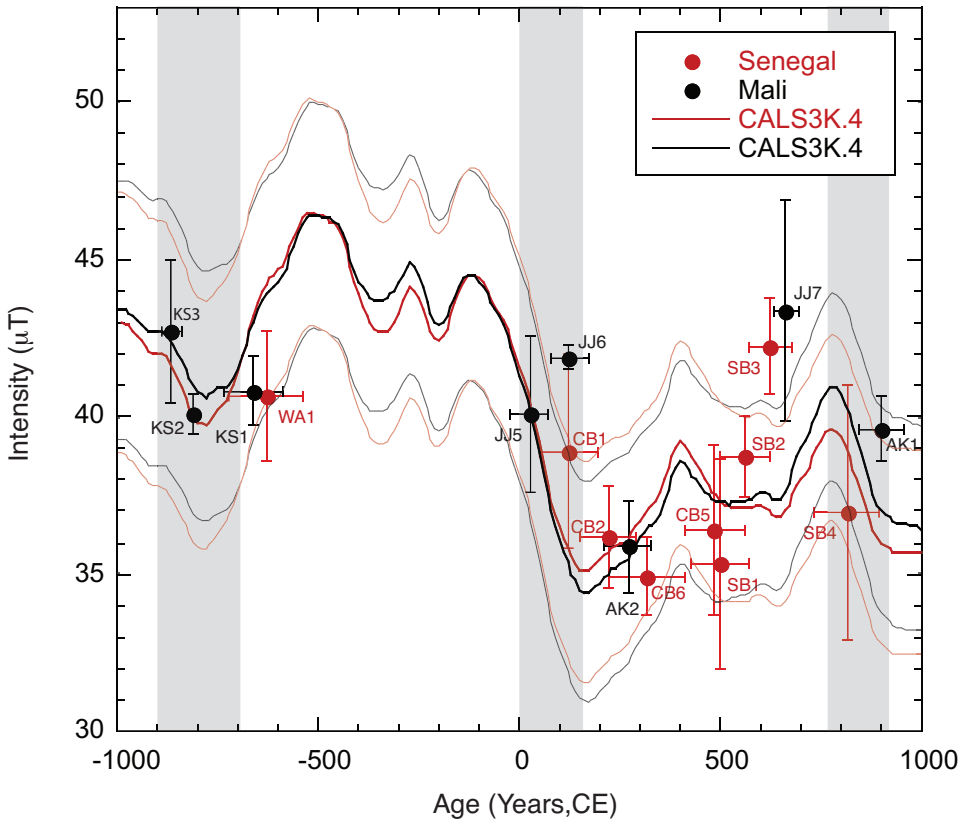


Figure 4.9: Intensities from Senegal and Mali and corresponding CALS3K.4 model predictions. Grey bars show "archeomagnetic jerk" periods of Gallet et al. (2003).

either longitudinally or latitudinally were used to estimate the median differences expected in VADM estimates within Africa. The latitudinal gradient of the field is predicted by CALS3K.4 to be ∼3.5% for every 10° but the longitudinal gradient would be much lower at ∼0.4% for a similar distance. More towards the east this gradient increases to ∼2%.

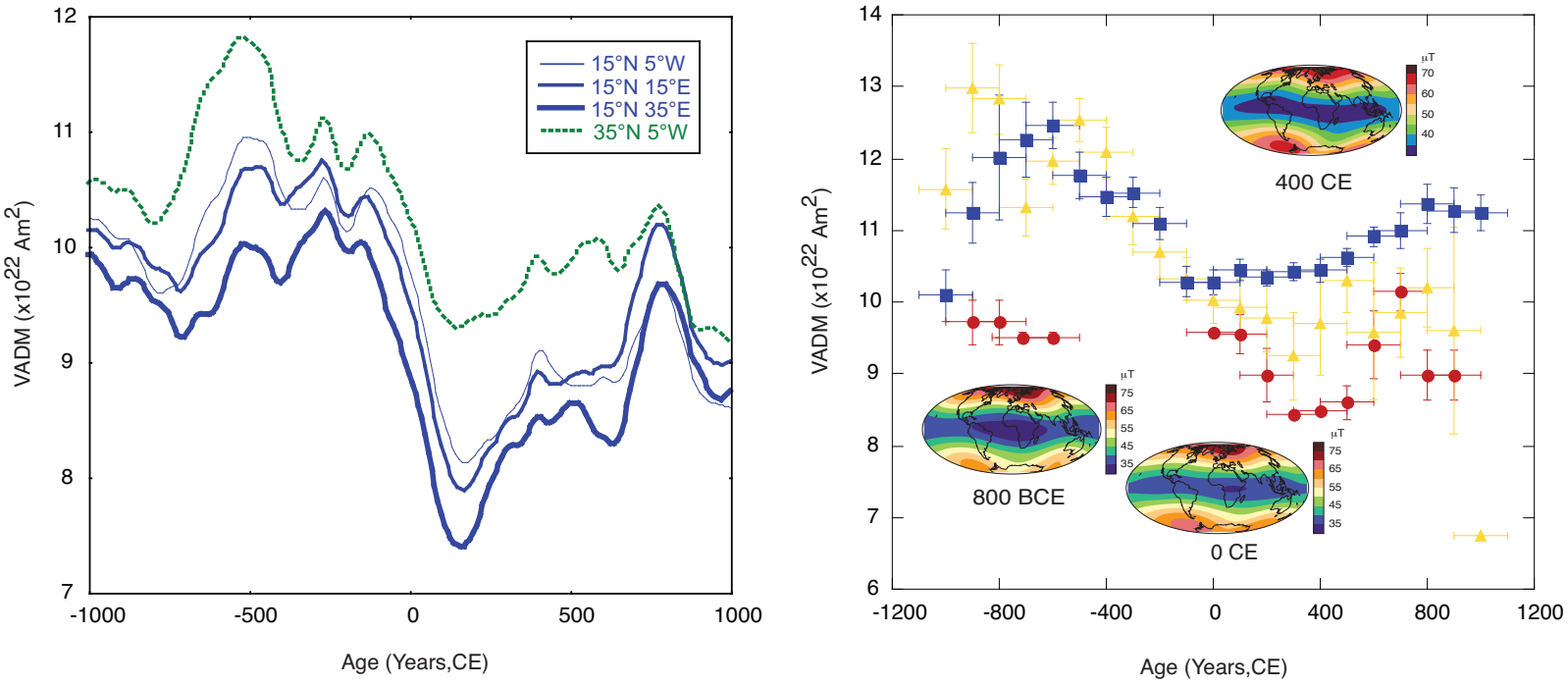


Figure 4.10: a) CALS3K.4 predictions for four different locations in Africa. b) Average VADM curves for 60°N to 40°N (blue squares), 40°N to 20°N (yellow triangles) and 20°N to 0 ° (red circles). The longitudinal extent of the data is between 20°W and 60°E. A 200 yrs moving window shifted by 100 yrs was used for the analysis. We used GEOMAGIA database (Korhonen et al., 2008; Donadini et al., 2009) and only paleointensity estimates obtained with a double-heating protocol were included in the analysis. Standard error is plotted on the y-axis and a fixed error of 100 yrs on the x-axis. Insets show the CALS3K.4 predictions at the surface for different periods in time.

In order to evaluate how the raw data from Africa compare with those from Europe we compiled average VADMs from different latitudinal bands (Fig. 4.10b). We have used the GEOMAGIA database (Korhonen et al., 2008; Donadini et al., 2009) and included only those data that were obtained with a double heating experimental protocol spanning the longitudinal band of 20°W to 60°E. An obvious problem with such a comparison is the extreme heterogeneity in sampling of the respective latitudinal bands. While the region between 40°N and 60°N has 690 intensity estimates (blue squares), the region between 20°N and 40°N has only 293 estimates (yellow triangles). This also explains the considerably smaller standard errors in the former. The southern-most 20° band, from 0° to 20°N, happens to be the least studied and this study is the only source of data (red circles). In spite of this heterogeneity some interesting observations can be made. Post 0 CE we find an increasing divergence in VADMs from the different latitudinal bands. African intensities are consistently lower than those from the more northerly and largely European data. Such a systematic variation in VADMs indicates a strong non-axial-dipolar contribution. Prior to 0 CE we see little evidence of such a difference, at least up to 500 BCE. Between 1000 BCE and 500 BCE, VADMs from 0°N to 20°N plot considerably lower than the other two latitudinal bands. A possible reason for the very high VADMs of 20°N to 40°N (yellow triangles) could be because of the sampling bias introduced by the Ben-Yosef et al. (2008) dataset. Ben-Yosef et al. (2008) sampled a very high resolution section viz., a slag mound. Multiple samples from the same slag mounds yielded 17 intensity estimates ranging from 11.02 to 25.08x10^{22}Am^2. When the same calculation was done with an average of these intensity estimates (14.83x10^{22}Am^2), instead of the 17 estimates, the VADMs for 900 and 800 BCE dropped lower to 11.34x10^{22}Am^2 and 11.75x10^{22}Am^2 respectively. Therefore, even after accounting for the possible bias, we do not see any significant difference in the VADMs from 40°N to 60°N (blue squares) and 20° to 40°N (yellow triangles) but both are considerably higher than the VADMs from 0° to 20°N (red circles). We can therefore conclude that

with the currently available data, significant non-axial-dipolar contributions are fairly evident from 0 CE to 1000 CE and possibly existed between 1000 BCE to 500 BCE as well.

The evidence for significant non-axial-dipolar contributions in this region also comes from the radial field simulation at the core mantle boundary by the CALS3K.4 model. It shows the presence of a persistent but highly mobile flux patch in this region, between 1000 BCE to 1400 CE (http://earthref.org/ERDA/1478/). The rate of drift in these flux patches could be as high as $\sim 0.2^{\circ}$ per year (Amit et al., 2011). As a consequence of this, the field at the surface of the earth would also show significant departure from axial-dipolar structure. For example, at 800 BCE and 400 CE we see that the time averaged field was considerably non-axial-dipolar in nature. Compared to that, the structure of the field at 0 CE was more axial-dipolar (Fig. 4.10).

A region influenced by such an oscillating flux patch can be argued to undergo rapid field changes on a spatial scale smaller than expected otherwise. A possible manifestation of such a drifting flux patch then, could be offset intensity highs from neighboring regions. For example, Fig. 4.9 shows the regions where Gallet et al. (2003) found rapid changes in field intensities, the so-called "archeomagnetic jerks". In our data we see a distinct offset of the peak defined in both Senegal and Mali by the highs SB3 and JJ7 as well as the flanking lows SB4 and AK1. One way of reconciling the two highs would be to ascribe the observed differences in the data to age uncertainties; either our samples suffer from old wood effects, i.e., the dated charcoals come from extraordinarily thick branches, or the archeological material used in Gallet et al. (2003) had to be from an archeological context older than that of its surroundings. Neither of these explanations seem plausible in our case. Exactly the same age offsets from the sites, viz., SB3 and JJ7 separated by 1200 km (see Fig. 4.9) indicates that old wood effect is unlikely to be the cause. Furthermore the radiocarbon dates coupled with stratigraphy and detailed pottery phase associations of our samples make the dating more robust

than would have been possible from using using any of them independently. The pottery fragment used in Genevey and Gallet (2002) was from a well-dated production site. Such associations, by their very nature, limit the possibility of the pot sherds being from an older context. We therefore argue that the offset we see is likely to be a geomagnetic feature.

4.5 Conclusion

We have provided well constrained archeointensity results from West Africa. The field varies between 35 μT and 43 μT and defines a decisive low around 300-500 CE. The data provide the first set of paleointensity estimates from Africa between 0 to 20°N. We do not see a marked difference between data from Senegal and Mali which are nearly at the same latitude and separated by 9° of longitude. The global CALS3K.4 model predicts a stronger gradient across the latitudes than the longitudes. This study provides experimental support for the model prediction - our data are significantly lower than those from Morocco (20° farther north). The CALS3K.4 model predicts a ∼3.5% difference for every 10° latitudinal separation. In the western part of Africa the longitudinal differences in intensities are minimal (also found in our study), amounting to ∼0.4% for every 10° of longitudinal separation. Further eastward this increases to ∼2% for the same longitudinal span.

Significant non-axial-dipolar components are also evident when we compare African and European data. The CALS3k.4 model, which is based on a global compilation of all the available data, shows the presence of a persistent and highly mobile flux patch at the core-mantle boundary between 1000 BCE to 1400 CE. We find further evidence of the flux patch in a pair of intensity highs observable in the dataset; a noticeable peak in intensity, observed in both Senegal and Mali is found considerably offset from the 'archeomagnetic jerk' at 800 CE (Gallet et al., 2003). We speculate that such asynchronous peaks should be more common in such regions and discovering them is critically dependent on the continuity of the

archeomagnetic dataset and proper age control. Archeomagnetic data by their very nature are discrete and discontinuous. Uncertainty in the age is usually a few hundreds of years. Together, these can be very effective in hiding true offsets in intensity highs in neighboring regions. It is therefore desirable to pay very close attention to the age control in any archeomagnetic study.

The substantial difference in VADMs observed in Africa and the offset intensity highs are a reminder of how restricted the reach of regional archeomagnetic curves for the purpose of dating can be. A corollary of that would be to not attribute offset intensity peaks/troughs in regional curves from adjacent regions to age uncertainties. The possibility of offset peaks/troughs being true geomagnetic features, controlled largely by the growth and decay of flux patches, should also be investigated. Additionally this study also shows that the scatter observed in compilations of archeomagnetic records from a region could be, in part, a telltale signature of true geomagnetic field variability.

4.6 Acknowledgement

We thank the NSF Arizona AMS laboratory for the fast processing of seven radiocarbon samples. The ^{14}C dates corroborated and supplemented the pre-exisiting archeological database. We thank Jason Steindorf for his help in the laboratory. RM thanks Ron Shaar for his thoughtful comments on many aspects this study. The authors thank Jeff Gee and Cathy Constable for their comments which greatly improved the quality of the manuscript. Part of this work has been funded by the NSF grants EAR 0944137 and 1013192 to LT.

Chapter 4, in full, has been submitted to Earth and Planetary Science Letters as: Mitra, R., Tauxe., L. and McIntosh, S.K., Two thousands years of archeointensity from West Africa. The dissertation author was the primary investigator and author of this paper.

4.7 Supplementary Material

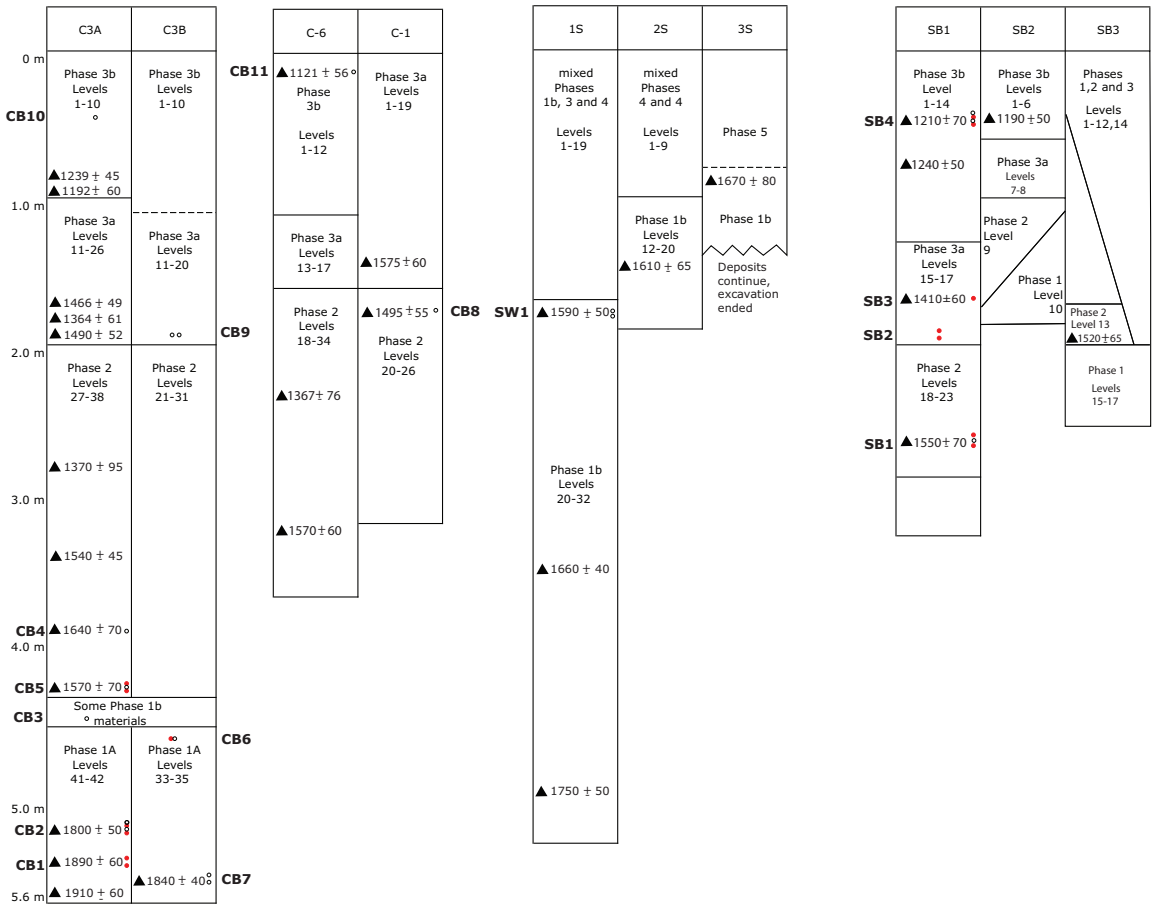


Figure 4.11: Stratigraphy of Cubalel, Siwré and Sincu Bara units. For simplicity, phases have been numbered without reference to their respective sites; eg., Phase CUB/S II (in the main text) is simply written as Phase 2 in the respective units. Units 2S, 3S, SB2 and SB3 yielded only charcoal samples for the current study. Triangles show radiocarbon samples and the corresponding uncalibrated date (BP). Solid red (Open black) circles shows samples at their excavation depths that passed (failed) the selection criteria of the paleointensity experiments. The paleomagnetic site names are recorded beside the samples.

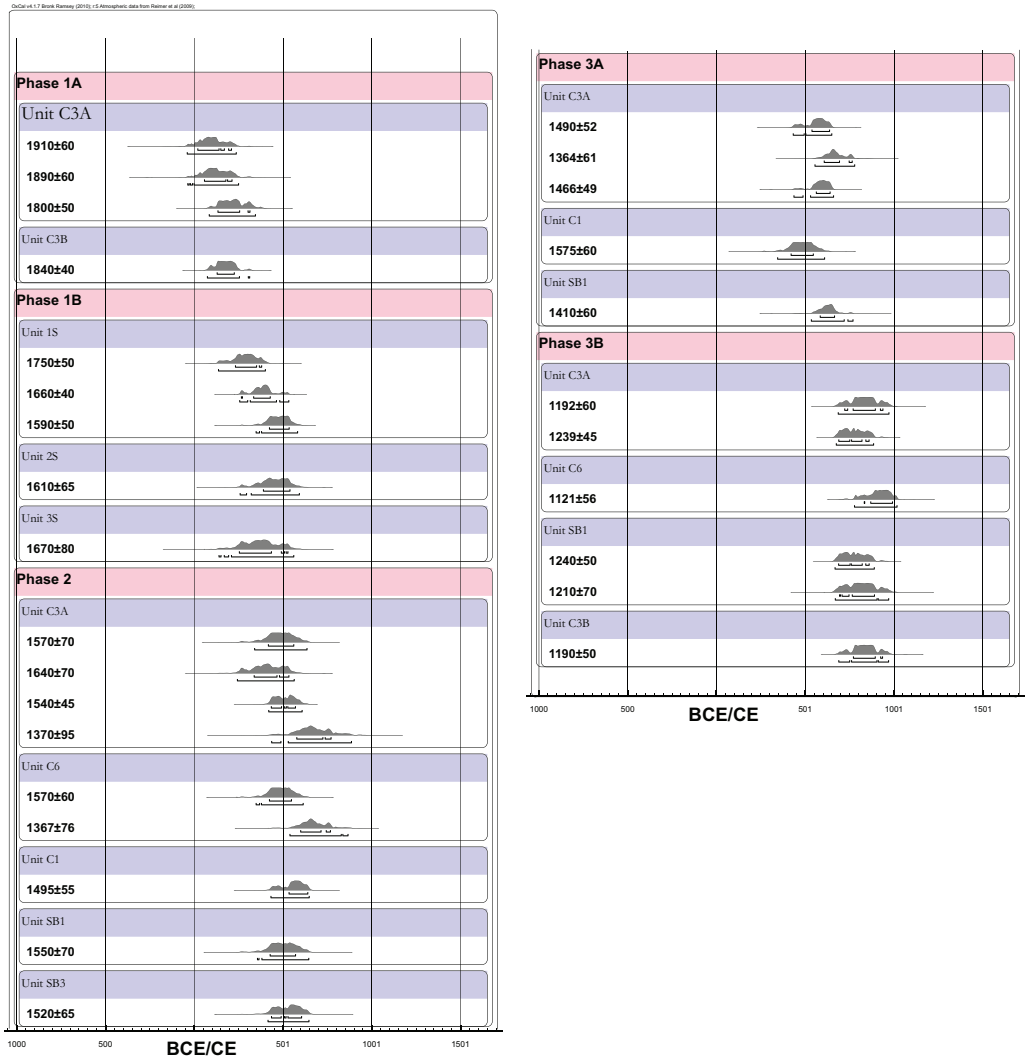


Figure 4.12: Calibrated radiocarbon dates from all the charcoal samples shown in Fig. 4.11. Uncalibrated ages of the charcoals are reported in the column and the corresponding output age distributions with 1- and 2-sigma brackets. Oldest dates appear at the top. Units (in blue) have dates ordered according to stratigraphic heights from which the charcoal samples were collected. The same pottery phase (in pink) could be found across multiple units hence many units can be part of the same phase. Since no information is available regarding the stratigraphic ordering of samples across the units, arrangement of units within a phase are arbitrary. For example, unit C3A has four dates from charcoals found associated with pottery showing distinct Phase 2 characteristics. Being in the same unit they could be stratigraphically ordered. But other Phase 2 potteries from units C1, SB1 and SB3 are listed under their respective units without any hierarchical significance.

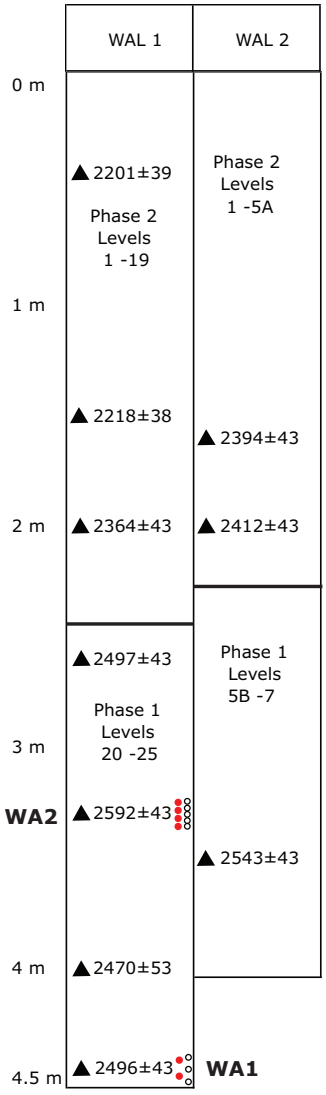


Figure 4.13: Stratigraphy of Walalde units. WA2, which was successful in the PI experiments (see Table 4.3) had contradicting stratigraphic and radiocarbon information and hence was not included in our study. Symbols have the same meaning as in Fig. 4.11.

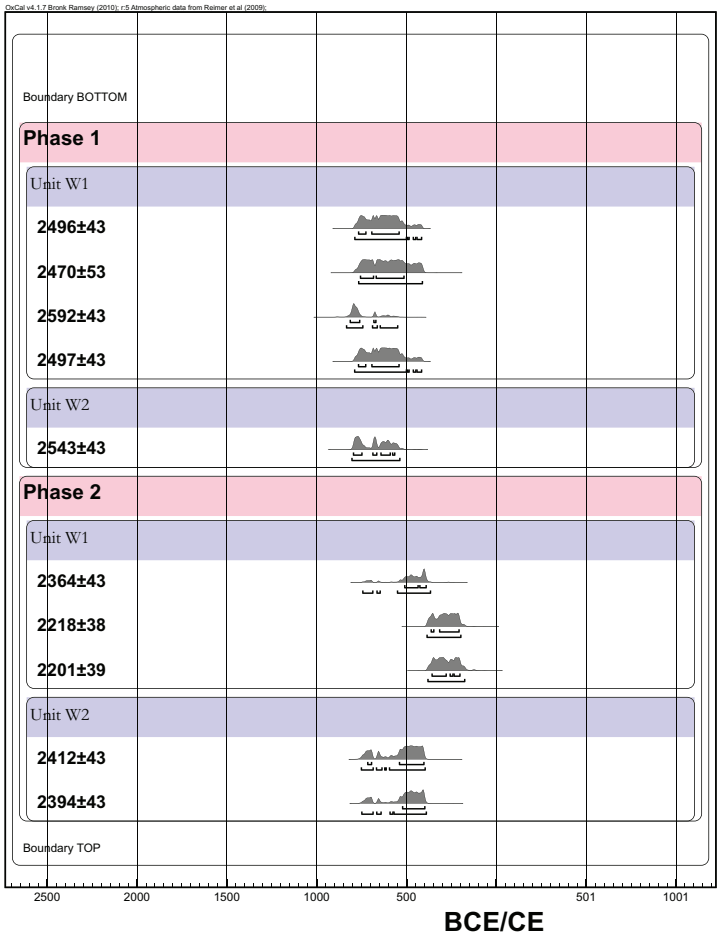


Figure 4.14: Calibrated radiocarbon dates from all the charcoal samples shown in Fig. 4.13. Convention as in Fig. 4.12.

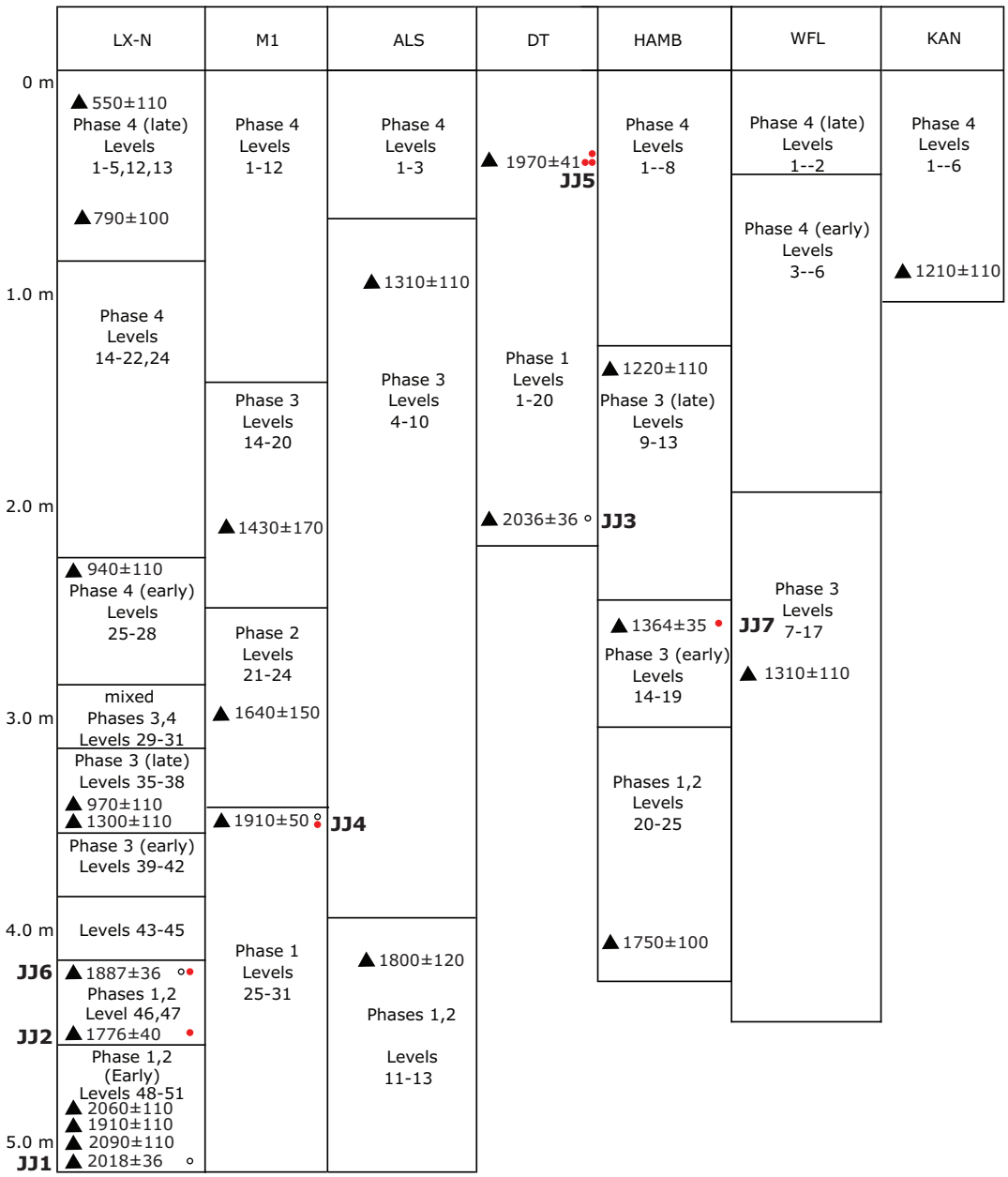


Figure 4.15: Stratigraphy of Jenné-Jeno and Hambarketolo units in Mali. Symbols have the same meaning as in Fig. 4.11. JJ2, which was successful in the PI experiments (see Table 4.3) had contradicting stratigraphic and radiocarbon information and hence was not included in our study. Units ALS, WFL and KAN yielded only charcoal samples that were used for the chronology.

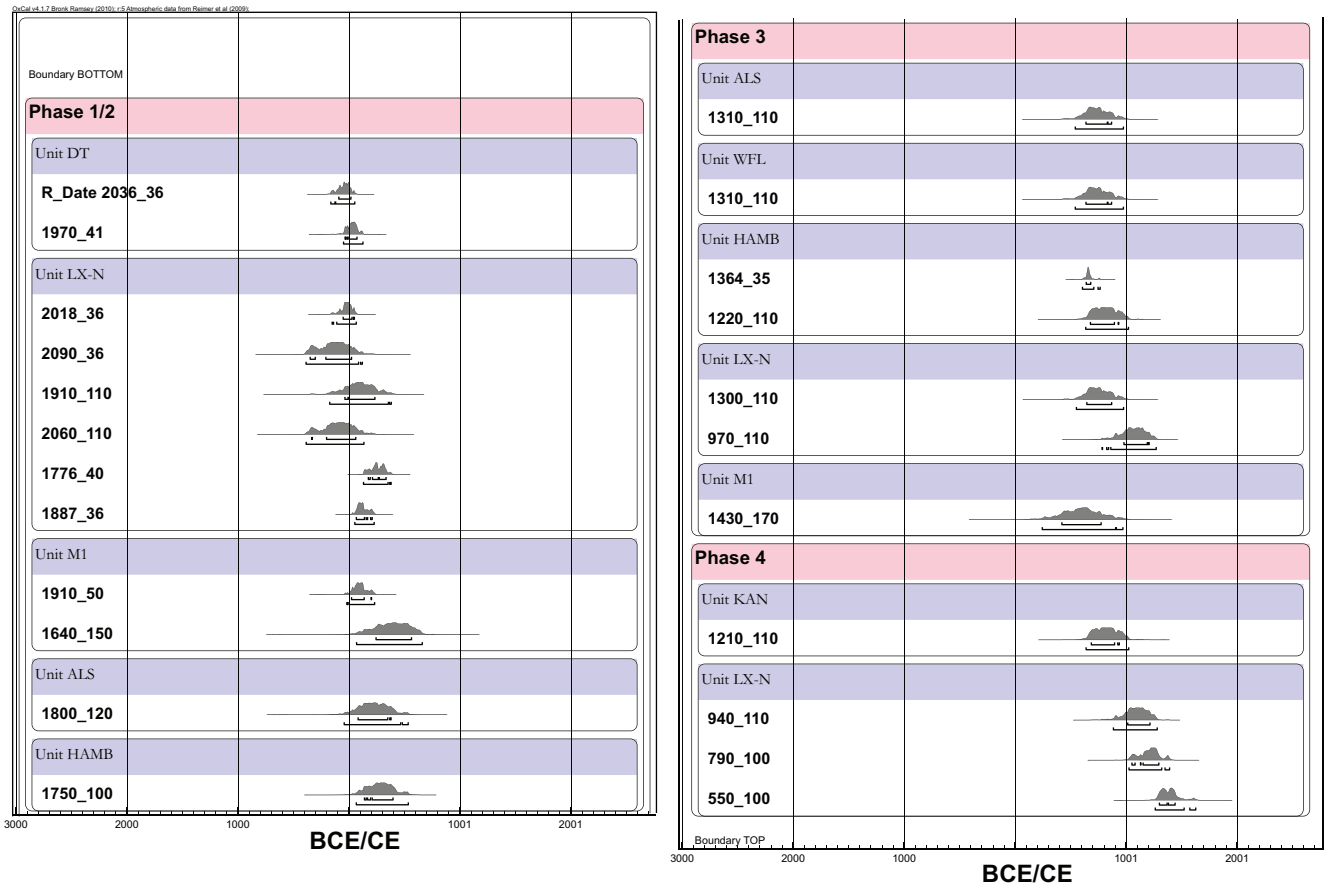


Figure 4.16: Calibrated radiocarbon dates from all the charcoal samples shown in Fig. 4.15. Convention as in Fig. 4.11.

Table 4.3: Paleointensity parameters of specimens selected for site level estimates. Z , the zig-zag parameter of Tauxe (2010). β, F_{coe} and Q as in Coe et al. (1978). F_{vds}, DANG and DRATS as in Tauxe and Staudigel (2004). MAD as in Kirschvink (1980). N is the number of double-heating steps used to constrain the paleofield estimate and T represents the corresponding temperature range.

Site Name	Specimen Name	Z	β	DANG	DRATS	F_{coe}	F_{vds}	Intensity (T)	MAD	N	Q	T(°C)
SB1	sb02a	1.4	0.036	0.7	2.1	0.656	0.719	3.52E-05	1.6	8	15.3	200-520
	sb02c	0	0.06	2.4	3.1	0.724	0.733	3.36E-05	3.7	8	10.2	200-520
	sb03a	1.5	0.029	2.5	7	0.583	0.647	4.39E-05	4.4	8	16.5	250-540
	sb03c	0	0.009	1.2	1.7	0.744	0.757	3.94E-05	1.7	9	73.7	300-585
SB2	sb05a	1.1	0.037	4.4	0.1	0.901	0.872	4.46E-05	4	10	20.8	100-540
	sb05b	1.3	0.025	2.3	2.5	0.897	0.868	4.29E-05	3	10	30.6	100-540
	sb05c	0	0.042	1.5	0.5	0.911	0.862	4.22E-05	2.1	10	18.7	100-540
	sb05d	0	0.029	0.4	9.3	0.93	0.909	4.32E-05	3.2	10	26.7	0-520
	sb06a	0	0.023	0.7	6.1	0.681	0.682	3.47E-05	2.5	9	24.7	300-585
	sb06c	0	0.059	1.4	7.8	0.75	0.744	4.25E-05	4.6	11	11.1	250-560
SB3	sb04a	0	0.012	0.2	1.3	0.856	0.859	4.62E-05	1.6	11	60.7	100-560
	sb04b	0	0.018	0.2	2.4	0.709	0.707	4.28E-05	3.7	9	33.5	100-560

Continued on next page

Table 4.3 – Continued from previous page

Site Name	Specimen Name	Z	β	DANG	DRATS	F_{coe}	F_{vds}	Intensity (T)	MAD	N	Q	T(°C)
	sb04c	0	0.032	0.5	1.3	0.894	0.875	4.64E-05	4	11	24.3	100-560
	sb04d	0	0.016	0.6	6.5	0.886	0.893	4.34E-05	2.6	11	46.7	100-560
	sb04e	0	0.022	1.3	5	0.926	0.888	4.29E-05	3.3	11	36.7	100-560
SB4	sb07a	1.2	0.018	1.3	2.6	0.942	0.963	4.43E-05	2.1	13	48	0-585
	sb07b	0	0.025	1.8	3.8	0.957	0.902	3.83E-05	5	12	34.8	100-585
	sb07c	0	0.014	1.7	1.3	0.841	0.812	4.18E-05	2.2	11	54	200-585
	sb08c	0	0.016	3.5	0.4	0.953	0.934	3.28E-05	5	12	54	100-585
	sb08w	0	0.053	2.9	4.9	0.887	0.863	3.35E-05	3.8	10	14.2	200-600
	sb08x	0	0.045	4.9	2.7	0.842	0.81	2.99E-05	4.9	10	15.7	200-600
WA1	wa08a	0	0.019	1.2	2.2	0.929	0.838	0.000045	4.7	12	42.7	100-585
	wa08b	0	0.049	1.9	9.4	0.92	0.826	0.0000428	4.9	10	16.6	100-540
	wa08x	0	0.025	1.2	1	0.888	0.829	0.0000434	4.6	10	30.9	200-600
	wa12a	0	0.016	1	4.6	0.643	0.706	0.0000463	1.7	9	34	200-560
	wa12b	0	0.018	1.5	8.3	0.627	0.678	0.000046	2.1	9	29.7	200-560
	wa12c	1.5	0.03	3.1	7.5	0.563	0.604	0.0000434	5	8	15.8	200-540
	wa12d	1.2	0.036	1.8	7.5	0.59	0.631	0.0000422	2.1	8	13.8	200-540

Continued on next page

Table 4.3 – Continued from previous page

Site Name	Specimen Name	Z	β	DANG	DRATS	F_{coe}	F_{vds}	Intensity (T)	MAD	N	Q	T(°C)
WA2	wa02w	2.9	0.057	1.5	4.7	0.868	0.83	0.0000566	2.4	8	13	200-540
	wa02x	0	0.018	1	9.5	0.893	0.863	0.0000549	2.3	10	41.5	200-600
	wa16a	0	0.029	2.3	2.2	0.771	0.76	0.0000452	3.2	8	22.4	200-540
	wa16b	0	0.024	0.6	9.4	0.903	0.916	0.0000496	0.9	10	32.3	200-600
	wa16c	0	0.027	1.7	9.1	0.882	0.869	0.0000471	2.3	9	27.1	100-540
	wa16d	0	0.023	0.7	9.2	0.775	0.743	0.0000448	3.2	8	28.3	200-540
	wa18a	1.1	0.021	0.1	9.9	0.835	0.895	0.0000563	0.9	10	34.4	200-600
	wa18b	1.5	0.017	0.6	0.5	0.827	0.879	0.0000658	1.8	10	42.6	200-600
	wa18c	0	0.019	0.4	8.4	0.731	0.828	0.0000617	2.7	9	32.9	250-600
	wa18d	0	0.024	1.2	9.8	0.706	0.816	0.0000668	2.5	9	24.3	250-600
	wa19a	1.5	0.045	2.6	0.6	0.748	0.758	0.0000452	2.9	9	14.2	250-600
	wa19b	0	0.039	1	3.2	0.661	0.672	0.0000409	4.8	8	13.7	300-600
CB1	cb01a	1.3	0.018	3.9	6	0.86	0.62	0.0000436	4.7	11	41.3	200-585
	cb01b	2.3	0.023	0.3	2.7	0.876	0.883	0.0000468	1.1	11	33.5	200-585
	cb01c	1.3	0.025	1.1	4.2	0.838	0.805	0.0000475	2.7	11	30.1	200-585
	cb02a	0	0.02	1.4	5.1	0.774	0.715	0.0000445	3.4	9	32.8	300-585

Continued on next page

Table 4.3 – Continued from previous page

Site Name	Specimen Name	Z	β	DANG	DRATS	F_{coe}	F_{vds}	Intensity (T)	MAD	N	Q	T(°C)
	cb02c	0	0.013	0.7	2.5	0.722	0.67	0.0000381	0.9	9	48	300-585
CB2	cb05a	0	0.029	2.4	0.1	0.727	0.705	0.0000379	4.9	9	21.8	200-540
	cb05b	0	0.031	1.9	1.5	0.815	0.816	0.0000451	4.4	10	22.7	200-560
	cb06a	0	0.018	1.7	1.7	0.82	0.739	0.000041	3.2	11	40.8	200-585
	cb06b	0	0.021	1.1	3.8	0.955	0.956	0.0000391	2.2	12	41.7	100-585
CB5	cb09a	1.3	0.04	1.1	4.8	0.589	0.676	0.0000458	3.2	7	12.2	400-585
	cb09b	1.4	0.024	2.1	4.3	0.676	0.745	0.0000392	4.5	8	24.1	350-585
	cb09w	0	0.015	1.7	2.8	0.615	0.725	0.000042	2.7	6	31.3	400-600
	cb09x	0	0.021	0.2	2.1	0.606	0.711	0.0000482	2.8	6	22.1	400-600
CB6	cb12a	0	0.012	1	0.6	0.726	0.739	0.0000387	1.2	10	50.8	250-585
	cb12b	0	0.017	2.8	1.2	0.829	0.615	0.0000352	5	11	41	200-585
	cb12w	0	0.01	1.7	1.7	0.781	0.806	0.0000348	2.5	8	65	250-560
	cb12x	1.5	0.017	1.3	3	0.745	0.824	0.0000337	3.2	8	36.5	250-560
JJ2	jj03a	0	0.032	4.5	8.8	0.622	0.624	3.48E-05	4.7	9	16.5	200-560
	jj03b	0	0.041	2.5	8.9	0.605	0.77	4.07E-05	2.9	9	12.9	200-560
	jj03c	0	0.032	2	6.6	0.631	0.674	4.67E-05	2.9	8	16.7	200-540

Continued on next page

Table 4.3 – Continued from previous page

Site Name	Specimen Name	Z	β	DANG	DRATS	F_{coe}	F_{vds}	Intensity (T)	MAD	N	Q	T(°C)
	jj03d	0	0.028	2	9.7	0.623	0.704	4.12E-05	3.9	9	18.9	200-560
JJ5	jj08a	2.4	0.057	4.8	8.9	0.928	0.945	4.38E-05	2.4	9	11.6	100-540
	jj08c	0	0.019	4.1	9.3	0.812	0.867	4.42E-05	2.5	7	26.6	100-450
	jj10c	0	0.04	4.7	2.2	0.52	0.625	3.99E-05	2.9	9	11.1	250-600
	jj10d	0	0.046	1.9	2.9	0.522	0.633	3.91E-05	3.5	9	9.6	250-600
	jj11a	0	0.035	0.9	7	0.766	0.765	4.84E-05	2.3	8	18.2	250-560
	jj11b	0	0.017	1.2	2.6	0.933	0.948	4.21E-05	1.7	11	48.8	100-600
	jj11c	0	0.04	2.1	0.1	0.868	0.869	4.07E-05	3.2	10	18.8	0-540
	jj11d	0	0.024	3	0.8	0.732	0.721	4.52E-05	2.4	7	24.4	100-600
JJ6	jj13b	0	0.039	3	5	0.748	0.655	4.45E-05	2.9	7	15.2	350-600
	jj13c	0	0.031	1.2	9.3	0.739	0.638	4.32E-05	1.6	7	18.3	350-600
	jj13d	0	0.037	1.4	8.7	0.782	0.656	4.54E-05	1.9	7	16.7	350-600
JJ7	jj14a	0	0.022	0.7	6.3	0.912	0.932	5.21E-05	2.2	10	36.5	200-600
	jj14b	1.8	0.041	2	9.3	0.905	0.832	5.74E-05	3.5	10	19.1	0-540
	jj14c	0	0.05	1.6	1	0.748	0.672	5.29E-05	4.9	7	12.2	200-500
KS1	ks01a	0	0.051	2.3	8.6	0.668	0.67	4.75E-05	3.3	6	10.3	300-540

Continued on next page

Table 4.3 – Continued from previous page

Site Name	Specimen Name	Z	β	DANG	DRATS	F_{coe}	F_{vds}	Intensity (T)	MAD	N	Q	T(°C)
	ks01b	0	0.036	1.6	4	0.756	0.684	4.24E-05	4	7	17.1	250-540
	ks01c	0	0.036	2.3	4.7	0.65	0.665	4.76E-05	4.4	7	15	250-540
	ks01d	0	0.047	3.4	2.9	0.663	0.634	4.23E-05	4.1	7	11.7	300-560
KS2	ks02a	1.4	0.026	1	4.9	0.846	0.902	4.49E-05	2.9	10	28.4	100-560
	ks02b	0	0.012	0.6	7.1	0.796	0.803	4.73E-05	2.4	9	56.2	200-560
	ks02c	0	0.013	0.4	9.5	0.826	0.808	4.89E-05	3.2	8	50.7	250-560
	ks02d	0	0.024	2.3	5.1	0.763	0.81	5.43E-05	2.4	9	28.1	200-560
KS3	ks03a	0	0.013	2.5	0.8	0.714	0.683	4.61E-05	3.9	8	43.4	200-600
	ks03b	0	0.029	4.3	1.6	0.825	0.801	5.08E-05	4.4	10	24.2	0-540
	ks03c	0	0.029	3	3.7	0.674	0.614	4.79E-05	3.7	6	17.8	200-540
	ks03d	0	0.023	2.3	6.7	0.837	0.82	4.65E-05	3	10	30.5	0-600
AK1	ak01a	2.6	0.057	0.5	1.9	0.641	0.601	4.07E-05	1.2	9	9.6	250-600
	ak01b	3	0.059	0.4	1.3	0.647	0.625	4.68E-05	2.3	9	9.4	250-600
	ak01c	1.1	0.014	0.5	3.8	0.696	0.676	4.23E-05	0.7	9	41.9	250-600
	ak01d	1.7	0.017	1.2	0.9	0.673	0.637	4.34E-05	2.3	9	33.3	250-600
AK2	ak04a	1	0.022	1.5	3.1	0.889	0.936	3.52E-05	2.3	10	34.6	200-600

Continued on next page

Table 4.3 – Continued from previous page

Site Name	Specimen Name	Z	β	DANG	DRATS	F_{coe}	F_{vds}	Intensity (T)	MAD	N	Q	T(°C)
	ak04c	0	0.022	1.2	3.6	0.891	0.95	4.14E-05	2.4	10	35.3	200-600
	ak04d	0	0.015	1.8	2.8	0.874	0.905	4.54E-05	3	10	51.8	200-600
	ak04b	0	0.011	0.7	6.4	0.873	0.897	3.62E-05	2	10	69.9	200-600

Bibliography

M. J. Aitken, A. L. Allsop, G. D. Bussell, and M. B. Winter. Geomagnetic intensity in Egypt and western Asia during the second millennium BC. *Nature*, 310(5975): 305–306, 1984.

M. J. Aitken, A. L. Allsop, G. D. Bussell, and M. B. Winter. Geomagnetic intensity variation during the last 4000 years. *Phys. Earth Planet. Int.*, 56(1-2):49–58, 1989.

M. J. Aitken, G. Bussell, R. Jones, and C. J. Shaw. Geomagnetic field intensity variations in the eastern Mediterranean within the period 5000 to 2000 BP. *Geophys. J. R. Astron. Soc.*, 65(1):267–267, 1981.

H. Amit, M. Korte, J. Aubert, C. Constable, and G. Hulot. The time-dependence of intense archeomagnetic flux patches. *J. Geophys. Res.*, 116, 2011.

E. Ben-Yosef, H. Ron, L. Tauxe, A. Agnon, A. Genevey, T. E. Levy, U. Avner, and M. Najjar. Application of copper slag in geomagnetic archaeointensity research. *J. Geophys. Res.*, 113(B8), 2008.

A. J. Biggin. Are systematic differences between thermal and microwave Thellier-type palaeointensity estimates a consequence of multidomain bias in the thermal results? *Phys. Earth Planet. Int.*, 182(3-4):199–199, 2010.

A. Chauvin, Y. Garcia, P. Lanos, and F. Laubenheimer. Paleointensity of the geomagnetic field recovered on archaeomagnetic sites from France. *Phys. Earth Planet. Int.*, 120(1-2):111–136, 2000.

R. S. Coe, S. Grommé, and E. A. Mankinen. Geomagnetic paleointensities from radiocarbon-dated lava flows on Hawaii and question of Pacific nondipole low. *J. Geophys. Res.*, 83(Nb4):1740–1756, 1978.

R. Day, M. Fuller, and V. A. Schmidt. Hysteresis properties of titanomagnetites : Grain-size and compositional dependence. *Phys. Earth Planet. Int.*, 13(4): 260–267, 1977.

A. Deme and S.K. McIntosh. Excavations at Walaldé: New light on the settlement of the Middle Senegal valley by iron-using people. *J. African Arch.*, 4(2):317–347, 2006.

M. H. Dodson and E. McClelland-Brown. Magnetic blocking temperatures of single-domain grains during slow cooling. *J. Geophys. Res.*, 85(Nb5):2625–2637, 1980.

F. Donadini, M. Korte, and C. G. Constable. Geomagnetic field for 0-3 ka: 1. New data sets for global modeling. *Geochem. Geophys. Geosyst.*, 10(Q06007), 2009. doi:10.1029/2008GC002297.

M. Dumberry and C. C. Finlay. Eastward and westward drift of the Earth's magnetic field for the last three millennia. *Earth Planet. Sci. Lett.*, 254(1-2): 146–157, 2007.

Y. Gallet, A. Genevey, and V. Courtillot. On the possible occurrence of 'archaeomagnetic jerks' in the geomagnetic field over the past three millennia. *Earth Planet. Sci. Lett.*, 214(1-2):237–242, 2003.

A. Genevey and Y. Gallet. Intensity of the geomagnetic field in western Europe over the past 2000 years: New data from ancient French pottery. *J. Geophys. Res.*, 107(B11), 2002.

A. Genevey, Y. Gallet, C. G. Constable, M. Korte, and G. Hulot. Archeoint: An upgraded compilation of geomagnetic field intensity data for the past ten millennia and its application to the recovery of the past dipole moment. *Geochem. Geophys. Geosyst.*, 9(Q04038), 2008. doi:10.1029/2007GC001881.

M. Gomez-Paccard, G. McIntosh, A. Chauvin, E. Beamud, F. J. Pavon-Carrasco, and J. Thiriot. Archaeomagnetic and rock magnetic study of six kilns from North Africa (Tunisia and Morocco). *Geophys. J. Int.*, 189:169–186, 2012.

S. L. Halgedahl, R. Day, and M. Fuller. The effect of cooling rate on the intensity of weak-field TRM in single-domain magnetite. *J. Geophys. Res.*, 85(Nb7):3690–3698, 1980.

G. A. Hartmann, A. Genevey, Y. Gallet, R. I. F. Trindade, C. Etchevarne, M. Le Goff, and M. C. Afonso. Archeointensity in Northeast Brazil over the past five centuries. *Earth Planet. Sci. Lett.*, 296(3-4):340–352, 2010.

A. G. Hussain. Archaeomagnetic investigations in Egypt - Inclination and field intensity determinations. *J. Geophys.*, 53(3):131–140, 1983.

A. G. Hussain. The secular variation of the geomagnetic-field in Egypt in the last 5000 years. *Pure Appl. Geophys.*, 125(1):67–90, 1987.

J. L. Kirschvink. The least-squares line and plane and the analysis of paleomagnetic data. *Geophys. J. R. Astron. Soc.*, 62(3):699–718, 1980.

K. Korhonen, F. Donadini, P. Riisager, and L. J. Pesonen. GEOMAGIA50: An archeointensity database with PHP and MySQL. *Geochem. Geophys. Geosyst.*, 9(Q04029), 2008. doi:10.1029/2007GC001893.

M. Korte and C. Constable. Continuous global geomagnetic field models for the past 3000 years. *Phys. Earth Planet. Int.*, 140(1-3):73–89, 2003.

M. Korte and C. Constable. Improving geomagnetic field reconstructions for 0-3 ka. *Phys. Earth Planet. Int.*, 188(3-4):247–259, 2011.

M. Korte and C. G. Constable. Continuous geomagnetic field models for the past 7 millennia: 2. CALS7K. *Geochem. Geophys. Geosyst.*, 6(Q02H15), 2005. doi:10.1029/2004GC000800.

M. A. Kovacheva. Some archaeomagnetic conclusions from 3 archaeological localities in Northwest Africa. *Dokladi Na Bolgarskata Akademiya na Naukite*, 37(2): 171–174, 1984.

R. Leonhardt, A. Saleh, and A. Ferk. Archaeomagnetic field intensity during the Roman period at Siwa and Bahryn oasis, Egypt: Implications for the fidelity of Egyptian archaeomagnetic data. *Archaeometry*, 52:502–516, 2010.

S. Levi and S. K. Banerjee. On the possibility of obtaining relative paleointensities from lake sediments. *Earth Planet. Sci. Lett.*, 29(1):219–226, 1976.

W. Lowrie. Identification of ferromagnetic minerals in a rock by coercivity and unblocking temperature properties. *Geophys. Res. Lett.*, 17(2):159–162, 1990.

E. McClelland-Brown. Experiments on TRM intensity dependence on cooling rate. *Geophys. Res. Lett.*, 11(3):205–208, 1984.

G. McIntosh, M. Kovacheva, G. Catanzariti, F. Donadini, and M. L. O. Lopez. High coercivity remanence in baked clay materials used in archeomagnetism. *Geochem. Geophys. Geosyst.*, 12(Q02003), 2011. doi:10.1029/2010GC003310.

G. McIntosh, M. Kovacheva, G. Catanzariti, M. L. Osete, and L. Casas. Widespread occurrence of a novel high coercivity, thermally stable, low unblocking temperature magnetic phase in heated archeological material. *Geophys. Res. Lett.*, 34(21), 2007.

R.J. McIntosh, S.K. McIntosh, and H. Bocoum. *Seeking the origins of Takrur : Archaeological excavations and survey in the Middle Senegal valley.* Yale University Publications in Anthropology, New Haven., 2012. (In press.).

S.K. McIntosh. *Excavations at Jenné-jeno, Hambarketolo, and Kaniana (Inland Niger Delta, Mali), the 1981 Season.* University of California Publications in Anthropology, 20. University of California Press, Berkeley, 1995.

S.K. McIntosh. Ceramics. In R.J. McIntosh, S.K. McIntosh, and H. Bocoum, editors, *Seeking the Origins of Takrur : Archaeological excavations and survey in the Middle Senegal valley.* Yale University Publications in Anthropology, New Haven., 2012. (In press.).

S.K. McIntosh and H. Bocoum. New perspectives in Sincu Bara, a first millennium site in the Senegal valley. *Afr. Arch. Rev.*, 77(1):124–178, 2000.

S.K. McIntosh and R.J. McIntosh. *Prehistoric Investigations in the Region of Jenné, Mali.*, volume 2 of *Camb. Mono. Afr. Arch.* Oxford: B.A.R., 1980.

T. Nagata, Y. Arai, and K. Momose. Secular variation of the geomagnetic total force during the last 5,000 years. *J. Geophys. Res.*, 68(18):5277–5281, 1963.

H. Odah. Improvement of the secular variation curve of the geomagnetic field in Egypt during the last 6000 years. *Earth Planets Space*, 51(12):1325–1329, 1999.

H. Odah, F. Heider, A. G. Hussain, V. Hoffmann, H. Soffel, and M. Elgamili. Paleointensity of the geomagnetic-field in Egypt from 4000 BC to 150 AD using the Thellier method. *J. Geomagn. Geoelectr.*, 47(1):41–58, 1995.

C. B. Ramsey, M. Dee, S. Lee, T. Nakagawa, and R. A. Staff. Developments in the calibration and modeling of radiocarbon dates. *Radiocarbon*, 52(3):953–961, 2010.

A. P. Roberts, Y. L. Cui, and K. L. Verosub. Wasp-waisted hysteresis loops - Mineral magnetic characteristics and discrimination of components in mixed magnetic systems. *J. Geophys. Res.*, 100(B9):17909–17924, 1995.

P. A. Selkin, J. S. Gee, L. Tauxe, W. P. Meurer, and A. J. Newell. The effect of remanence anisotropy on paleointensity estimates: A case study from the Archean Stillwater Complex. *Earth Planet. Sci. Lett.*, 183(3-4):403–416, 2000.

D. Strangway, R. M. Honea, B. E. Mcmahon, and E. E. Larson. Magnetic properties of naturally occurring goethite. *Geophys. J. R. Astron. Soc.*, 15(4):345–359, 1968.

L. Tauxe. *Essentials of Paleomagnetism.* University of California Press, Berkeley, 2010.

L. Tauxe, T. A. T. Mullender, and T. Pick. Potbellies, wasp-waists, and superparamagnetism in magnetic hysteresis. *J. Geophys. Res.*, 101(B1):571–583, 1996.

L. Tauxe and H. Staudigel. Strength of the geomagnetic field in the Cretaceous Normal Superchron: New data from submarine basaltic glass of the Troodos ophiolite. *Geochem. Geophys. Geosyst.*, 5(Q02H06), 2004. doi:10.1029/2003GC000635.

O. Thellier, E. Thellier. Sur l'intensité du champ magnétique terrestre dans le passé historique et géologique. *Ann. Géophys.*, 15:285376, 1959.

T. Togola. Archaeological investigations of Iron Age sites in the Mema region, Mali (West Africa). *BAR IS1736*, Oxford: Archaeopress, 2008.

D. Walton. Re-evaluation of Greek archaeomagnitudes. *Nature*, 310(5980):740–743, 1984.

D. Walton. The intensity of the geomagnetic-field in the eastern Mediterranean between 1600 BC and AD 400. *J. Geomagn.Geoelectr.*, 42(8):929–936, 1990.

D. Walton and H. Balhatchet. Application of a new technique to Greek archaeomagnitudes. *J. Geomagn. Geoelectr.*, 40(12):1503–1510, 1988.

Chapter 5

Archeointensity in India: New constraints for the Iron Age

Very few archeomagnetic studies have been conducted in India despite its archeological wealth stemming from some of the most ancient civilizations. In order to address the paucity of data we conducted an archeointensity study on artifacts collected in and around the ancient city of Varanasi. We provide four new archeointensity estimates in this study and place them in the context of the published data. Our data are in agreement with other data from this region. Together these demonstrate a sharp drop in field intensity by ∼40% in the first half of the first millenium BCE and the field might have stayed low for the entire first millenium CE. An additional motivation behind this study was to test the potential of iron slags as paleointensity recorders but all the slag specimens in our study suffered from extensive alteration and were unsuitable for archeointensity.

5.1 Introduction

In the recent past, archeomagnetic datasets have proved extremely useful in reconstructing the Anthropocene geomagnetic field. Some parts of the world, such as northern Europe and the Middle East are well represented with data from

the past few millennia owing to a combination of rich cultural heritage and active interest by certain investigators. Other parts of the world, such as India or South America, remain relatively uncharted despite having some of the oldest known civilizations in history. The vast difference in the regional coverage of data is often a cause for concern as it affects the accuracy of global field models such as the CALSxK generation of models, where x stands for the time span of the models in millenia (Korte and Constable, 2003, 2005, 2011). Regional differences predicted in field intensities from these models could either stem from the regional influence of non-axial-dipole features or result from inadequate data coverage from some parts of the world (see Genevey et al., 2008). Gradual progress is being made to expand the archeointensity database into new frontiers as new studies are being conducted in poorly represented regions (Hartmann et al., 2010).

To illustrate the difficulty in studying geomagnetic field behavior, we plot data in Fig. 5.1 from two parts of the world with vastly different data coverage, Europe and the Middle East (hereafter called "Europe") versus Central and Southeast Asia (hereafter called "Central Asia"). Virtual axial dipole moments (VADMs) transform locally observed magnetic intensities to a global reference by using an axial dipole approximation for the magnetic field. Observed differences in VADMs are therefore usually attributed to non-axial-dipole contributions to the total magnetic field. While both the European and the Central Asian curves show a high field value in the second half of the first millennium BCE, the drop in intensity in Central Asia seems to be much more rapid than in Europe and the field seems to have reached a much lower value. Also, in Europe the intensity seems to have steadily recovered in the first millenium CE while in Central Asia the average intensity remained low although there seems to have been significant fluctuation in the field evolution. While these distinct regional trends could result from significant non-axial dipolar contributions to the field, it is difficult to draw any conclusion because of the big difference in data density from the two regions; in Europe we have 752 intensity estimates while for central Asia we only have 188.

Therefore, part of the observed differences in the regional VADMs, for example the fluctuation observed in Central Asia, could be the result of inadequate and/or poor data. In order to address the obvious need for high quality data from Central Asia, we decided to tap into the resources of Prof. Vibha Tripathy, an Indian archeologist.

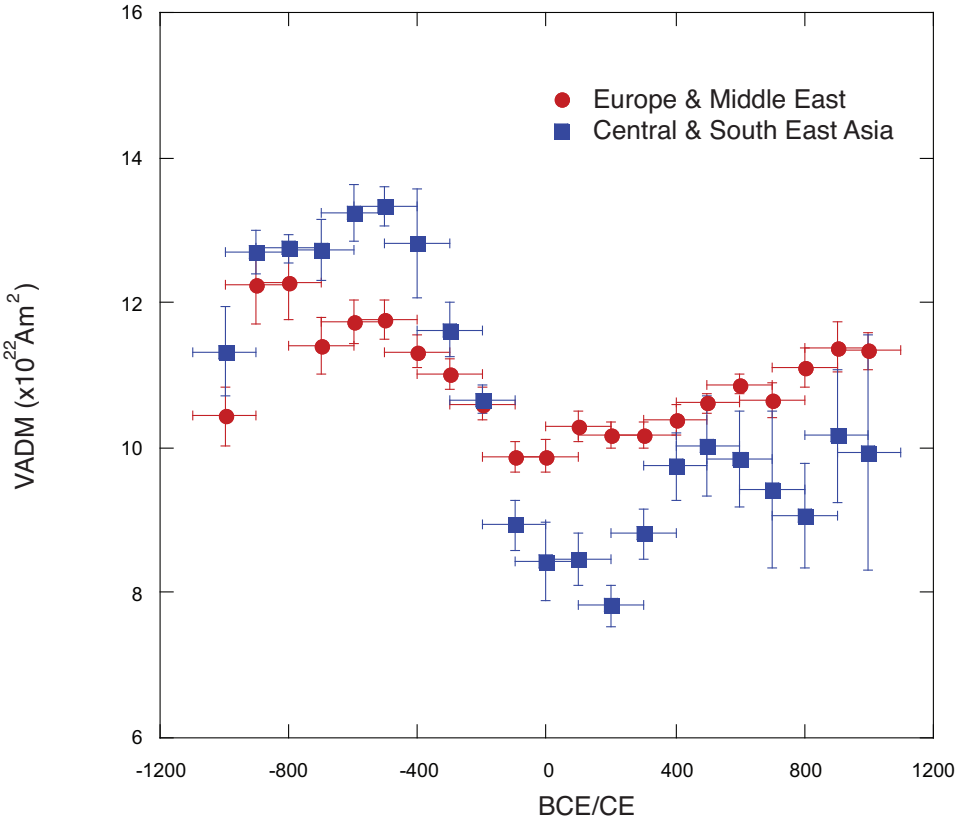


Figure 5.1: Average VADMs for Europe and Middle East (30-60°N, 20-50°E) and Central to South-East Asia (10-40°N, 50-80°E). A moving window of 200 yrs shifted every 100 yrs was used for the analysis. Standard error is plotted on the y-axis and a fixed error of 100 yrs on the x-axis. We used GEOMAGIA database found at http://geomagia.ucsd.edu (Korhonen et al., 2008; Donadini et al., 2009) and only paleointensity estimates obtained with a double-heating protocol were included in the analysis.

Ben-Yosef et al. (2008) found copper slags to be excellent paleointensity recorders and this study was initially designed to see whether slags from the Iron Age in India could be used in a similar manner. All the slags showed marked

alteration during the paleointensity experiments and had to be rejected. Some potsherds and furnace clay were collected along with the slags and they provided four new archeointensity estimates. Being the only recent study from India, this data is intended as a starting point for obtaining more intensity estimates from the subcontinent using advanced paleomagnetic techniques. With the data presented here, we find evidence of a drop of $\sim 26\ \mu$T in the second half of the first millennium BCE. Also, the field likely remained at a low value for the first millenium CE.

5.2 Archeology

The samples used in this study belonged to the Iron Age period in India (2000 BCE to 1000 CE). The samples included mostly iron slags, some potsherds and one furnace clay. All the samples were collected during excavations at localities within 100 kilometers of the city of Varanasi (25.31°N, 82.96°E) in northern India. Age was constrained by the archeologists in a variety of ways including pottery phase, coin inscriptions, stratigraphy and ^{14}C dates (Table 5.1).

5.3 Rock Magnetic Experiments

To identify the major magnetic mineral phases in the samples, we carried out three-axis IRM demagnetization experiment (Lowrie, 1990). IRM demagnetization involved giving the specimen three DC pulse fields of 1.2 T, 0.4 T and 0.2 T successively, in orthogonal directions. The samples were then thermally demagnetized up to 680°C. Subsequently hysteresis loops were measured on the same samples at a maximum field of 1T. Together these reveal the varying contributions of different phases of magnetite and hematite.

The Lowrie tests revealed a dominant soft component which unblocked gradually up to 580°C (Fig. 5.2). Some specimens showed minor goose-necking (sensu Tauxe et al., 1996) that indicated a significant high coercivity contribution

(Fig. 5.2b). The minor harder fraction sometimes sometimes showed a strong unblocking near 200°C and could be composed of a substituted hematite phase, first observed by McIntosh et al. (2011).

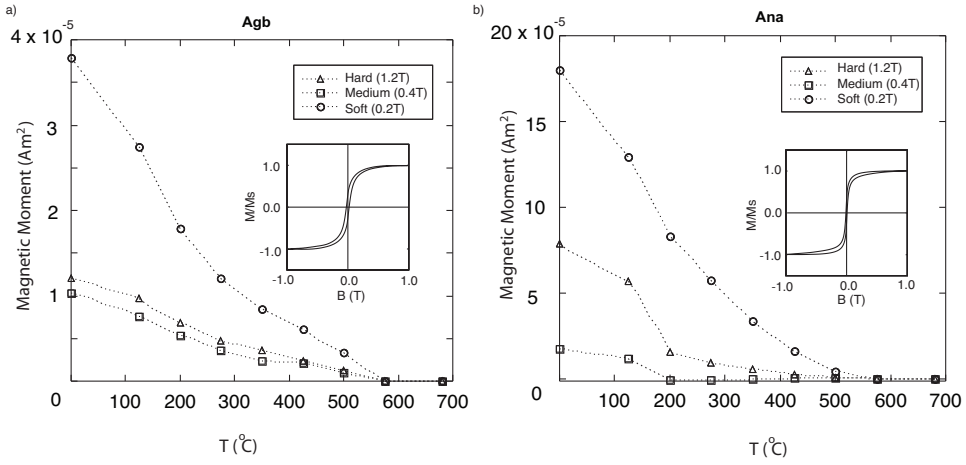


Figure 5.2: Rock magnetic measurements on sister specimens from samples a) Agb and b) Ana. Three component IRM demagnetization experiments with insets of the corresponding hysteresis loop of the specimens at 1T.

5.4 Archeointensity Experiments and Results

Raw paleointensity estimates were obtained using the IZZI protocol (Tauxe and Staudigel, 2004). In this method the in-field (I) and zero-field (Z) heating steps are alternated at each temperature steps. Additionally, pTRM checks were conducted at every alternate step to detect alteration. 13 double heating steps between 100°C and 600°C were used for the experiments with steps of 50°C between 100°C and 500°C and steps of 25°C between 500°C and 600°C.

We used a stringent set of criteria for choosing successful specimens which included DRATS <10, MAD<7, DANG<7°, $\beta < 0.06$ and F_{vds} >0.5 with at least 7 double heating steps to constrain the primary remanence. Our quality criteria let us select only those specimens which yielded straight Arai plots (Nagata et al., 1963) and with a single component of remanence that decayed to the origin, in

an objective manner. Thus while va12i (Fig. 5.3a) was selected, bhu2a (Fig. 5.3b) and bhu4c (Fig. 5.3c) were rejected. AARM was used to correct for anisotropy in the samples (McCabe et al., 1985; Selkin et al., 2000; Ben-Yosef et al., 2008). Cooling rate corrections (Dodson and McClelland-Brown, 1980; Halgedahl et al., 1980) were performed on sister specimens of successful samples assuming a 10 hour ancient cooling time. This was achieved by keeping the fan in the ovens switched off during the entire length of cooling. The correction factor varied between 0.91 and 0.93 (see Chapter 4 for details of the experiments).

Of the 111 specimens, 93 were rejected primarily owing to alteration during the experiment (Table 5.1). This included all the slag specimens which comprised almost 70% of the samples. These altered even at low temperatures of 200°C and were found to be unsuitable for paleointensity experiments. Two estimates from ∼500 BCE show moderately high fields of 59.92 ± 3.27 μT and 52.57 ± 2.01 μT. When converted to VADM these translate to 12.43 $\times 10^{22}$ Am^2 and 10.91 $\times 10^{22}$ Am^2 respectively. Thereafter we see a marked drop in intensity of 26 μT between 500 BCE to 150 CE . In the first millenium CE we have two sites which yield low estimates, 33.9 ± 2.87 μT at 150 CE and 33.04 ± 1.43 μT at 900 CE, that suggest the field might have remained low for the entire first millenium CE (Fig. 5.4).

5.5 Discussion

Only a very limited number of studies have looked at paleosecular variation in India (Athavale, 1966; Ramaswamy et al., 1985; Ramaswamy and Duraiswamy, 1990; Aitken et al., 1989; Manoharan et al., 2008a,b) (see Fig. 5.4). Although Athavale (1966) was among the pioneers who tried paleointensity with archeological samples, there seems to have been a precipitous drop in the production of archeointensity data from the region after him. In that study, thirty radiometrically dated (uncalibrated) archeological sites ranging in age from 350 BP to 4200 BP furnished successful paleointensity estimates. The experimental technique was

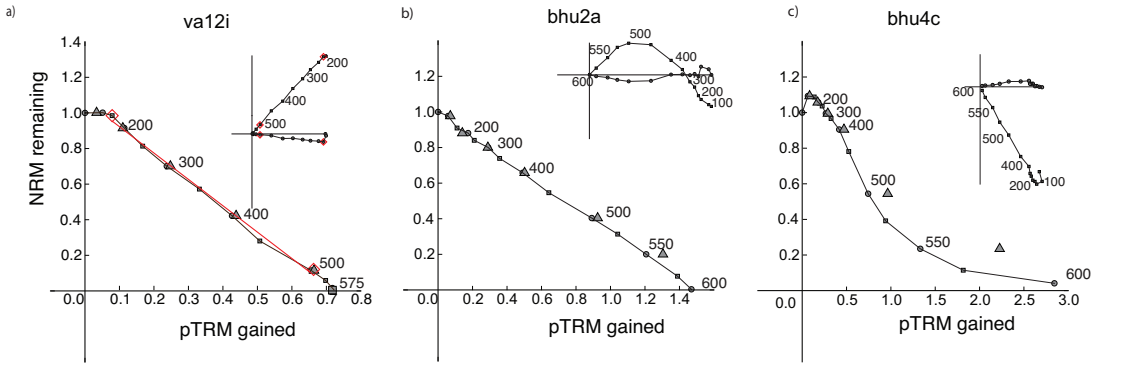


Figure 5.3: IZZI experiment results: Arai plots with insets of Zijderveld diagrams of a) representative specimens which passed the selection criteria and b-c) representative specimens which failed the selection criteria. The temperature interval used for isolating the characteristic remanence in a) is marked with a red line. Insets show the vector components of the zero field steps with x in the abscissa and y, z in the ordinate. The circles are (x, y) pairs and the squares (which have the temperature steps marked alongside) are (x, z) pairs. The directions are in the specimen coordinate system. The laboratory field was applied along the z-axis in the in-field steps.

similar to the then recent work by Thellier (1959) but used only two temperature steps and alteration potential was measured only on sister specimens. Based on the description of the samples - red pottery with no grey core - and our experience with Indian samples, it could well be that the samples were indeed resistant to significant alteration and using sister specimens to gauge alteration did not introduce substantial error. Also, a rudimentary selection criterion was used and if the fields obtained at the two temperature steps differed by more than 30% they were discarded. The next set of studies, by (Ramaswamy et al., 1985) and (Ramaswamy and Duraiswamy, 1990), together yielded 32 estimates from the southern tip of India. They used closely spaced temperature steps (100°C). They also aligned field direction with the NRM direction to reduce the effect of anisotropy. These innovations were distinct improvements over the approach of Athavale (1966). However, they performed no additional tests to detect alteration. The effect of cooling rate was taken into account by cooling for 7 hrs during the in-field step. Together these three studies form the bulk of the Indian archeointensity data. Aitken et al.

(1989) included pottery samples from India in a study involving ceramics from many different parts of the world and used stricter quality criteria. Cooling rate experiments were done systematically with a sister specimen from each core and anisotropy effects were also taken into account. Five paleointensity estimates were generated in this study. The remaining two studies each yielded one data point (Manoharan et al., 2008a,b). It is noteworthy that there is no directional datum from the subcontinent for the past few millenia.

Data from South India, especially from Ramaswamy et al. (1985) and Ramaswamy and Duraiswamy (1990), show a steep drop in intensity in the region between 500 and 0 BCE. As the sites are all located in a small geographic region in the southern tip of India (Fig. 5.4a), it is difficult to tell whether this feature is local or more widespread. Data from Athavale (1966) have a high scatter overall and this is the only study we have from the northern parts of India (Fig. 5.4b). In spite of that, the markedly high scatter observed in the dataset around 300 CE indicates a more regional nature of this drop in intensity. The study of Aitken et al. (1989) also show a large intensity drop. This study confirms that the intensity drop which is apparent in the data from South India is indeed a regional feature. The intensity near Varanasi is likely to have dropped by $\sim$40% in this period. As the data from Ramaswamy et al. (1985); Ramaswamy and Duraiswamy (1990) and this study are from sites separated by of 20° of latitude, it could point to a more regionally homogenous field than that observed in Africa (see Chapter 4). Our data matches the CALS3K.4 model predictions reasonably well although it must be pointed out that both paleointensity estimates from the first millenium CE are much lower than the model predictions. The sample from Sikandarpur has a large age error because only pottery style was used to determine its age. Pottery style generally persisted over long time periods and hence it is more difficult to constrain the ages of samples based only on the style of pottery. Unlike in Chapter 4, where stratigraphy, ^{14}C and pottery style were used in tandem (and only those samples where all three fixed the date unequivocally were retained), this study

used artifacts for which any of those three methods (and coin inscriptions) were used to constrain age. This often leads to more uncertainty in the age estimates. In spite of this the sample from Sikandarpur showed that the field in India was likely quite low in the first millenium CE.

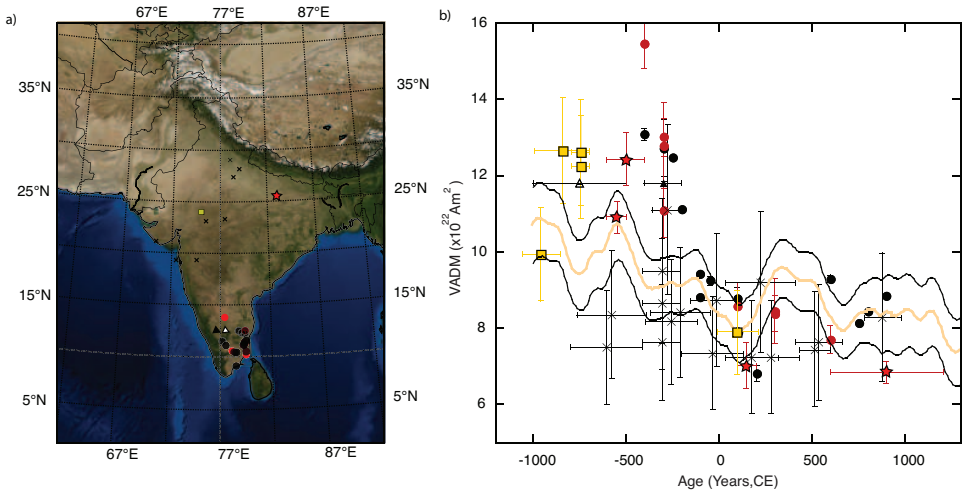


Figure 5.4: a) Compilation of archeointensity site locations from Athavale (1966) (black cross), Ramaswamy et al. (1985) (black dots), Ramaswamy and Duraiswamy (1990) (red dots), Aitken et al. (1989) (yellow square), Manoharan et al. (2008a) (black triangle), Manoharan et al. (2008b) (white triangle). Red star marks the location of this study. b) Compilation of archeointensity data from India. Symbols correspond to the map. The CALS3K.4 prediction with one-sigma bounds are also shown.

5.6 Conclusion

One goal of this study was to test the suitability of iron slags as a recorder of the paleofield and we were unable to get any reliable paleointensity estimates from the slags because of extensive alteration. An additional goal was to obtain new data to complement the rather thin dataset from this region. Further, given the datedness of the previous studies this study was also intended to test some of the trends observed in the earlier studies.

Data from the pottery samples confirmed the broad trend observed in the

existing data from this region; a substantial drop of ∼40% in the last half of the first millenium BCE. Furthermore, the field seems to have remained low for the entire first millenium CE. Our data broadly agrees with CALS3K.4 predictions but the field in the first millenium CE could have been lower than that predicted by the model.

The existing model predictions do not account for our data very well with markedly lower variability in the field in India at that time. Additional high quality data from India would improve the PSV models and thereby our understanding of the Holocene field variability.

Table 5.1: Archeointensity results from Varanasi, India. B_{raw}, B_{anis} and B_{cool} are the raw, anisotropy corrected and cooling rate corrected intensities respectively. B_{site} and $VADM_{site}$ are the site level intensities and virtual axis dipole moment respectively. Uncertainties in the paleointensity are calculated as one standard deviation of the mean. All the samples are potsherds except Kha which is a furnace clay.

Sites (Samples)	**Specimens**	**Dating Method**	**Age** BCE/CE	$\mathbf{B}_{raw}$ μT	$\mathbf{B}_{anis}$ μT	$\mathbf{B}_{cool}$ μT	$\mathbf{B}_{site}$ μT	$\mathbf{VADM}_{site}$ x10^{22}Am^2
Khairadih, Balia	va11a	Coins and inscription	150±50	38.95	39.96	37.1628		
(Kha)	va11b			41.29	34.76	32.3268	33.9±2.87	7.01±0.6
25.7°N, 84°E	va11c			30.14	33.12	30.8016		
	va11d			40.73	37.96	35.3028		
Anai, Varanasi	va12f	^{14}C aided	-500±100	71.61	70.137	64.52604		
(Ana)	va12g			62.24	64.484	59.32528	59.92±3.27	12.43±0.68
25.45°N, 82.85°E	va12h			67.5	66	60.72		
	va12i			60.95	60.213	55.39596		
	va12j			59.5	64.84	59.6528		
Agiabir, Mirzapur	va13f	^{14}C aided	-550±50	53.64	55.97	52.6118		
(Agb)	va13g			54.12	52.945	49.7683	52.57±2.01	10.95±0.42
25.13°N, 82.55°E	va13h			57.47	57.918	54.44292		
	va13i			64.02	56.868	53.45592		
Sikandarpur, Chandauli	bhu3a	Pottery style	900±300	35.24	35.7	32.487		
(Skn)	bhu3b			33.91	34.85	31.7135		
25.25°N, 83.25°E	bhu3c			37.3	35.53	32.3323	33.04±1.43	6.87±0.3
	bhu3d			34.18	36.54	33.2514		
	bhu3e			40.62	38.91	35.4081		

Bibliography

M. J. Aitken, A. L. Allsop, G. D. Bussell, and M. B. Winter. Geomagnetic intensity variation during the last 4000 years. *Phys. Earth Planet. Int.*, 56(1-2):49–58, 1989.

R. N. Athavale. Intensity of geomagnetic field in India over past 4000 years. *Nature*, 210(5043):1310–1312, 1966.

E. Ben-Yosef, H. Ron, L. Tauxe, A. Agnon, A. Genevey, T. E. Levy, U. Avner, and M. Najjar. Application of copper slag in geomagnetic archaeointensity research. *J. Geophys. Res.*, 113(B8), 2008.

M. H. Dodson and E. McClelland-Brown. Magnetic blocking temperatures of single-domain grains during slow cooling. *J. Geophys. Res.*, 85(Nb5):2625–2637, 1980.

F. Donadini, M. Korte, and C. G. Constable. Geomagnetic field for 0-3 ka: 1. New data sets for global modeling. *Geochem. Geophys. Geosyst.*, 10(Q06007), 2009. doi:10.1029/2008GC002297.

A. Genevey, Y. Gallet, C. G. Constable, M. Korte, and G. Hulot. Archeoint: An upgraded compilation of geomagnetic field intensity data for the past ten millennia and its application to the recovery of the past dipole moment. *Geochem. Geophys. Geosyst.*, 9(Q04038), 2008. doi:10.1029/2007GC001881.

S. L. Halgedahl, R. Day, and M. Fuller. The effect of cooling rate on the intensity of weak-field TRM in single-domain magnetite. *J. Geophys. Res.*, 85(Nb7):3690–3698, 1980.

G. A. Hartmann, A. Genevey, Y. Gallet, R. I. F. Trindade, C. Etchevarne, M. Le Goff, and M. C. Afonso. Archeointensity in Northeast Brazil over the past five centuries. *Earth Planet. Sci. Lett.*, 296(3-4):340–352, 2010.

K. Korhonen, F. Donadini, P. Riisager, and L. J. Pesonen. GEOMAGIA50: An archeointensity database with PHP and MySQL. *Geochem. Geophys. Geosyst.*, 9(Q04029), 2008. doi:10.1029/2007GC001893.

M. Korte and C. Constable. Continuous global geomagnetic field models for the past 3000 years. *Phys. Earth Planet. Int.*, 140(1-3):73–89, 2003.

M. Korte and C. Constable. Improving geomagnetic field reconstructions for 0-3 ka. *Phys. Earth Planet. Int.*, 188(3-4):247–259, 2011.

M. Korte and C. G. Constable. Continuous geomagnetic field models for the past 7 millennia: 2. CALS7K. *Geochem. Geophys. Geosyst.*, 6(Q02H15), 2005. doi:10.1029/2004GC000800.

W. Lowrie. Identification of ferromagnetic minerals in a rock by coercivity and unblocking temperature properties. *Geophys. Res. Lett.*, 17(2):159–162, 1990.

C. Manoharan, K. Veeramuthu, R. Venkatachalapathy, and R. Ilango. Studies on rock magnetic and paleointensity of some archaeological artifacts from Tamil-Nadu, India. *J. Zhejiang Univ.*, 9(7):988–993, 2008a.

C. Manoharan, K. Veeramuthu, R. Venkatachalapathy, T. Radhakrishna, and R. Ilango. Spectroscopic and ancient geomagnetic field intensity studies on archaeological pottery samples, India. *Lith. J. Phys.*, 48(2):195–202, 2008b.

C. McCabe, M. Jackson, and B. B. Ellwood. Magnetic anisotropy in the Trenton limestone : Results of a new technique, anisotropy of anhysteretic susceptibility. *Geophys. Res. Lett.*, 12(6):333–336, 1985.

G. McIntosh, M. Kovacheva, G. Catanzariti, F. Donadini, and M. L. O. Lopez. High coercivity remanence in baked clay materials used in archeomagnetism. *Geochem. Geophys. Geosyst.*, 12(Q02003), 2011. doi:10.1029/2010GC003310.

T. Nagata, Y. Arai, and K. Momose. Secular variation of the geomagnetic total force during the last 5,000 years. *J. Geophys. Res.*, 68(18):5277–5281, 1963.

K. Ramaswamy, M. Dheenathayalu, and S. Bharathan. Archaeomagnetic determination of the ancient intensity of the geomagnetic-field in Tamil Nadu, India. *Phys. Earth Planet. Int.*, 40(1):61–64, 1985.

K. Ramaswamy and D. Duraiswamy. Archaeomagnetic studies on some archaeological sites in Tamil-Nadu, India. *Phys. Earth Planet. Int.*, 60(4):278–284, 1990.

P. A. Selkin, J. S. Gee, L. Tauxe, W. P. Meurer, and A. J. Newell. The effect of remanence anisotropy on paleointensity estimates: A case study from the Archean Stillwater Complex. *Earth Planet. Sci. Lett.*, 183(3-4):403–416, 2000.

L. Tauxe, T. A. T. Mullender, and T. Pick. Potbellies, wasp-waists, and superparamagnetism in magnetic hysteresis. *J. Geophys. Res.*, 101(B1):571–583, 1996.

L. Tauxe and H. Staudigel. Strength of the geomagnetic field in the Cretaceous Normal Superchron: New data from submarine basaltic glass of the Troodos ophiolite. *Geochem. Geophys. Geosyst.*, 5(Q02H06), 2004. doi:10.1029/2003GC000635.

O. Thellier, E. Thellier. Sur l'intensité du champ magnétique terrestre dans le passé historique et géologique. *Ann. Géophys.*, 15:285376, 1959.